Graz University of Technology

Hydro Governor as Damping Device

Doctoral Thesis

Submitted by
Michael Weixelbraun

Head of Institute: Univ.-Prof. DI Dr.techn. Lothar Fickert
A - 8010 Graz, Inffeldgasse 18-I
Phone: (+43 316) 873 – 7551
Fax: (+43 316) 873 – 7553
http://www.ifea.tugraz.at
http://www.tugraz.at

Supervisor
Ao. Univ.-Prof. DI Dr.techn. Herwig Renner

Reviewer
Ao. Univ.-Prof. DI Dr.techn. Herwig Renner

Reviewer
Professor, dr.ing. Kjetil Uhlen

University of Technology Graz
Institute of Electrical Power Systems

10/2013

Abstract
This thesis presents a novel approach to damp low frequency electromechanical oscillations utilizing the governor of hydro power plants. The focus is thereby on weak grid conditions from the generator's perspective such as high connection impedance, high line loadings and weak voltage conditions. Especially for these conditions the classical Power System Stabilizer (PSS) is subjected to limitations concerning the interaction with the voltage regulation and the mutual coupling with other generators.

The overall approach is divided in two steps:
In the **Single Machine Infinite Bus Model** the linear characteristics of the governor system are derived and compared to the voltage control path. Furthermore the damping and synchronizing torque components of the governor system are investigated utilizing the extended Heffron-Phillips Model.
In the **Multi Machine Model** the hydro governor as a damping device is applied to act on low frequency oscillations during the mentioned grid conditions and is compared to the classical solution.

It is shown that the hydro governor is principally capable to act as a damping device. For weak grid conditions it is thus decoupled from the voltage control path and furthermore implies a favorable damping behavior. In addition the generator side damping with the classical Power System Stabilizer is extended towards low oscillations frequencies and weak grid conditions.
The technical limitation of the hydro governor for oscillation damping is given by the actuator speed limits, respectively the target oscillation frequency. These parameters are determinant for the contribution of the governor to the system damping.

Kurzfassung
In der vorliegenden Arbeit wird der Einsatz des Turbinenreglers von Wasserkraftwerken zur Dämpfung niederfrequenter, elektromechanischer Oszillationen untersucht. Der Fokus liegt dabei auf dem Einsatz bei besonderen Netzverhältnissen, wie beispielsweise hohen Anschlussimpedanzen oder hohen Leitungsauslastungen und damit schwierigen Spannungsverhältnissen. Speziell während dieser Betriebszustände ist die Wirkung des klassischen „Power System Stabilizers" aufgrund der gegenseitigen Beeinflussung mit der Spannungsregelung und der gegenseitigen, elektrischen Kopplung mit anderen Generatoren in der elektrischen Umgebung begrenzt.

Die Untersuchungen werden prinzipiell in zwei Abschnitte unterteilt:
Im Ein-Maschinen-Modell werden die linearen Eigenschaften des Turbinenreglers hergeleitet und in weiterer Folge mit den Eigenschaften der Spannungsregelung verglichen. Weiters werden die Komponenten des dämpfenden und des synchronisierenden Drehmoments des Turbinenreglers auf Basis eines erweiterten Heffron-Phillips-Modells untersucht.
Im Mehr-Maschinen-Modell wird der Turbinenregler unter den erwähnten netztechnischen Rahmenbedingungen zur Dämpfung eines Inter-Area-Modes eingesetzt.

Es kann gezeigt werden, dass der Turbinenregler grundsätzlich zu Dämpfungszwecken eingesetzt werden kann und speziell bei den genannten netzbetrieblichen Rahmenbedingungen und niederen Oszillationsfrequenzen (unter 1Hz) ein verbessertes Dämpfungsverhalten aufweist. Damit kann der Einsatzbereich der klassischen generatorseitigen Dämpfung hinsichtlich niedriger Oszillationsfrequenzen und erschwerten netzbetrieblichen Rahmenbedingungen erweitert werden.
Die technische Begrenzung der Wirksamkeit des Turbinenreglers zur Erhöhung der Systemdämpfung richtet sich dabei vorwiegend nach der maximalen Stellgeschwindigkeit der mechanischen Anlagen bzw. der jeweiligen Oszillationsfrequenz.

STATUTORY DECLARATION

I declare that I have authored this thesis independently, that I have not used other than the declared sources / resources and that I have explicitly marked all material which has been quoted either literally or by content from the used sources.

…… ……..

date (signature)

Acknowledgements
The author acknowledges especially Professor Herwig Renner from Graz University of Technology, Institute of Electrical Power Systems for supervision of the work and all the support during the whole research project.
Professor Kjetil Uhlen at NTNU (Norwegian University of Science and Technology) is acknowledged for being the second reviewer and examiner.
Also the involved members at the Norwegian Transmission System Operator STATNETT, where most of the work has been hosted, Jan Ove Gjerde, Oystein Kirkeluten and Stig Lovlund are acknowledged for their input and discussions as well as for the provision of operational experiences.
The author also wants to thank Professor Nina Thornhill from Imperial College London and all other key persons involved for the central coordination of the IAPP Project that enabled the secondment in Norway.

Content

1. List of symbols

A	System state matrix
AVR	**A**utomatic **V**oltage **R**egulator
B	Input matrix
C	Feed forward matrix
D	Output matrix
D	Damping coefficient
DFIG	**D**oubly **F**ed **I**nduction **G**enerator
d_w	Rotor speed deviation
E	Rotor voltage
f	Frequency
F	Participation factor matrix
G_{max}	Maximal governor gate limit
G_{min}	Minimal governor gate limit
H	Inertia constant
HF1, HF4	System state **H**igh **F**requency band 1 and 4 of multiband PSS
IF1, IF4	System state of **I**ntermediate **F**requency band 1 and 4 of multiband PSS
Imag	Imaginary part of complex term
K_D	Damping torque component
KD	Turbine damping
K_d	Differential gain
$K_{D\,\Delta Te}$	Damping torque component of electrical torque
$K_{D\,\Delta Tm}$	Damping torque component of mechanical torque
K_I	Integrative gain
K_P	Proportional gain

K_{PSS-G}	Proportional gain PSS-G
K_S	Synchronizing torque component
$K_{S\,\Delta Te}$	Synchronizing torque component of electrical torque
$K_{S\,\Delta Tm}$	Synchronizing torque component of mechanical torque
m	Number of lead/lag terms for PSS
M_P	Peak value of amplitude response
P	Right eigenvector matrix, modal matrix
p	Number of pole pairs
P	Active power
P_d	Accelerating power, difference between mechanical input active power and electrically dissipated active power
P_D	Damping power
P_m	Mechanical power
P_r	Rated generator active power
PSS	Power System Stabilizer
PSS-E	Power System Stabilizer – Excitation
PSS-G	Power System Stabilizer – Governor
Real	Real part of complex term
RG CE	Regional Group Central Europe
R_P	Static droop constant
R_T	Transient droop constant
sca	Scaling factor
SISO	**S**ingle **I**nput **S**ingle **O**utput
T_{decay}	Decay time constant calculated based on real part of eigenvalue
T_G	Gate servo time constant
t_j	Mechanical starting time
T_{Lead} / T_{Lag}	Lead / lag time constant

T_m	Mechanical torque
$T_{m,r}$	Rated mechanical torque
T_P	Pilot servo time constant
T_R	Transient droop time constant
T_s	Measuring time constant
TSO	**T**ransmission **S**ystem **O**perator
T_W	Washout time constant
V	Voltage
v_{gmax}	Actuator speed limit, opening gate
v_{gmin}	Actuator speed limit, closing gate
V_s	Generator **s**tator voltage
WAMPAC	**W**ide **A**rea **M**onitoring, **P**rotection **A**nd **C**ontrol
WAMS	**W**ide **A**rea **M**onitoring **S**ystem
$\mathbf{x}$	Vector of system states
$\mathbf{y}$	Output vector
β_{comp}	Angle to be compensated by damping device
ζ	Damping ratio
θ	Angle difference
ϑ	Rotor angle
λ_i	Eigenvalue of state matrix
Ψ_{fd}	Flux linkage of field winding
Ψ_{kd}	Flux linkage of damper winding
ω	Actual rotational speed
ω_n	Natural frequency
ω_r	Rated speed

2. Introduction

2.1. Changes in Power System Environment

Transmission grids in Europe are progressively facing critical operational situations, characterized by high line loadings, volatile and geographically centralized generation and possible violations of operational security limits. The reasons are manifold, reaching from the increased number of actors in the liberalized electricity markets to massive integration of renewables and sagging realization of grid extension plans. Conventional generating units, mostly synchronous generators are partly but persistent substituted by renewable units. These circumstances lead to a volatile change in the grid's oscillatory behavior, resulting from a permanently change in the constitution of the type of active generation units and thus changes in grid inertia.
The situation is in principle similar for most member countries of the ENTSO-E association with varying influences and consequences for the overall system operation and stability.

In the last decade various factors have influenced and changed the traditional view of the power system. In this section the most important ones are briefly described and their impact on power system characteristics is mentioned.
The liberalization of the electricity market at the beginning of the 21st century has split the traditional vertical organized utilities into horizontally organized energy companies. Power plant operators, traders and other market players face each other in competitive market structures, while grid operators remain regulated by the national regulatory authorities and the international regulator (ACER[1]) respectively. Besides the effect of an increased unpredictability of power flow, the increasing electricity trade and the increased price pressure led to a higher utilization of the power system on the one hand and to melting capacity reserves in generation and transmission on the other hand.
In parallel the power demand still increases constantly, shortly interrupted by the economic crises from 2008 until 2010.
In general the energy system undergoes a radical change. Political efforts to create a low carbon-economy and to fulfill the goals of a sustainable and renewable energy supply provide the energy industry, in particular the electrical industry, with new challenges.
The system change, accompanied by market phenomena and massive extension and further integration of fluctuating, renewable energy sources, is merging in a significant change in the oscillation behavior and the control characteristic of the power system. High power and frequency gradients combined with the decreasing respectively fluctuating grid inertia require ambitious efforts in power system monitoring and control in the future.
The dimension of additional stress for the mechanical system of generators is determined by the number and duration of oscillation events and considerable frequency deviations. Hence, the additional actuator movement needs to be put in relation to the increased, meanwhile inherent governor action due to deterministic frequency deviations, exemplary shown in Figure 1 [1].

[1] ACER – Agency for the Cooperation of Energy Regulators (http://www.acer.europa.eu/)

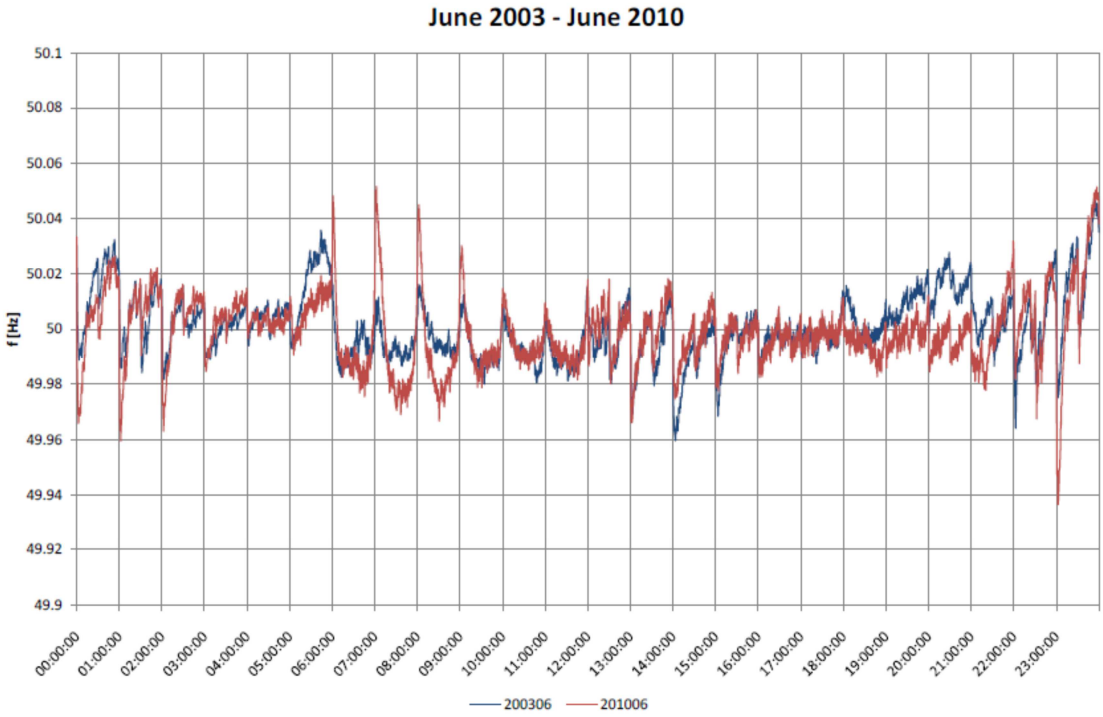

Figure 1: Frequency in Continental Europe, comparison June 2003 and June 2006 [1]

Further details, regarding the impact of deterministic frequency deviations to system operation and power plant operation, are given in [1].

The omnipresent linger in approval processes of power lines in many countries, caused by multiple reasons, has the consequence, that the expansion of the power system can hardly keep up with the changes in operational characteristics and the generation situation.
These developments, resulting in an increase of stressed power system conditions, have encouraged various stability incidents in the recent past. In the historical past mainly transient stability problems were causing major blackouts, whereas voltage stability, frequency stability and angle stability problems have created more concern in the resent past and in the present [2]. Two measured examples from the synchronous Central European System and from the Nordic Power System are described in chapter 3.2.3.

As one of the many consequences the small signal stability has become a topic of increasing attention in the last decade, mainly resulting from highly stressed systems or inadequate parameterization of various control devices resulting in low damped inter area oscillations. Generators in different grid areas, swinging against or with each other, are causing unwanted active power flows over thousands of kilometers. Under these conditions system stability is endangered preliminary due to two major factors:

- The danger of generation losses as a consequence of loss of synchronism

- The violation of transmission grid security limits, depending on the actual system loading.

The worst case scenario in this manner is a cascading line tripping, resulting from overloads and furthermore leading into major blackouts.
Several circumstances dominate the damping behavior of an electrical system. Influencing factors in the central European system are power flow situations from the periphery to the center of Europe, occurring during high renewable generation or cases of weak coupled grid areas for example the Iberian Peninsula or Turkey.
Especially in power systems with appropriate topological conditions conductive for the development of inter area oscillations and a long history of occurring events (e.g. WECC[2] or the Nordic Power System characterized by large groups of synchronous generators connected by long tie lines) utilities have gained experiences with oscillation. Lessons learned from the last decades identify insufficient damping as a considerable factor for grid separation [3].

The damping situation in the Nordic Power System is mainly dominated by the grid structure resulting from the longitudinal geographical shape of these countries. Centralized consumption and generation in the south, connected via long power lines across the north of the countries, are beneficial for weak oscillatory behavior under certain conditions. Also powerful industry sites connecting to weak grids can cause stability problems, although most of them of local nature.
Some incidents in the last years, related to the oscillation behavior of power systems, caused the central European system getting close to security limitations and blackouts.
Based on this development great effort has been undertaken in academia and industry to identify root cause scenarios. Many inventions have been worked out, control systems have been designed to improve the system's oscillatory behavior and thus to increase the damping.
The development of Wide Area Measurement Systems WAMS has been driven forward and implemented to monitor the system with improved accuracy. This feature has been approved and settled over the last years and is applied in most of the operation centers of the transmission grid operators and some distribution grid operators. By feeding processed WAMS signals into damping devices one speaks of WAMPAC (Wide Area Monitoring, Protection And Control) systems. This topic is under intensive investigation and delivers promising results for future automatic coordinated damping control systems across wide geographical areas.

[2] WECC – Western Electricity Coordinating Council is a Regional Entity coordinating Electric System reliability in the Western Interconnection. WECC is geographically the largest and most diverse of the eight Regional Entities that have Delegation Agreements with the North American Electric Reliability Corporation (NERC). WECC's service territory extends from Canada to Mexico. For further details see http://www.wecc.biz/Pages/Default.aspx

2.2. Motivation

The main motivation for this work is the cumulative occurrence of weakly damped, low frequency oscillations between large areas of power systems. In the past these oscillation phenomena have received subordinate attention whereas in the recent past increased effort has been made to develop solutions in academia and industry to improve the system damping. The superordinate intention of the approach is to contribute to a reliable and stable energy supply, considering the aspect of changing fundamental system characteristics. According to the developments in power grid characteristics, described in chapter 2.1, an increase of operational situations with critical damping and poor grid conditions can be expected for the future.

Among the various classes of damping devices the proposed approach is allocated to synchronous generator side damping.

The commonly used Power System Stabilizer is used to increase the damping of low frequency oscillations, acting via the excitation path. If the generator is connected to high grid impedances, the operational effectiveness is subjected to limitations which significantly reduce the beneficial impact on the respective inter area oscillation. Typical output limits are in the range of 3% up to 5% of the actual terminal voltage. The main reason is the mutual influence among the PSS-E device and the voltage control respectively the voltage control of neighboring generators. Furthermore in case of poor, local voltage conditions around the generator connection point, the reduced efficiency in power oscillation damping can affect a wide range of the power system.

In contrast, hydro governor systems are expected to provide beneficial control behavior regarding mutual interference. Furthermore, actuator speed limits of most of the governor systems are expected to be sufficient for low oscillation frequencies. Beyond the expected beneficial technical characteristics of a single device, a great number of potential generators in hydro power plant dominated countries in central Europe like Austria or Switzerland and in parts of Scandinavia offer the possibility to utilize the existing control infrastructure. In Norway, where the author absolved a research secondment at the Norwegian TSO STATNETT, the investigation of the potential governor damping device was of great interest.

Additionally new digital governor systems, applied in new generation units or repowered units, offer new possibilities regarding the implementation of new applications, flexibility in parameterization and accuracy in frequency control. Frequency deviations of ±1 mHz can already result in a change in active power output on the generator shaft.

Generally is it believed by the author that adequate system damping behavior is achieved by interaction of various technologies depending on the type of oscillation they should act on and on their optimal operational range.

From the author's perspective, there is a great need for the future to extend the classical generator side damping via the excitation path towards low oscillation frequencies and more independent from the predominant grid conditions. The advantage of existing infrastructure shall thereby be utilized and furthermore improve the generator side damping to a broader and more robust application.

Changing requirements for damping devices as a consequence of continuously changes in the oscillation behavior of the power system, accompanied with new possibilities of digital governing systems, are thus the main motivation for this work.

2.3. Objectives

The main objectives of this thesis are:

- To investigate potential of the hydro governor to act as a damping device. The classical generator side damping via the excitation control path shall thereby be extended by the utilization of the active power control path.
- To improve the damping behavior of low frequency oscillations under weak grid conditions from the generator's perspective.
- To utilize a single machine infinite bus system for the derivation of principle characteristics of the governor system, equipped with the PSS-G.
- To investigate the damping behavior of the PSS-G, acting on an inter area target mode, based on a multi machine model.

For each model the investigations are based on linear theory as well as on time domain simulations, taking into account nonlinear behavior of the system.

2.4. Scope of Research

In this work the generator side damping is of major concern. The active power control device for hydro power plants, the hydro governor, is investigated in frequency domain and in time domain regarding the potential to act as a damping device, additionally to the basic function of primary control. The basis of investigation is formed by two dynamic, nonlinear simulation models. Basically the investigations rely on linear analysis as well as on time domain simulations.

The linear analysis, a modified Heffron-Phillips model on the one hand, and the state space representation of the power system on the other hand, are utilized.

Simulations in time domain are done according to the nonlinear simulation models. Parameterizations of synchronous generators, automatic voltage regulators, transformers and power lines are derived from standard parameterizations. Hydro governors have been partly parameterized with recommended values or recommended parameterization routines.

Regarding the modal spectrum of the target frequencies, the focus is on low frequency inter area oscillation, were common hydro governors are believed to be able to play a role in the achievement of the formulated objectives. Exception thereby is the utilized single machine infinite bus system, which is used to derive principle relationships between the excitation system, the governor system and system damping.

The devices are fed by local signals such as speed deviation and accelerating power as well as from simplified Wide Area Measurement Systems, such as active power deviations or voltage angle deviations taken from an intertie power line.

Beyond the scope of this work is the investigation of the impact on the hydraulic path of the governor system. Also the used control signals are synthesized signals. Measured signals have not been utilized.
Also the impact of the system load, depending on its characteristics and dynamic modeling, is not addressed in this work. Further information regarding the load behavior and the damping of the system is referenced in [4] and [5].

2.5. Terminology and Assumptions

To distinguish between the Power System Stabilizer PSS in the excitation path an in the governor path the notation PSS is expanded. In the following the damping device **PSS-G** is for the PSS in the **governor** control loop and **PSS-E** is in the **excitation** control loop. Similar notations have been used by Milanovic in [4] regarding governors for multi-stage double reheat turbines whereas in [6] the Phase Compensated Governor PCG was applied to gas turbine systems.
In the following the mechanical and electrical torques are set equal to the respective electrical and mechanical powers in good approximation. This assumption is good practice in small signal stability studies. For small deviations of the quantities from the steady state operational point one can set the terms in per unit $P \approx T$ for $\omega \approx \omega_r$.
Wide Area Signals, utilized as input signals for the damping device, are consequently modeled without time delays from the measurement unit and the data transmission. This assumption is valid for all used devices whereby a comparison of the performances is assumed to be admissible.

2.6. Previous Work

2.6.1. State of the Art of Excitation System Representations and PSS-E Modeling in Small Signal Analysis

The basement for the modeling of excitation systems and PSS-E devices is summarized in the IEEE standard in [7]. Also typical parameter sets are included, which are satisfying the requirements for most stability studies.
In linearized systems the excitation system, including PSS-E, can be effectively modeled by using the Heffron-Philipps Model, first described in [8] and derived in more detail in [5]. The electrical system of the generator, including the excitation system, is therein represented by the constants K1-K6. Thus the Heffron-Phillips model is also found in literature as K-constant model. This representation allows the calculation of damping and synchronizing torque components in dependency of the rotor speed deviation, respectively the rotor angle deviation due to the analysis of fundamental transfer functions. The parameterization approach is therefore named “Damping Torque Approach”, described in detail by Pal in [9]. Several other approaches, like the frequency response approach or the state space approach are also summarized in [9]. In the past, several modified Heffron-Phillips model modifications have been developed in order to implement information from various signals. In [10] for example, the authors derive modified equations for the K-Constants in dependence of the secondary bus at the high voltage side of the step up transformer.

The Heffron-Phillips model has been extended to a multi machine representation in [11]. Therein the authors describe the effect of one particular machine on the overall system damping. The respective transfer functions are described and categorized by their influence on the target eigenvalue. The mentioned model is also used for deriving parameters for excitation systems and damping devices. The possibility of a Heffron-Phillips model setup, based on measured data, is described in [12]. The method is based on closed loop subspace identification and does not require any prior data of the generator.

2.6.2. **State of the Art of Governor Modeling in Stability Studies**

The contribution of hydro turbine control systems to system damping in the past has mainly focused on the suppression of negative, thus exciting damping contributions. This was achieved by the adjustment of parameters and restricting the control activity on certain oscillation frequencies [13].
Governor modeling in general can be performed in nonlinear time domain models or linear models, depending on the aim of the study. According to the principal functional realization, respectively the type of actuators, governors can be subdivided into the following categories [5]:

- Mechanical
- Mechanical hydraulic
- Electromechanical
- Electrohydraulic actuators

Several governor realizations are standardized and can be found combined with common parameter sets in [14] and [15]. The authors in [16] provide a software package with commonly used governors and hydraulic turbine models with accurate parameterizations and summarize their behavior in transient and small signal studies.
The impact of hydro governors on small signal stability is, under certain conditions, usually neglected.
Linear hydro governor models are an important and essential tool for the parameterization. In [17] the authors describe the validation of a linear governor model, based on transient field tests. The result is a black box model, derived by the state space identification method described in [18]. Tuning of hydro governors due to the comparison of parameters with typical value ranges of frequency and time domain parameters is described in detail in [15].
The governor as damping device applied to power plants connected via high impedances was also investigated in [13]. The enhancement was achieved by the insertion of positive damping and synchronizing torques. The theoretical results were verified by field tests.
The use of the governor system of gas turbines, as well as steam turbine governors and hydro governors, to improve transient stability and oscillatory stability, based on local measurements, has been carried out in [6], [19], [4] and [20]. All authors describe the governor control loop as robust to changes in system parameters. Additionally several investigations have been made to combine the action of the PSS in the excitation control loop and the PSS in the governor control loop to improve transient stability.

For the simplified considerations of a steam governing system in [21], the authors introduce a boundary frequency where a damping torque is induced. Above this frequency no damping torque or a slight negative damping torque is introduced. As a result the authors assume the boundary frequency to be independent from the controller gain. For hydro turbines the boundary frequency is said to be between 0.1 Hz and 0.3 Hz. The influence of the governor around the boundary frequency is therefore neglected whereas below or above the governor system provides an impact to the damping behavior of the considered system.

In [22] the influence of steam governor deadbands on small signal stability is studied. The authors conclude that governing systems can have a significant impact on low frequency inter area oscillations, even though their influence on local electromechanical oscillations can be neglected. Frequency deviations within the chosen deadband can result in a destabilizing effect on the target inter area mode.

Furthermore, in [6], [19] and [4] it has been shown that governor systems can introduce negative damping components and consequently weaken the oscillation damping of the system.

In [23] the authors mention that the governor dynamics are also weakly coupled to the rest of the power system, whereas in contrast the exciter control loop is affected by the operating conditions of the power system. The authors also describe the possibility of locally synthesizing the governor PSS, so that the controller design is reduced to a single machine problem.

In [24] the authors describe the damping of local modes, caused by large disturbances such as short circuits or line faults by controlling the water hammer of a low head hydroelectric power plant.

Generally many concepts are based on the improvement of transient stability mostly using steam- or gas turbines with fast valving actuators.

Hydro governors have also been applied to nonlinear, coordinated control structures to improve transient stability. The insertion of probing signals by the governor and/or the exciter to identify poorly damped modes under ambient conditions also requests further investigations. This method appeared in literature several times and it allows the detection of poorly damped modes even with low amplitudes.

The impact of inter area oscillations on the hydraulic system can be done using linear representations in various degree of detail. A stepwise description, starting from the simplified hydraulic model to a high order representation including penstock, surge tank and elastic water column, is given in [25]. The models are compared in frequency domain as well as in time domain.

2.7. The New Approach – Hydro Governor as Damping Device for Inter Area Oscillations during weak Grid Conditions

Governor systems have been used for stability improvement in the past. Hydro Governors have been utilized to improve transient stability (local) including the stabilization of the water hammer in case of large rotor excursions. Furthermore the governors of gas and

steam turbines have been adapted for the improvement of oscillatory stability. Further details are described in chapter 2.6.2.
The main scientific contribution of this thesis is the utilization of hydro governor system to improve the small signal stability. Therefore the application range of the classical generator side damping is extended towards low oscillations frequencies particularly under weak grid conditions.
In case of rotor oscillations due to active power swings, the resulting mechanical torque on the generator shaft provided by the governor should be decreased in the acceleration period, and increased in the decelerate period of the rotor movement. To introduce a pure damping torque to the system the mechanical torque deviation has thus to be ideally in phase opposition to the speed deviation. Essential is therefore the phasing of the speed deviation of the rotor $\Delta\omega$ and the inserted deviation of the mechanical torque by the PSS-G.
In Figure 2 the principle significance of the phasing of the generator output power vector P_m is drawn into a $\Delta\omega/\Delta\delta$ plain. The phase shift between $\Delta\omega$ and P_m of more than 90 ° has, at a certain synchronizing component P_s, a negative, thus exciting component P_d. Due to phase compensation by the angle θ, the resulting sign of the component P_d is inversed and thereby a damping behavior is achieved.

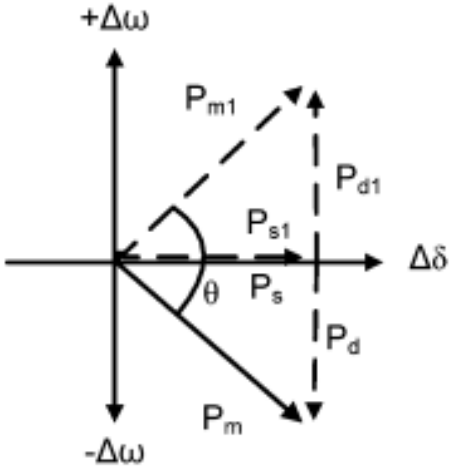

Figure 2: Effect of the phasing of generator output power P_m on the synchronizing and damping torque provided by the governor; $\Delta\omega$ speed deviation, P_m mechanical output power, P_d damping power component, P_s synchronizing power component; [19]

As the phase difference between mechanical output and speed deviation further decreases, P_{d1} increases to a maximum.
The description shown in Figure 2 is based on the K-Constant or Heffron-Phillips model, used for small signal stability studies. It is strongly coupled to the damping torque approach, regarding the design of PSS-E devices, wherein the changes of the resulting electrical torque are split into components in phase with rotor deviation $\Delta\omega$, thus damping torques, and in components in phase with the rotor angle deviation $\Delta\delta$, named synchronizing torques.

In this work this concept is applied to the hydro governor and is described in more detail in chapter 4.3.2.
From the basic concept interactions with the functionalities during normal operation, such as primary control, shall be avoided. Figure 3 shows the principle signal routing for the PSS-G.

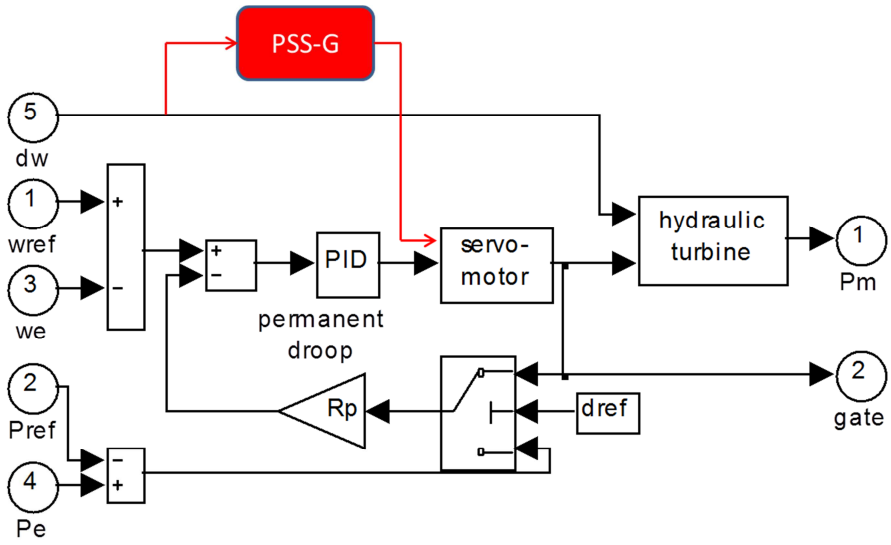

Figure 3: Principle signal routing for the PSS-G; PID controller, R_p permanent controller droop, d_w mechanical speed deviation, w_{ref} speed value reference, w_e actual speed value, P_{ref} active power reference, P_e actual active power, P_m mechanical power output

One can see that the primary control path is bypassed and not influenced by the power oscillation damping control path. This separation of fundamental functionalities is based upon the wanted insensibility of the primary control path of usually ±10 mHz, whereas the power oscillation damping path should react as sensitive as possible to a certain mode of oscillation.

2.8. Outline of the Thesis

In **chapter 3** electromechanical oscillations are categorized in terms of system stability following the general scheme provided by [5]. Furthermore the basic framework of electromechanical oscillations is briefly described adducing the nature and root causes of oscillations and their mathematical formulation. The focus is thereby on small deviations from the initial steady state operating point. Also two measured examples accentuate the practical relevance of low frequency oscillations.

In **Chapter 4** the most important and most utilized damping devices are described. The focus thereby is on the classical Power System Stabilizer PSS-E and the hydro governor. The PSS-E impact on system damping is derived utilizing the Heffron-Phillips model. The impact of the hydro governor is derived, based on the extended Heffron-Phillips model.
The major aim of this section is to give an overview of the application of damping devices, as well as the introduction of the new damping device PSS-G.

Chapter 5 describes the methods, applied for the parameterization of the PSS-E and PSS-G devices. The emphasis is drawn on the analysis of relevant residues, connected to the respective oscillation modes of interest.

Chapter 6 contains the major results and scientific outcome of this thesis. The conceptual structure is based on principal investigations, utilizing a single machine infinite bus model. For more detailed and application-oriented investigations a two area, multi machine model, related to the well-known Prabha Kundur model, is used. Therein the robustness and control behavior of the PSS-G is elaborated. Furthermore the performance for low oscillation frequencies is investigated in comparison to the PSS-E and the conclusions are drawn.

3. Power System Stability, Electromechanical Oscillations and Damping

In this chapter the concept of system stability is described, as well as the nature and the different types of electromechanical oscillations in power systems are briefly illuminated. The physical background to the occurrence of oscillations and their mathematical description is also part of this chapter. Furthermore recent examples of measured oscillations and their relevance to actual system stability issues are given.

3.1. Categories of System Stability

The electric power system is a highly nonlinear and complex system with arising multidimensional coherency of different states and constantly changing environment. It is facing continuous changes in its operation point while the state variables influence each other at the same time. The ambition to keep the system in a stable operating point and maintain a safe und sustainable supply of energy at high quality is from fundamental importance. Based on the definition of the "IEEE/CIGRE Joint Task Force and Stability Terms and Definitions" power system stability can be defined as follows:

> *"Power system stability is the ability of an electric power system, for a given initial operating condition, to regain a state of operating equilibrium after being subjected to a physical disturbance, with most system variables bounded, so that practically the entire system remains intact"* [2].

This qualitative statement points out the importance of the system state before the disturbance occurs and is valid for local or inter area problems.
Due to the number of components and the complexity of an interconnected power system, the assessment of stability problems is often referred to the usage of dynamic simulation models. Depending on the investigated stability issue, the real system is modeled in the required detail. Large power systems are therefore reduced in size and optimized regarding the individual stability problem. From this point of view the fragmentation of the general definition of system stability into several categories and subcategories is essential for the optimization of the simulation model regarding the issued stability problem and hence for the success of this approach.
Figure 4 gives an overview of the categorization, provided by the IEEE/CIGRE Joint Task Force and Stability Terms and Definitions.

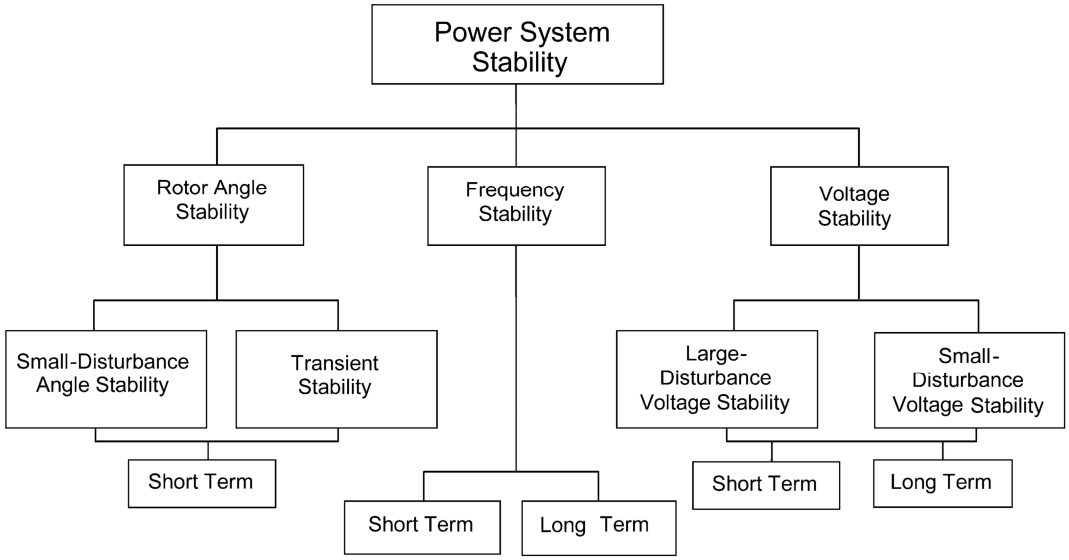

Figure 4: Categories of Power System Stability [2]

Rotor angle stability reflects the ability of the power system to refer to an operational equilibrium point and remain in synchronism after being exposed to a disturbance. It can be divided in the subcategories small signal stability (or small disturbance stability) and transient stability. Both kinds can be assigned to reflections in short term.
Frequency stability implies the ability of a power system to maintain system frequency during severe system upsets followed by a significant imbalance between generation and load and is considered in short term as well as in long term.
The third category is named voltage stability and covers the ability of a power system to retain system voltages after being exposed to a disturbance.
In the historic past the predominant number of blackouts or partial blackouts could be referred to the issue of transient stability, whereas in the last years up to the present mostly small signal stability and voltage stability issues were dominant [2].
This thesis is placed in the field of small signal stability covering the issue of oscillatory instability.

3.2. Electromechanical Oscillations in large Power Systems

3.2.1. Introduction

Electromechanical oscillations in power systems are inherent to the operation of power systems and can be referred to the characteristic of synchronous machines to exchange active power among each other at a common synchronous base frequency. Depending on the geographical expansion of the interconnected power system, this active power can, in certain areas, be transferred over thousands of kilometers, causing unwanted power losses and possibly comparatively high capacity reserves regarding the transmission grid.
System stability in this general manner is defined in [5] as the ability of a power system to remain in operation equilibrium (synchronous operation) in normal operation and after being exposed to a disturbance. Based on an initial condition the system can revert to the

same operating or any other operating point that fulfills the stability criterion after being excited by a physical disturbance.
The dynamic transition from one stable stationary operating point to another stable stationary operating point is characterized by different types of oscillations, subdivided in categories mainly depending on their oscillation frequency and amplitude.
In case of small deviations from the initial operating point, in this manner small signal stability is addressed, the rotor excursions are small enough to be able to linearize the system and assume bounded linearity. This approach is valid for a multiplicity of study cases. The distinction of different oscillation qualities can be made following [9]:

- Torsional mode oscillations
- Controller mode oscillations
- Intraplant mode oscillations
- Local plant oscillation modes and
- Inter area oscillation modes.

Severe rotor excursions from the initial stationary operating point have a nonlinear character and are constituted as transient rotor excursions in literature. The system response is thereby characterized by the nonlinear behavior of the respective system elements, in particular the nonlinear relationship between active power and rotor angle of the synchronous generators. The assessment of stability in these cases can be done analytically by solving the general swing equation or, for more complex systems, with the use of time domain simulation models. Qualitative analysis for the nonlinear case can also be accomplished by the investigation of the equal area criterion looking at the coherence between the rotor angle and the active power.
Furthermore the type of oscillation excitation can be classified in ambient oscillations due to load noise, transient oscillations and forced oscillations. In Figure 5 and Figure 6 several examples are shown.

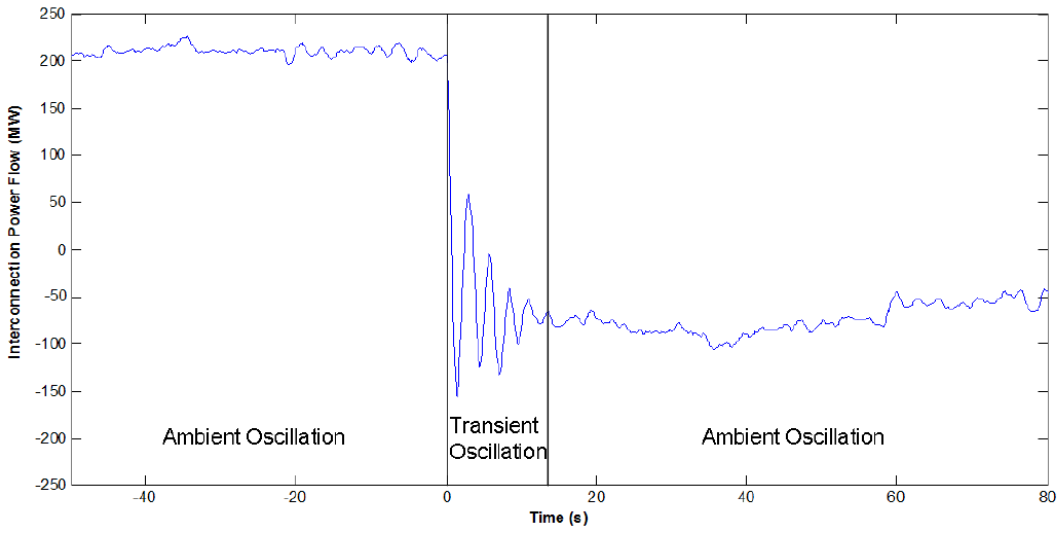

Figure 5: Example of ambient oscillations and transient oscillations, transition from one into another stable operating [26]

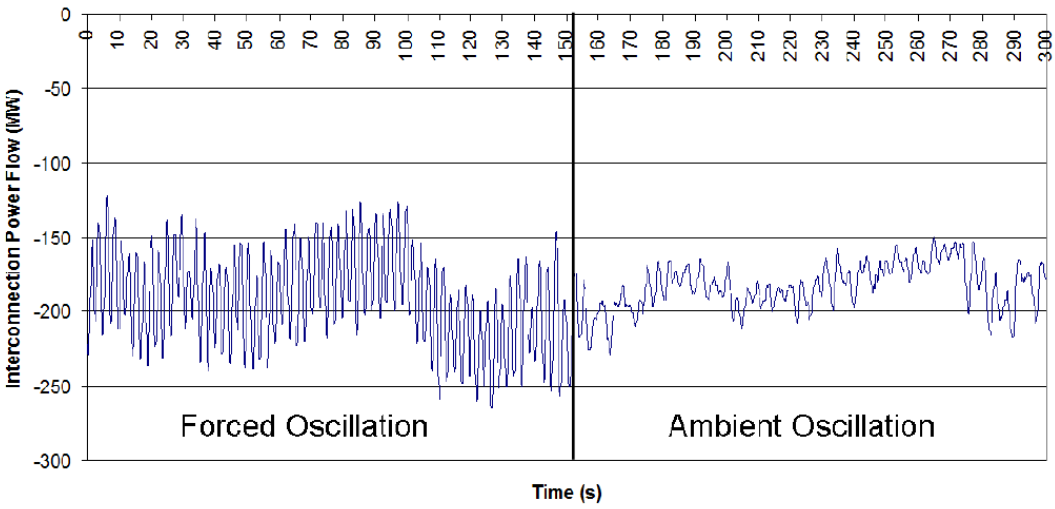

Figure 6: Example of forced oscillations and ambient oscillations [26]

Oscillations can be excited due to manifold causes, such as short circuits, load or generation losses or switching actions.
In section 3.2.2 the general nonlinear equations for the rotor motion have been illuminated.

3.2.2. **Mathematical Formulation**

The electrical power system is continuously exposed to disturbances and power imbalances. The following electromechanical oscillations of the synchronous rotors can be referred to the general swing equation, exemplary assuming a single machine swinging against an infinite power system.
For the following principal considerations (single machine infinite bus system) several assumptions have to be considered:

- Resistances of synchronous machines, transformers and lines are neglected
- The synchronous machine is modeled as an ideal voltage source behind the reactance (classical constant flux model)
- Voltages and currents are assumed to be symmetrical so that only the positive sequence system is investigated
- Deviations in speed from the rated value are small
- Mechanical damping of the generator D is set to zero

$$J \cdot \frac{d\omega_m}{dt} = T_m - T_e \qquad \textbf{3-1}$$

The inertia of the rotating masses J is including the turbine set, ω_m is the mechanical angular velocity, T_m and T_e are the mechanical and the electrical torques, respectively. The rotational masses on the left side of equation 3-1 are decelerated or accelerated if an imbalance between the mechanical and electrical torque occurs on the left side of the equation.
Transforming 3-1 in terms of per unit and electrical quantities lead to

$$\frac{2H}{\omega_r} \cdot \frac{d\omega}{dt} = P_m - P_e \qquad \textbf{3-2}$$

where ω_r is the rated angular velocity, ω is the electrical angular velocity and P_m and P_e are the active powers in per unit.
The left side of 3-2 represents the oscillation behavior of the rotating masses as a result of disturbances propagated due to an imbalance of mechanical and electrical power on the right side.
The inertia constant H is defined as

$$H = \frac{0.5 \cdot J \cdot {\omega^2}_{m,r}}{S_n} \qquad \textbf{3-3}$$

and is given in seconds. The inertia constant H is the time that elapses, when a rotor at synchronous speed is decelerated to standstill by extracting rated power $P_n = S_n$. The nominator in 3-3 is thereby the kinetic energy, stored in the rotating mass of the rotor at a certain speed.
Also used in literature is the mechanical starting time t_j as the time that is needed to accelerate the rotor from standstill to rated speed when rated mechanical torque is fed into the shaft.
The basis equation for this case is derived from 3-1:

$$J \cdot \frac{d\omega_m}{dt} = T_{m,r} \qquad \textbf{3-4}$$

$$\omega_{m,r} = \int_0^{tj} \frac{d\omega_m(t)}{dt} \cdot dt = \frac{T_{m,r}}{J} \cdot t_j \qquad \textbf{3-5}$$

$$t_j = \frac{J \cdot \omega_{m,r}}{T_{m,r}} = \frac{J \cdot {\omega_{m,r}}^2}{P_m} \qquad \textbf{3-6}$$

Comparing 3-3 and 3-6 the correlation between H and t_j is given with

$$t_j = 2 \cdot H \qquad \textbf{3-7}$$

The mechanical power P_m in 3-2 is provided by the respective governors and their actuators feeding controlled mechanical power into the generator. Depending on amplitude and the frequency of the considered oscillations this term is assumed to be

constant for the investigations of oscillatory stability. The reason are the time constants of the actuators that are usually in the range of several seconds.
Neglecting the resistance of the stator, the electrical power P_e of a salient pole synchronous generator, connected to an infinite bus, using the Park formulation[3], is given by

$$P_e = \frac{E \cdot V}{X_d} \cdot \sin(\vartheta) + \frac{V^2}{2} \cdot \left(\frac{1}{X_q} - \frac{1}{X_d}\right) \sin(2\vartheta) \qquad \textbf{3-8}$$

where E is the induced voltage, V is the terminal voltage, X_d is the synchronous reactance and ϑ is the rotor angle.

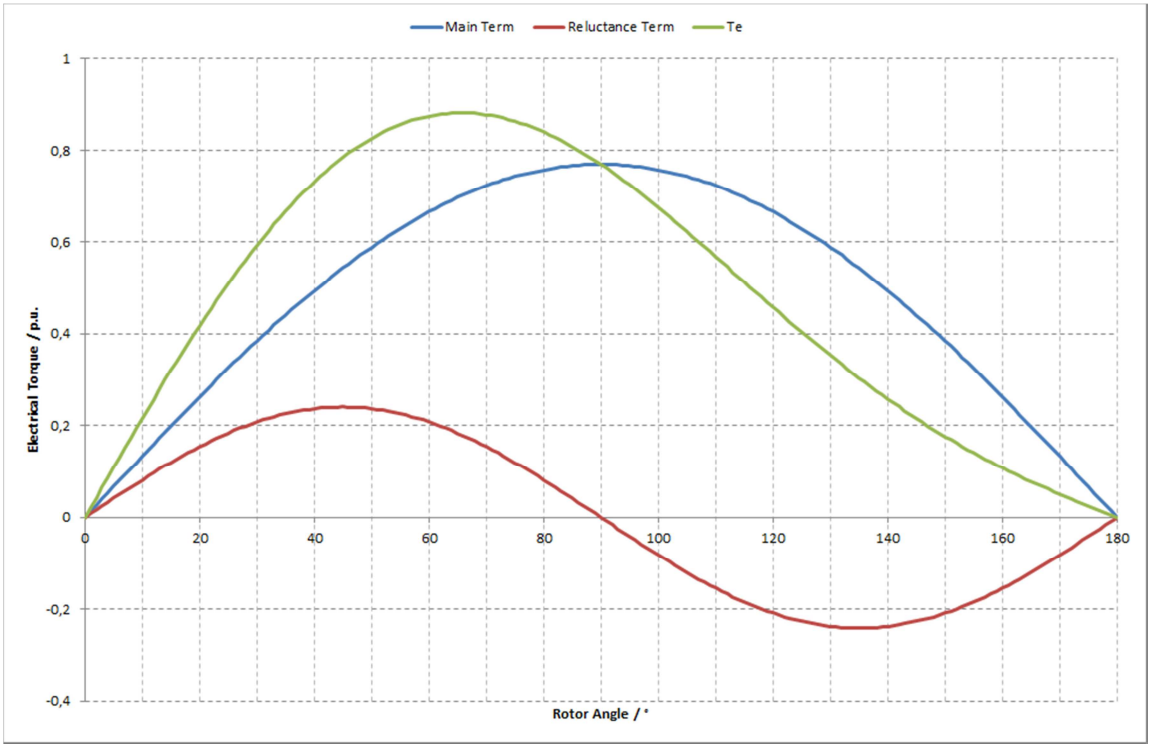

Figure 7: Illustration of the terms in 3-8, active power, the main term and the reluctance term of the power equation of a general salient pole synchronous machine, E/V = 1, X_d = 1.3p.u., X_q = 0.8p.u.

Figure 7 illustrates the main term and the reluctance term of 3-8. The reluctance term represents the power regarding an unexcited rotor that is moved by the passing rotating field of the stator windings. The reluctance term is only effectual for salient pole rotors and can contribute to stability [27].

[3] The Park transformation is a commonly used tool to transfer the three phase quantities a,b,c into a d,q,0 System (that rotates synchronously with the rotor speed) due to the use of an appropriate linear transformation. The aim is to simplify the classical formulation which implies the immanent change in self and mutual inductances due to the rotor movement. For more details see [2].

Depending on the excitation voltage and assuming the relation $X_q = (0.5 - 0.7)X_d$ for salient pole rotors, the reluctance term can be half of the value of the main term. Furthermore the resulting maximum power of P is shifted towards a lower rotor angle than 90 °.
In the case that the disturbance in torque balance leads to a relative movement of the rotor compared to the synchronously rotating field, the electrical power of the salient pole synchronous machine gets

$$P_e = \frac{E' \cdot V}{X_d{}'} \cdot \sin(\theta) + \frac{V^2}{2} \cdot \left(\frac{1}{X_q{}'} - \frac{1}{X_d{}'} \right) \sin(2\theta) + D \cdot \dot{\theta} \qquad \textbf{3-9}$$

The synchronous reactance is substituted by the transient values as well the internal voltage E is turning to E'.
The damping coefficient D gives respect to the induced currents in the excitation- and damper windings due to the relative movement of the rotor compared to the synchronous speed of the rotating stator field.

3.2.3. **Measured Examples**

In the following, two examples regarding oscillatory stability are illuminated. The first case deals with the incident on February 19th and 22nd 2011. The second case is referred to a parameterization problem of a SVC unit in the Norwegian power Grid.
These examples show the potential danger of weakly damped active power swings causing line trips (depending on the protection philosophies in different countries) and possible cascading effects and thus for the stability of the power system.

ENTSO-E Central Europe, Synchronous Power System
Two occurrences of inter oscillations in the ENTSO-E system were recorded on February 19th and 22nd 2011. The analysis of the measurement data showed frequency deviations with more than +/- 100 mHz (Figure 8) and active power oscillations with an amplitude up to +/- 150 MW on certain power lines (Figure 9). The oscillations could be allocated to a superposition of the central European east-west mode (0.18 Hz) and the north south mode (0.25 Hz) [28].

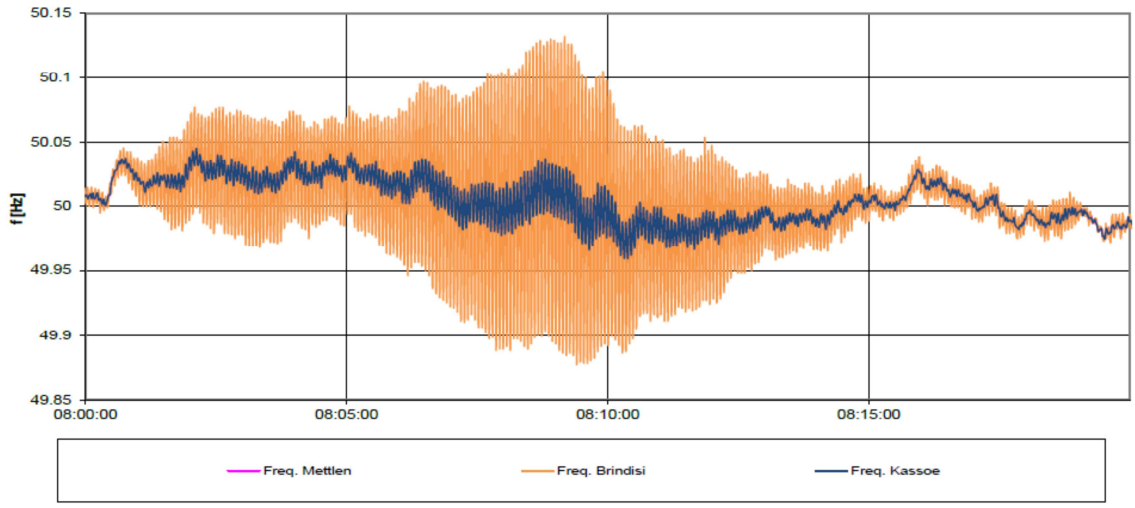

Figure 8: Frequency oscillations during the incident February 19th 2011 at the nodes in Mettlen (CH), Brindisi (IT) and Kassoe (DK) [28]

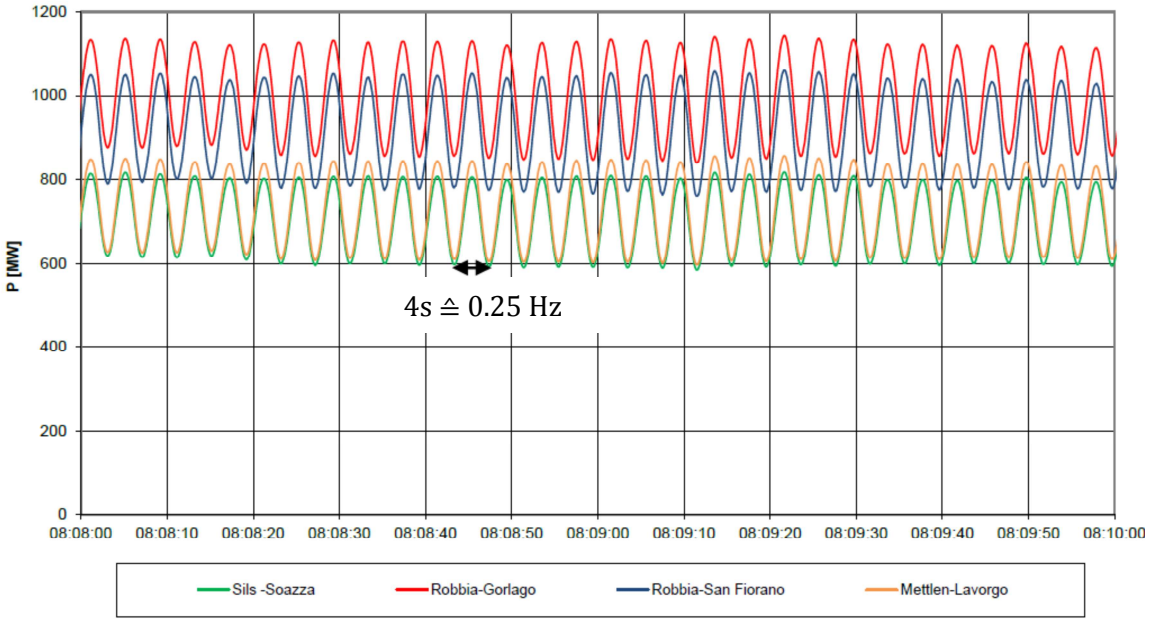

Figure 9: Active power oscillations on the border from Switzerland to Italy [28]

A more detailed description on that case is given in [28].

Nordic Power System

Figure 10 and Figure 11 show an example of the Norwegian power system. The active power oscillation is in the frequency range of 0.5 Hz. The oscillation can be seen at around 54 min in Figure 10 and lasts for about two minutes.

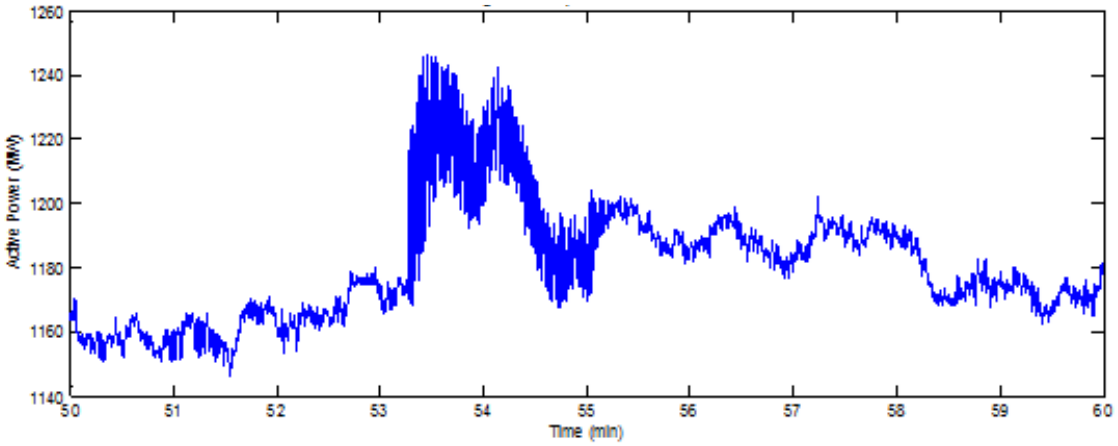

Figure 10: Active power measurements, oscillation between t=53.5 min and 55 min

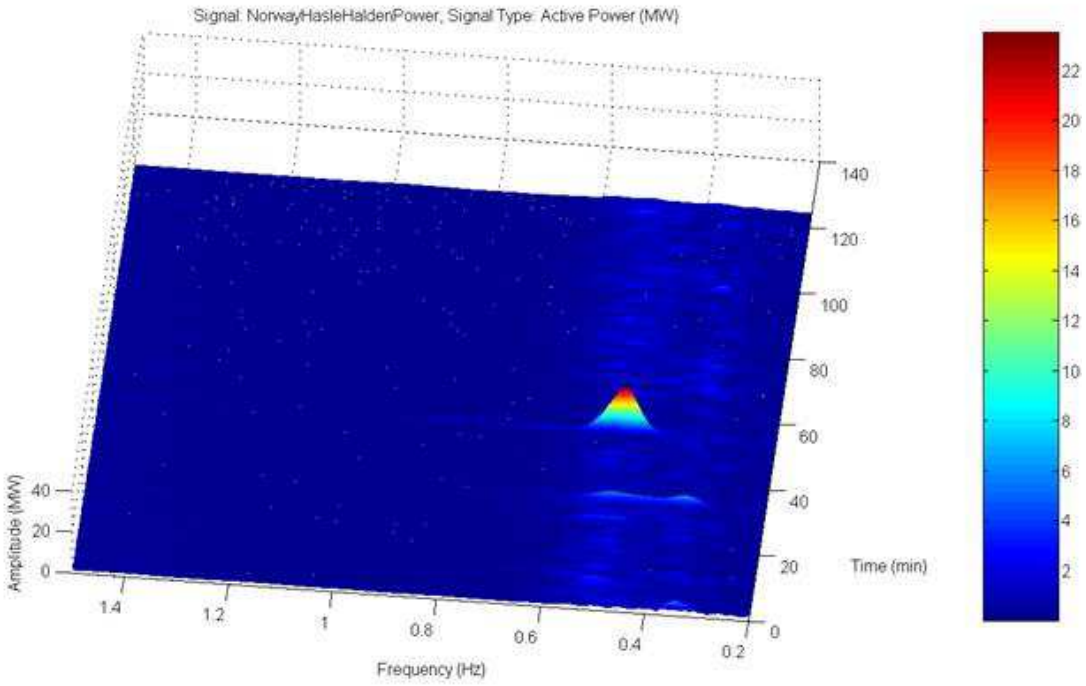

Figure 11: Oscillation amplitude as a function of frequency and time

The amplitude of this active power swing is rather high, with a value around ±40 MW on the measured power line. Although this oscillation is categorized as a forced oscillation incident by the local the exact root cause is unknown.

3.3. Small Signal Stability Analysis

The categorization of small signal stability in the field of system stability has already been given in chapter 3.1. It is defined as the ability of the system to remain in stable operation when it is exposed to small disturbances around the operating point. Therefore rotor angle

excursions of the respective synchronous machines are small and a linearization of nonlinear elements is allowed.
Instability can occur in the way that one or several synchronous machines fall out of step due to continuously increasing rotor angles in consequence of the lack of synchronizing torque. Furthermore, instabilities can occur due to increasing amplitudes of rotor oscillations in the case of missing damping torque.
For the investigations, nonlinear power systems are linearized in the operation point of interest.
The system is said to be asymptotically stable in the small, if the trajectories of the system state variables (t - > ∞) return to the original state or a finite region in the surrounding of the original state.

In this thesis only small signal stability is investigated and therefore it is described in the necessary detail.

3.3.1. **State Space Representation**

The basis is the description of the physical system due to a set of first order differential equations. Physical states are represented by an arbitrary selection of linear independent state variables in the vector **x** and can, for example, involve electrical or mechanical angles, voltages or any mathematical analogue giving information about the dynamic behavior of the system. The system states in general contain the information about the dynamic behavior of the system.
The following overview of equations is based on the more detailed descriptions of chapter 12 in [5]. Here only the substantial derivations related to the topic of this thesis are described briefly to give a solid picture of the theoretical background.

The inputs of the state space system influencing the system state are written in the input **u** vector with the number of inputs r, whereas the number of outputs of the system m is written in the output vector **y**. The vectors **f** and **c** represent a set of functions relating the system states and the input variables to the output variables. Underlying an autonomous system, e.g. a system without explicit dependency of time, the vectors and the differential equations of the physical states can be written as follows:

$$\mathbf{x} = \begin{bmatrix} x_1 \\ x_2 \\ \vdots \\ x_n \end{bmatrix} \quad \mathbf{u} = \begin{bmatrix} u_1 \\ u_2 \\ \vdots \\ u_r \end{bmatrix} \quad \mathbf{y} = \begin{bmatrix} y_1 \\ y_2 \\ \vdots \\ y_m \end{bmatrix} \quad \mathbf{f} = \begin{bmatrix} f_1 \\ f_2 \\ \vdots \\ f_n \end{bmatrix} \quad \mathbf{c} = \begin{bmatrix} c_1 \\ c_2 \\ \vdots \\ c_n \end{bmatrix} \qquad \textit{3-10}$$

$$\dot{\mathbf{x}} = \mathbf{f}(x_1, x_2, \dots x_n;\ u_1, u_2, \dots u_r) \qquad i = 1,2, \dots n$$
$$\mathbf{y} = \mathbf{c}(x_1, x_2, \dots x_n;\ u_1, u_2, \dots u_r) \qquad i = 1,2, \dots n$$

Assuming that the nonlinear equations in 3-10 are locally differentiable, the system can be linearized around the operation point of interest where the system state can be described with

$$\dot{\mathbf{x}}_0 = \mathbf{f}(\mathbf{x}_0, \mathbf{u}_0) = 0 \qquad \textit{3-11}$$

and

$$\mathbf{x} = \mathbf{x}_0 + \boldsymbol{\Delta}\mathbf{x} \qquad \mathbf{u} = \mathbf{u}_0 + \boldsymbol{\Delta}\mathbf{u} \qquad \textit{3-12}$$

The linearized system can be expressed in terms of a Taylor series expansion for the linear terms and gets

$$\begin{aligned} \boldsymbol{\Delta}\dot{\mathbf{x}} &= \mathbf{A} \cdot \boldsymbol{\Delta}\mathbf{x} + \mathbf{B} \cdot \boldsymbol{\Delta}\mathbf{u} \\ \boldsymbol{\Delta}\mathbf{y} &= \mathbf{C} \cdot \boldsymbol{\Delta}\mathbf{x} + \mathbf{D} \cdot \boldsymbol{\Delta}\mathbf{u} \end{aligned} \qquad \textit{3-13}$$

This is the well-known form of the state space representation with the system matrix **A**, the input matrix **B**, the output matrix **C** and the feedforward matrix **D**.
Applying the Laplace transformation to 3-13 the solution of the system equations in the frequency domain gets

$$\begin{aligned} \mathbf{s}\boldsymbol{\Delta}\mathbf{x}(\mathbf{s}) - \boldsymbol{\Delta}\mathbf{x}(\mathbf{0}) &= \mathbf{A} \cdot \boldsymbol{\Delta}\mathbf{x}(\mathbf{s}) + \mathbf{B} \cdot \boldsymbol{\Delta}\mathbf{u}(\mathbf{s}) \\ (\mathbf{sE} - \mathbf{A})\boldsymbol{\Delta}\mathbf{x}(\mathbf{s}) &= \mathbf{B} \cdot \boldsymbol{\Delta}\mathbf{u}(\mathbf{s}) + \boldsymbol{\Delta}\mathbf{x}(\mathbf{0}) \\ \boldsymbol{\Delta}\mathbf{x}(\mathbf{s}) &= (\mathbf{sE} - \mathbf{A})^{-1}[\mathbf{B} \cdot \boldsymbol{\Delta}\mathbf{u}(\mathbf{s}) + \boldsymbol{\Delta}\mathbf{x}(\mathbf{0})] \end{aligned} \qquad \textit{3-14}$$

$$\begin{aligned} \boldsymbol{\Delta}\mathbf{y}(\mathbf{s}) &= \mathbf{C} \cdot \boldsymbol{\Delta}\mathbf{x}(\mathbf{s}) + \mathbf{D} \cdot \boldsymbol{\Delta}\mathbf{u}(\mathbf{s}) \\ \boldsymbol{\Delta}\mathbf{y}(\mathbf{s}) &= \mathbf{C} \cdot (\mathbf{sE} - \mathbf{A})^{-1}[\mathbf{B} \cdot \boldsymbol{\Delta}\mathbf{u}(\mathbf{s}) + \boldsymbol{\Delta}\mathbf{x}(\mathbf{0})] + \mathbf{D} \cdot \boldsymbol{\Delta}\mathbf{u}(\mathbf{s}) \end{aligned} \qquad \textit{3-15}$$

Above equations lead to the conclusion that $(\mathbf{sI} - \mathbf{A})^{-1}$ imply valuable information about the dynamic behavior of the system. The poles of the expression

$$(\mathbf{sE} - \mathbf{A})^{-1} = \frac{\mathbf{adj}(\mathbf{sE} - \mathbf{A})}{\mathbf{det}(\mathbf{sE} - \mathbf{A})} \qquad \textit{3-16}$$

can be determined with

$$\mathbf{det}(\mathbf{sE} - \mathbf{A}) = \mathbf{0} \qquad \textit{3-17}$$

3-17 is called the characteristic equation and its solutions are the eigenvalues of the system state matrix **A**.

3.3.2. **Eigenproperties of the System State Matrix**

From 3-13 one can see that the derivation of each state variable depends theoretically on the linear combination of the motion of every other state variable. As mentioned above, the selection of the system state variables is not unique and therefore the basis for an analytical investigation is the decoupling of system states.

Eigenvalues and Eigenvectors

Due to a regular state transformation the original dependent set of state variables can be transferred into another set of state variables with the demand of the linear independence of the state variables.

Starting from the linearized system in equation 3-13 the indicator Δ for the small perturbation of the system can be omitted. The transformation can thus be done with

$$\mathbf{x} = \mathbf{P} \cdot \mathbf{z} \qquad \textit{3-18}$$

were $\mathbf{P}$ is a transformation matrix with definite properties.

Substituting in 3-13 gets

$$\begin{aligned} \dot{\mathbf{z}} &= \mathbf{P^{-1}} \cdot \mathbf{A} \cdot \mathbf{P} \cdot \mathbf{z} + \mathbf{P^{-1}} \cdot \mathbf{B} \cdot \mathbf{u} \\ \mathbf{y} &= \mathbf{C} \cdot \mathbf{P} \cdot \mathbf{z} + \mathbf{D} \cdot \mathbf{u} \end{aligned} \qquad \textit{3-19}$$

3-13 gets

$$\begin{aligned} \dot{\mathbf{z}} &= \mathbf{\Lambda} \cdot \mathbf{z} + \mathbf{\Theta} \cdot \mathbf{u} \\ \mathbf{y} &= \boldsymbol{\psi} \cdot \mathbf{z} + \mathbf{\Omega} \cdot \mathbf{u} \end{aligned} \qquad \textit{3-20}$$

with the demand to the new system state matrix $\boldsymbol{\Lambda}$ being a diagonal matrix of the form

$$\mathbf{P^{-1}} \cdot \mathbf{A} \cdot \mathbf{P} = \mathbf{\Lambda} = \mathbf{diag}(\lambda_i) = \begin{bmatrix} \boldsymbol{\lambda_1} & \mathbf{0} & \dots & \mathbf{0} \\ \mathbf{0} & \boldsymbol{\lambda_2} & \mathbf{0} & \vdots \\ \vdots & \mathbf{0} & \ddots & \mathbf{0} \\ \mathbf{0} & \dots & \mathbf{0} & \boldsymbol{\lambda_n} \end{bmatrix} \qquad \textit{3-21}$$

Rearranging 3-21 and looking at the columns of the transformation matrix $\mathbf{P}$ leads to

$$\mathbf{A} \cdot [\mathbf{p_1} \quad \mathbf{p_2} \quad \dots \quad \mathbf{p_n}] = [\mathbf{p_1} \quad \mathbf{p_2} \quad \dots \quad \mathbf{p_n}] \cdot \begin{bmatrix} \boldsymbol{\lambda_1} & \mathbf{0} & \dots & \mathbf{0} \\ \mathbf{0} & \boldsymbol{\lambda_2} & \mathbf{0} & \vdots \\ \vdots & \mathbf{0} & \ddots & \mathbf{0} \\ \mathbf{0} & \dots & \mathbf{0} & \boldsymbol{\lambda_n} \end{bmatrix} \qquad \textit{3-22}$$

The vectors $\mathbf{p_i}$ that fulfill above equation, are called the right eigenvectors of matrix A and imply the impact of an excited mode (according to an eigenvalue λ_i) to the system state variables. The matrix **P,** containing all eigenvectors, is called the modal matrix.
The fundamental equation for the determination of the eigenvalues and eigenvectors can be written as

$$(\boldsymbol{\lambda} \cdot \mathbf{E} - \mathbf{A}) \cdot \boldsymbol{P} = \mathbf{0} \qquad \textit{3-23}$$

And for the nontrivial solution the eigenvalues are determined by

$$\boldsymbol{det}(\boldsymbol{\lambda} \cdot \mathbf{E} - \mathbf{A}) = \mathbf{0} \qquad \textit{3-24}$$

The eigenvalues derived from 3-24 can be real or complex. Real eigenvalues represent a decaying mode, leading into aperiodic instability, if the value is positive.
Complex eigenvalues appear as conjugate pairs in the form

$$\lambda \mathrm{i} = \delta \pm \mathrm{j}\omega \qquad \textit{3-25}$$

and can be referred to an oscillatory mode, characterized by the damping ratio ζ and the oscillation frequency of the damped oscillation f.

$$\zeta = -\frac{\delta}{\sqrt{\delta^2 + \boldsymbol{\omega}^2}} \qquad \mathrm{f} = \frac{\boldsymbol{\omega}}{2 \cdot \pi} \qquad \textit{3-26}$$

The resulting decoupled system for the free motion can now be given as

$$\dot{\mathbf{z}} = \boldsymbol{\Lambda} \cdot \mathbf{z} \qquad \textit{3-27}$$

One can see that the new state variables **z,** which describe the unique dynamic state of the system, are decoupled and the solutions of the differential equations are a first order problem. The solution for the free motion of the dynamic system differential equation gets

$$\begin{aligned} \dot{z_i} &= \lambda_\mathrm{i} \cdot z_i \qquad & \mathrm{i} = 1{,}2 \ldots \mathrm{n} \\ z_i(t) &= \mathrm{e}^{\lambda \mathrm{i} \cdot \mathrm{t}} \cdot z_i(0) \qquad & \mathrm{i} = 1{,}2 \ldots \mathrm{n} \end{aligned} \qquad \textit{3-28}$$

Every complex eigenvalue λ_i is therefore corresponding to an oscillatory mode. The solution of the free motion in 3-28 leads to a damped oscillation, when the real part of the eigenvalue is negative thus in the left complex half plane. The oscillation is undamped, if the real part of an eigenvalue is zero. If the real part of the respective mode is positive the oscillation amplitude is increasing and is donated an unstable mode.
The transformed state variables can also be retransferred into the original system states. This is done by rearranging 3-18

$$\mathbf{z} = \mathbf{P^{-1}} \cdot \mathbf{x} \qquad \textit{3-29}$$

and

$$z_i(0) = Q_i \cdot x(0) \qquad \textit{3-30}$$

where $P^{-1} = Q$ is the left eigenvector of the original state matrix A.

Combining 3-18, 3-29 and 3-30 the solution of the original state variables in time domain can be given as a linear combination as

$$\Delta x_i(t) = \sum_{i=1}^{n} e^{\lambda i \cdot t} \cdot P_i \cdot Q_i \cdot \Delta x(0) \qquad \textit{3-31}$$

The solution of the original state variable x_i in time domain is a linear combination of the decoupled eigenproperties of the original state matrix A, namely the eigenvalue corresponding to a certain mode of oscillation and the respective column and row of the right and left eigenvector.
The right eigenvector p_i in 3-18 can be interpreted as the contribution of each mode (corresponding to each new state variable z_i) to a certain state variable x_i, whereas the left eigenvector q_i is consequently a measure of the contribution of a certain state variable x_i to an excited mode, represented by the transformed state variable z_i.

Participation Factors
As mentioned above, the right eigenvectors for all modes give the modal matrix thus the reaction of the state variables to a certain mode. The conclusion which state variables impose high impact on the respective mode cannot be made easily since the states are given in their respective physical units.
Therefore the participation factor matrix is developed, using the elements of the right and left eigenvectors.

$$\mathbf{F} = [\mathbf{f_1} \quad \mathbf{f_2} \quad \dots \quad \mathbf{f_n}] \qquad \mathbf{f_i} = \begin{bmatrix} f_{1i} \\ f_{2i} \\ \vdots \\ f_{ni} \end{bmatrix} = \begin{bmatrix} p_{1i} \cdot q_{i1} \\ p_{2i} \cdot q_{i2} \\ \vdots \\ p_{ni} \cdot q_{in} \end{bmatrix} \qquad \textit{3-32}$$

The result is a matrix **F** that provides a percentage of contribution of each state variable to a certain oscillation mode and vice versa.

3.3.3. **Synchronous Generators in Small Signal Analysis**

For small excursions of the rotor, relative to the synchronously rotating field, the linearized system is a sufficient approximation for the nonlinear system.

For relative movement of the rotor against the synchronous field, asynchronous torques are arising due to the induction of currents in the field windings as well as in the amortisseur windings of the rotor. These asynchronous torques in general attempt to damp oscillations.
The resulting torque is therefore differing essentially from the torque balance while the generator is operating at synchronous speed.
In the following the different torques are illuminated and their impact on the oscillation behavior is derived in principle by the use of a single machine infinite bus system.

Inter area phenomena can be assigned to small signal stability for large scale system investigations. Rotor excursions are small and can be assumed to stay within a finite region around the actual operating point. The general nonlinear equations can thus be linearized around the stationary operating point with satisfying accuracy. Consequently the handling of such problems can be done, for example, in the state space representation, described in section 3.3.1, using the advantages of the powerful and clear structured mathematical formulation.
In this chapter the principle impact of the excitation system and the classical power system stabilizer PSS-E on the generator side are illuminated.
In a first step the constant flux model with a constant ideal voltage source behind the transient generator reactance is used to derive the principle of the damping- and synchronizing torque of a synchronous generator. In the next step the influence of the change in field flux, the voltage regulator and the PSS-E is illuminated. The basis is a single generator model connected to an infinite bus system .This is, of course, not representative for large scale system, but gives a good insight, especially for the impact of the PSS-E. The following descriptions in the chapters 4.2 and 4.5 are based on the explanations in [5], p189ff.

With adequate accuracy, the following simplifications are made:

- The terms $\frac{d\Psi_d}{dt}$ and $\frac{d\Psi_q}{dt}$ in the stator voltage circuits are neglected. These terms account for the transient changes in stator voltage and can be reduced in case of slow rotor movements. Based on this assumption the steady-state, nonlinear correlations for the representation of the connected network can be used in the ordinary way.
- The deviations of the rotor speed have no effect on the stator voltages since the deviations are assumed to be small; in other words $\Delta\omega \approx \omega_r$ = 1p.u., changes in stator voltages due to deviations in speed are neglected.
- All resistances in stator and rotor circuits are neglected.
- The reluctance term for salient pole rotors is neglected for a more clearly derivation

The General Swing Equation in State Space Representation

The constant flux model is the principle model, usually used for short analysis time periods, compared to T_{d0}' of the generator. It is modeled with a constant ideal voltage source behind the transient reactance X_d'. The principle diagram is shown in Figure 12.
It is the basis for the derivation of the Heffron-Phillips model, developed by Heffron and Phillips, described in [8].

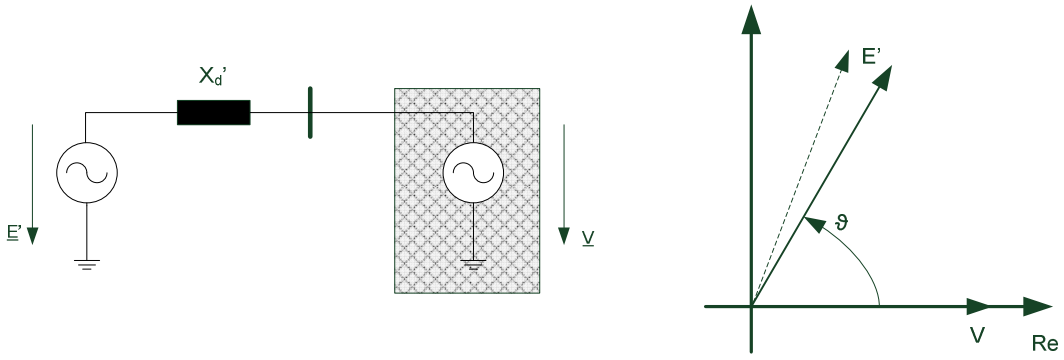

Figure 12: Constant flux model, phasor diagram of voltage angle deviation

The general swing equation with above assumptions leads to

$$2H \cdot \frac{d\omega}{dt} = T_m - T_e \qquad \textbf{3-33}$$

whereas values in per unit and neglected stator resistances as well as the relation $P_e = T_e$ is presupposed.
To derive the expression for the steady state electrical output power $P_{e,0}$ the general nonlinear equation

$$P_e = T_e = \frac{E' \cdot V}{X_d'} \cdot \sin(\vartheta) \qquad \textbf{3-34}$$

is linearized around the operation point with Taylor's expansion for the linear terms. Notating Δ for small perturbations and with $f(x_0)$ for the steady-state

$$f(x_0 + \Delta x) = f(x_0) + \frac{df(x_0)}{dx} \cdot \Delta x \qquad \textbf{3-35}$$

the electrical torque terms get

$$\Delta T_e = \frac{E' \cdot V}{X_d'} \cdot \sin(\vartheta_0) + \frac{E' \cdot V}{X_d'} \cdot \cos(\vartheta_0) \cdot \Delta\vartheta = T_{e,0} + K_{S\,\Delta Te} \cdot \Delta\vartheta \qquad \textbf{3-36}$$

Substituting in 3-33 and adding the term for the inducted damping due to the relative movement of the rotor leads to the linearized swing equation for the simplified model in Figure 12.

$$2H \cdot \frac{d\Delta\ddot{\vartheta}}{dt} = T_{m,0} + \Delta T_m - \left\{T_{e,0} + K_{S\,\Delta Te} \cdot \Delta\vartheta + D \cdot \Delta\dot{\vartheta}\right\} \qquad \textit{3-37}$$

$$T_{e,0} = \frac{E' \cdot V}{X_d{}'} \cdot \sin(\vartheta_0)$$
$$K_{S\,\Delta Te} = \frac{E' \cdot V}{X_d{}'} \cdot \cos(\vartheta_0)$$

Under the condition that $P_{m,0}$ and $P_{e,0}$ are balanced (operating point) the swing equation can be written as

$$2H \cdot \frac{d\Delta\ddot{\vartheta}}{dt} + \Delta T_m - D \cdot \Delta\dot{\vartheta} - K_{S\,\Delta Te} \cdot \Delta\vartheta = 0 \qquad \textit{3-38}$$

with

$$\frac{d\Delta\vartheta}{dt} = \Delta\omega \cdot \omega_n \qquad \textit{3-39}$$

The swing equation can be rewritten in the form of the state space representation as

$$\begin{bmatrix}\Delta\dot{\omega}\\ \Delta\dot{\vartheta}\end{bmatrix} = \begin{bmatrix}-\frac{D}{2H} & -\frac{K_{S\,\Delta Te}}{2H}\\ \omega_n & 0\end{bmatrix} \cdot \begin{bmatrix}\Delta\omega\\ \Delta\vartheta\end{bmatrix} + \begin{bmatrix}\frac{1}{2H}\\ 0\end{bmatrix} \cdot \Delta T_m \qquad \textit{3-40}$$

$K_{S\,\Delta Te}$ is the synchronizing torque and is proportional to the rotor angle ϑ. It can be seen as the gradient of the active power – angle relationship in the initial operating point at $\vartheta = \vartheta_0$. Therefore the maximum synchronizing torque appears in a no load condition. The stabilizing effect of the synchronizing torque can be referred to the ability of synchronous machines to exchange active power when one or more machines adept a change in their rotor angle. For example, the increased rotor angle of one machine causes a higher active power output, following the (linearized) nonlinear relationship of active power and rotor angle. This leads to an increased takeover of load and consequently to a decrease in rotor speed whereas other synchronous machines adept a decrease in their loading, followed by a speed up of the respective rotors until the new point of equilibrium is reached. These considerations are based on the assumptions, listed at the beginning of this chapter as well as on a constant load and on a constant mechanical power input for the consideration period.

The damping coefficient D takes into account the mechanical losses due to friction (neglected for most practical applications) as well as the impact of the armature windings and is proportional to the rotor speed deviations.
Small signal instability can thus either occur due to the lag of synchronizing torque resulting in an aperiodic drift of the rotor angle or due to the lag of damping torque resulting in oscillatory instability.

Oscillation Frequency and Damping
Substituting the system state matrix of 3-40 into 3-24, the eigenvalues of the state matrix can be derived solving

$$\det\begin{bmatrix} -\lambda - \frac{D}{2H} & -\frac{K_{S\,\Delta Te}}{2H} \\ \omega_n & -\lambda \end{bmatrix} = 0 \qquad \textbf{3-41}$$

The natural frequency f_{nat} is thus given by

$$f_{nat} = \frac{1}{2 \cdot \pi} \cdot \sqrt{\frac{K_{S\,\Delta Te} \cdot \omega_0}{2 \cdot H}} \qquad \textbf{3-42}$$

and the damping factor can be written as

$$\zeta = \frac{1}{2} \cdot \frac{D}{\sqrt{K_{S\,\Delta Te} \cdot 2 \cdot H \cdot \omega_0}} \qquad \textbf{3-43}$$

Detailed Heffron-Phillips Model
In the detailed illumination the influence of the automatic voltage regulator (AVR) and the PSS-E on the damping and the synchronizing torque component (explanations in [5] p758ff and [8]) are used as a basis. The shown K-factor representation is derived by expressing the units of the physical states in terms of defined state variables. Thus the damping and synchronizing component of each generator in the system can be directly derived from the analysis of the transfer functions from $\Delta\omega$ and $\Delta\vartheta$ to ΔT_e.
Figure 13 shows the block diagram of the expanded constant flux model from previous chapter, taking into account the changes in flux linkage, the controlled field voltage due to the action of the AVR as well the field dynamics and transducer time constants.

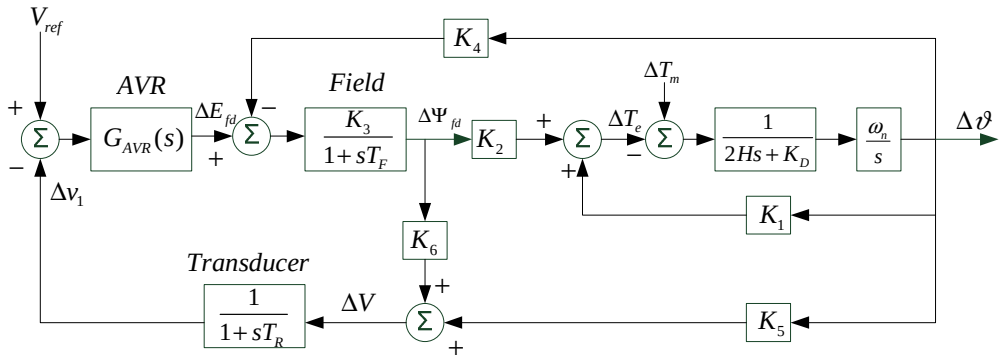

Figure 13: Block diagram of detailed system, including changes in field flux linkage variation, AVR realized as excitation system ST1A[4] in K-constant representation [5]

The damping torque coefficient from previous constant flux model is depending on the speed deviation Δω and is therefore written together with the rotor representation.
The changes in electrical torque ΔT_e can thus be influenced by various variables.

- Torque component represented by $K_1 \cdot \Delta\vartheta$ (synchronizing torque component)
- Changes in field flux linkage $\Delta\Psi_{fd} \cdot K_2$ (synchronizing and/or damping torque component)due to
  - the action of the AVR and excitation system
  - Demagnetizing effect due to the armature reaction, represented by $K_4 \cdot \Delta\vartheta$

The general equation for of the torque components, provided by the changes in field flux linkages can be written as

$$\Delta T_{e(\Delta\Psi_{fd})} = \Delta\Psi_{fd} \cdot K_2 = \pm K_S(\Delta\vartheta) \pm K_D(j\Delta\vartheta) \qquad \textbf{3-44}$$

The factors K_2, K_3, and K_6 are usually positive values, whereas the factor K_5 can be positive or negative and can thus have a significant impact on the overall synchronizing and damping torque components. The factor K_5 can provide positive or negative values depending on the generator output power and the connection impedances of the generator to the external grid.
A qualitative view of Figure 13, looking at the signs of the signals, leads to the conclusion that a positive factor K_5 provides a negative synchronizing torque component and a positive damping component.
High loadings, meaning higher values of the rotor angle of the respective generators, and high grid impedances lead to negative values of K_5 and thus to positive components of synchronizing torque and negative component of damping torque. A possibility to improve the damping behavior of the generator in such cases and to add damping to the system proportional to speed changes is the use of a PSS-E. In this matter also the AVR controller

[4] Static excitation system, for further details see [7]

gain can have a cumulative effect of the negative damping component. On the one hand it is obvious that the parameterization of the AVR should provide a good transient behavior and support the synchronizing torque, meaning a high controller gain. On the other hand for bad grid conditions and high loadings this could have a compromising effect on the damping behavior. Thus the parameterization of both, the AVR and the PSS-E need to be balanced, especially for the application in multi machine systems. In [29] a coordinated design procedure for PSS-E and AVR is developed, considering their strong coupling. The result is a near-optimal set of parameters for PSS-E and AVR for an improved small signal stability- and transient stability performance.

The factor K_4 is also positive and thus provides a negative contribution to the synchronizing torque. This effect can be referred to the demagnetizing of the armature. Compared to other positive components the impact on the overall synchronizing torque is small.

4. Description of Active and Passive Damping Devices and their Representation in Small Signal Stability Manners

This section provides a general overview of the most common damping devices with the major aim to damp inter area oscillations, classified in active or passive damping devices. The aim of this listing is to provide a round picture of commonly used damping devices and to give a detailed insight into the technical aspects of those devices that play an important role in the following investigations

4.1. Classification

Commonly used damping devices can be classified into passive and active damping devices. Passive damping devices are characterized by indirect impact on the damping without using a foreseen control signal. In contrast, active damping devices are based on a parameterized control unit acting on an adequate input signal. Some devices, like the Synchronous generator can be used as a passive damping device as well an active damping device with an activated PSS.

This chapter gives attention to commonly used damping devices and damping effects of electrical components of the grid. Besides the more detailed description of the synchronous generator in chapter 3.3.3 and the impact of the PSS-E and the PSS-G, a brief overview of other damping devices is provided.

4.2. The Classical Power System Stabilizer PSS-E

The classical power system stabilizer PSS-E is an embedded function in modern AVRs. Its purpose is to provide additional damping torque component to the system.

4.2.1. Heffron-Phillips Model

The PSS-E in Figure 14 uses the speed deviation of the rotor as an input signal and can thus provide a pure damping signal to the system, if the phase shift between $\Delta v_{PSS\text{-}E}$ and ΔTe is fully compensated.

The changes in electrical torque, derived from Figure 14, in terms of damping and synchronizing torque components are

$$\boldsymbol{\Delta T_e = \Delta \Psi_{fd} \cdot K_2 + K_1 \Delta \vartheta}$$

$$\boldsymbol{\Delta T_e = \frac{G_{PSS-E}(s) \cdot G_{AVR}(s) \cdot K_3 \cdot K_2}{1 + sT_F + K_3 \cdot K_6 \cdot G_{AVR}(s)} \cdot \Delta \omega + \left[\frac{K_2 \cdot K_3 \cdot K_5 \cdot G_{PSS-E}(s) + K_2 \cdot K_3 \cdot K_4}{1 + sT_F + K_3 \cdot K_6 \cdot G_{AVR}(s)} + K_1 \right] \cdot \Delta \vartheta}$$

4-1

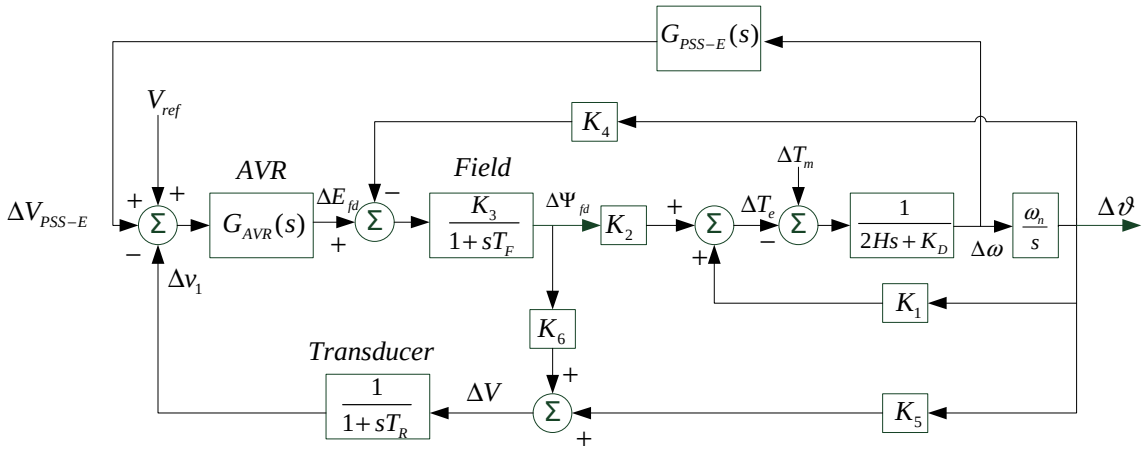

Figure 14: Block diagram of detailed system including changes in field flux linkage variation, AVR realized as excitation system ST1A[5] and the effect of the PSS-E in K-constant representation [5]

In 4-1it is obvious from that the transfer function of G_{PSS-E} ,representing the Power System Stabilizer, influences the damping term and the synchronizing term. Additionally one can see the influence of the PSS-E on the voltage regulation path, since it is multiplied with the transfer function of the voltage regulator.

Depending on the overall amplitude and phase characteristic of the damping and the synchronizing term and taking into account 3-44, the phase of the ΔT_e provided by the change in field flux linkage, can be illustrated as shown in Figure 15.

It shows the principle conditions of assuming a negative factor K_5 and therefore a positive synchronizing torque (in phase with $\Delta\vartheta$) as well as a negative damping torque (in phase with $\Delta\omega$).

Figure 15 a) shows the positive synchronizing torque component $K_S \cdot \Delta\vartheta$ and the negative damping toque component $K_D \cdot \Delta\omega$. Assuming a pure damping torque, provided by the PSS-E compensation $K_D' \cdot \Delta\omega$ the resulting change in electrical torque due to the changes in field flux linkage $\Delta T_e(\Psi_{fd})$ gets a positive damping torque component with a constant synchronizing torque component $K_S \cdot \Delta\vartheta$. In Figure 15 b) the situation at under- and overcompensation is shown.

These situations differ from the full compensation in a) due to an additive positive or negative synchronizing torque component. Therefore, in most applications a slight undercompensation due to the PSS-E is wanted, in order to achieve a positive damping torque component as well as an increased synchronizing torque component.

[5] Static excitation system, for further details see [7]

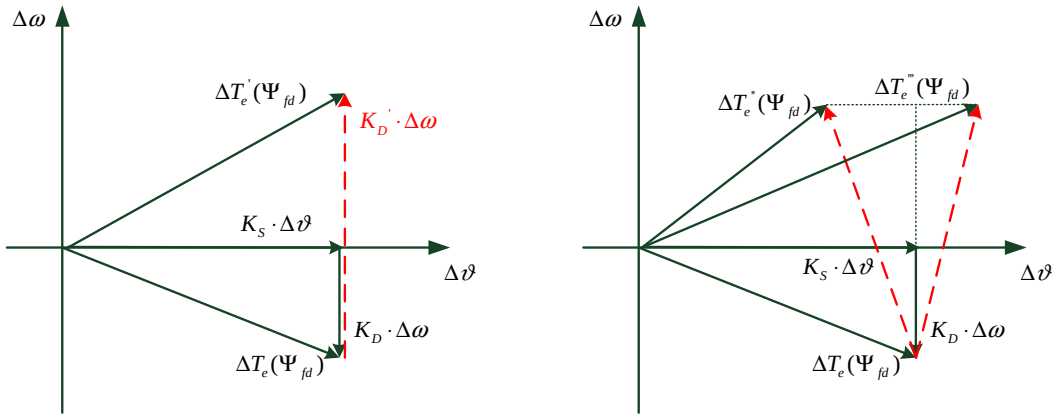

a) ***b)***

Figure 15: Full compensation of negative damping torque component resulting in $\Delta T_e^{'}(\Psi_{fd})$ ***due to*** $K_D^{'} \cdot \Delta\omega$ ***in a). Overcompensation resulting in*** $\Delta T_e^{''}(\Psi_{fd})$ ***and undercompensation resulting in*** $\Delta T_e^{'''}(\Psi_{fd})$ ***in b)***

4.2.2. **Derivation of Excitation Impact**

To derive the respective damping and synchronizing terms for any given system operating point, the constants K1-K6 need to be recalculated and set into 4-1. More practical is the calculation of the respective transfer functions from the model by defining an adequate system input and output and derive a single input single output (SISO) configuration. For any given system operating point, respectively eigenvalue of interest, the SISO transfer function delivers a real and imaginary part.

Simplifying Figure 14 by summarizing the electrical loop, the following Figure 16 is obtained. The electrical system is summarized in $G_{Electrical}(s)$, also containing the optional PSS-E, whereas an additional input from speed deviation would have to be inserted. Based on this compact illustration, the transfer functions can be analyzed and the real and imaginary parts can be converted into damping and synchronizing terms.

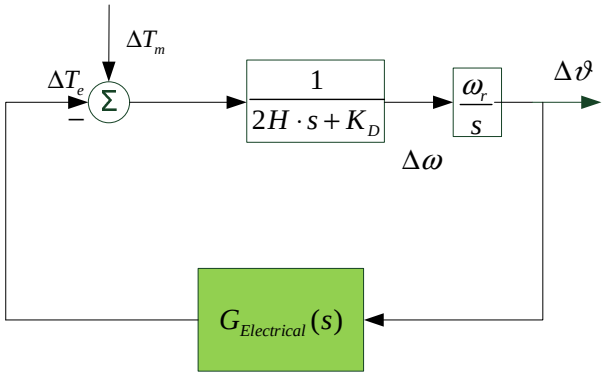

Figure 16: Summarized Heffron-Phillips model, excitation control path

For the electrical system of the generator, summarized in $G_{Electrical(s)}$, the transfer of the real and imaginary parts of the frequency response, at a certain frequency, into damping and synchronizing components, is based on the transfer function according to Figure 16 and can be written as

$$\Delta T_e = G_{Electrical}(s) \cdot \Delta\vartheta = \\ = Real\{G_{Electrical}(s)\} \cdot \Delta\vartheta + j \cdot \Delta\vartheta \cdot Imag\{G_{Electrical}(s)\} \quad \textit{4-2}$$

$$\Delta\vartheta = \frac{\omega_r}{s} \cdot \Delta\omega \quad \textit{4-3}$$

Finding a substitute for $j \cdot \Delta\vartheta$ by rearranging 4-3 gets

$$\Delta\omega = \frac{s}{\omega_r} \cdot \Delta\vartheta = \frac{Real\{\lambda\}}{\omega_r} \cdot \Delta\vartheta + j \cdot \Delta\vartheta \cdot \frac{Imag\{\lambda\}}{\omega_r} \cdot \quad \textit{4-4}$$

and hence

$$j \cdot \Delta\vartheta = \frac{\omega_r}{Imag\{\lambda\}} \cdot \Delta\omega - \frac{Real\{\lambda\}}{Imag\{\lambda\}} \cdot \Delta\vartheta \quad \textit{4-5}$$

Substituting 4-16 for the expression $j \cdot \Delta\vartheta$ in 4-2 results in

$$\Delta T_e = Real\{\Delta T_e\} \cdot \Delta\vartheta + Imag\{\Delta T_e\} \cdot \left[\frac{\omega_r}{Imag\{\lambda\}} \cdot \Delta\omega - \frac{Real\{\lambda\}}{Imag\{\lambda\}} \cdot \Delta\vartheta\right] = \quad \textit{4-6}$$
$$= \underbrace{\left[\frac{Imag\{\Delta T_e\} \cdot \omega_r}{Imag\{\lambda\}}\right]}_{K_{D\,\Delta Te}} \cdot \Delta\omega + \underbrace{\left[Real\{\Delta T_e\} - \frac{Imag\{\Delta T_e\} \cdot Real\{\lambda\}}{Imag\{\lambda\}}\right]}_{K_{S\,\Delta Te}} \cdot \Delta\vartheta$$

Applying 4-2 and 4-6 to any eigenvalue of interest, the damping and synchronizing term of the electrical transfer function of the generator can be calculated.
The damping and synchronizing torque concept, applied to the single machine model of chapter 6, is expanded to the multi machine model for the PSS-E in [30]. Based on the linearized multi machine model, the use of the respective transfer functions in Figure 17 leads to the contribution of each generator to an oscillation mode.

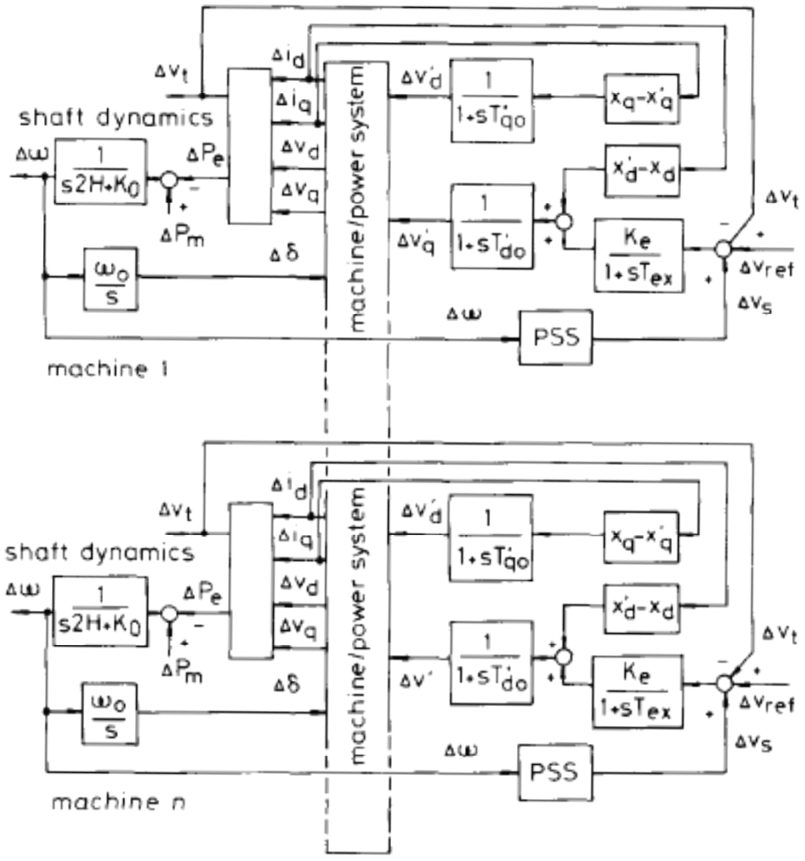

Figure 17: Linearized multi machine model, simplified shaft dynamics [30]

In Figure 17 it is obvious that the change in electrical torque due to speed deviations for generator i consists of two fractional paths, given by the path due to the rotor angle δ and the PSS-E.

$$H_{\delta ii}(s) = \left.\frac{\Delta P_{ei}(s)}{\Delta \omega_i(s)}\right|_{\delta} \qquad H_{Pii}(s) = \left.\frac{\Delta P_{ei}(s)}{\Delta \omega_i(s)}\right|_{P} \qquad \textbf{4-7}$$

Following the signal path of 4-7 in Figure 17, the relationship of the damping and synchronizing torque coefficients of the voltage and therefore the PSS-E path is also dependent on the respective network conditions. Especially for high connection impedances, the coupling of the PSS-E path and the voltage regulation is stronger resulting in a higher voltage control interference of the PSS-E.
The mutual interaction of generator i with a PSS-E active with generator j can be written as

$$H_{\omega ij}(s) = \frac{\Delta P_{ei}(s)}{\Delta \omega_j(s)} \qquad \textbf{4-8}$$

The calculation of 4-7 and 4-8, described in more detail in [30], and the subsequent conversion in terms of damping and synchronizing terms, as shown in 4-19, allows therefore the quantification of the contribution of generator i to the respective mode.
In a similar manner the transfer functions can be set up for the governor path by determination of the transfer functions. Keeping the notation from above, it leads to

$$H_{\omega ii}(s) = \left.\frac{\Delta P_{mi}(s)}{\Delta \omega_i(s)}\right|_{PSS-G} \qquad H_{\omega ii}(s) = \left.\frac{\Delta P_{mi}(s)}{\Delta \omega_i(s)}\right|_{Governor} \qquad \textbf{4-9}$$

Applying 4-6 on the real and imaginary parts of the transfer functions, at the eigenvalue of interest, result in the respective damping and synchronizing torques again.

4.2.3. **Practical Applications**

The PSS-E as a damping device has a wide spread field of applications. The operational frequency range depends on the respective target frequency and the parameterizations. Usually it is operated in the frequency range from 0.1 Hz up to 2.5 Hz, and is thus used to damping enhancement in the inter area oscillation sector as well as for higher oscillation frequencies, assigned to local oscillation phenomena or intra plant oscillations. Due to the fact that the PSS-E is operating in the voltage control path, the parameterization has to take into account the control behavior and the requests for the AVR parameters.

Inter Area Oscillations
The effect of the PSS-E action on damping inter area oscillations, using local signals, is limited due to the restrictions of the output signal, concerning allowable stator voltage deviations. Another reason is the limited observability of inter area information in local signals. Therefore so called global signals, provided by Wide Area Measurement Systems – WAMS, are fed into the PSS-E, increasing the effectiveness considerably. In the recent past many investigations on Wide Area Monitoring, Protection and Control systems (WAMPAC) have been made.

Local Oscillations
The local oscillation phenomena can be categorized in the field of small signal stability, as seen in section 3.1. In their geographical expansion they are limited to generators within a power plant or a small section of a power grid, swinging against the rest of the grid. The oscillation frequency is from 0.8 Hz up to 2.5 Hz. Manifold investigations and parameterization methods for PSS-E devices have been carried out in the past. Local oscillations are propagated due to the coupling of generators via the electrical system. As an input, local signals such as speed or electrical power are used.
In [31] for example, the IEEE-type PSS2B is parameterized to enhance the damping of a power plant mode. The oscillations are caused by changes in mechanical torques from the turbine due to vortex rope torque oscillations. The authors also take into account the electrical coupling of the generators within a plant, which is required especially for weak

couplings of the power plant to the grid. As a result, an advanced parameter set is derived to enhance the damping in the simulation model. Nevertheless, the authors mention a drawback of the PSS-E, meaning an influence on the reactive power flow due to the action of the PSS-E.

Drawbacks

Even though the PSS-E is operating via the excitation system very fast and can provide a positive impact on the damping behavior for unfavorable grid conditions and high generator connection impedances, the output of the device and thereby the impact on damping needs to be limited. The dependency of the damping behavior on the operating point of the generator and thus on the steady state rotor angle, implies that the optimal settings for a PSS-E vary with the changes in grid conditions and the operating point of the respective generator. This implies challenges for the parameterization of the PSS-E. In order to solve these problems, several robust parameterizations techniques have been developed, such as H_∞ methods, linear matrix inequalities or supervisory level power system stabilizers [32]. Optimization algorithms, addressing the immanent change in operation conditions are presented in [33].

Furthermore, looking at the block diagram in Figure 14, it is obvious that the positive impact on the damping behavior has an inverse impact on the voltage regulation. In [31] the authors also mention the propagation of reactive power imbalances due to the electrical coupling of generators.

4.3. Hydro Turbine Governor as Damping Device

4.3.1. General issues

As discussed in section 2.6, there have been several approaches applying the governor system of steam and gas turbines as a damping device.

The focus in this work is on the behavior of hydro governors and their actuators in case of low frequency oscillations. The oscillation frequency range of interest, where the investigation focuses on, is defined in the region of low oscillation frequencies where the contribution of the governor is believed to be realistic. This range is assumed to be below 1 Hz and therefore, dedicated to inter area oscillations. The limiting factor for the governor, to act as a damping device, is its actuator speed limit, depending on the respective type of hydro power plant (impulse turbine with or without deflector system, Francis turbine, Kaplan). A more detailed investigation on the governor characteristics, regarding time domain and frequency domain, is given in chapter 4.3.3 and chapter 6.3.3.

For most of the small signal stability investigations the contribution of the hydro governor, respectively the governors in general, has been neglected. This is founded in dead bands in the primary control path as well as in slow parameterized governor settings. Furthermore it has been assumed that the speed limits of the actuators restrict the movement of the governor due to low frequency oscillations.

From the authors perspective this is absolutely true for local oscillations and intraplant oscillations at frequencies around 1 Hz to 2.5 Hz.

Practical examples in the recent past have shown that the occurrence of oscillations with frequencies below 1 Hz are present and can also show weak damping behavior. Two cases with measured data have been given in chapter 3.2.3. In this frequency region the PSS-E has also shown weaknesses especially in combination with bad grid connection conditions with high connection impedances. Due to the weak coupling of the excitation and governor control path, parameterizations and changes in the control characteristic of the governor control path can be made without influencing the excitation behavior significantly.
The investigations comprise the contribution of the governor to the damping and synchronizing torque components in the basic configuration as well as in combination with the PSS-G. Structurally this is divided in investigations concerning a single machine infinite bus model and a multi machine model.
The overall aim is to give insight into the possibility of utilizing the hydro governor as damping device, acting on low frequency inter area oscillations.

4.3.2. **Approach and Derivation of Governor Impact**

The general approach is structured stepwise, starting from a small, principle simulation model to a more complex multi machine model. Principle relationships and feasibility considerations are based on a single synchronous generator connected to an infinite bus. In a four generator multi machine model interactions between two areas and the mutual interactions between control loops on inter area oscillations are illuminated.

The investigations are generally based on two pillars:

- As this work focuses on small signal stability the **linear system theory** is a compact and mathematically powerful approach to investigate a snapshot of the linearized relationships of the respective physical state variables.
- To get a full picture of the system behavior, based on the results of the linear system, **time domain simulations** are the complement of the linear investigations.

Conceptually, the approach is based on the extension of the Heffron-Phillips model for the PSS-E described in [8]. From the basic idea, the constants K1-K6 are derived by putting the system parameters in relation to the generator speed deviation and rotor angle deviation. In Figure 18, the extended Heffron-Phillips representation of the synchronous generator with PSS-E, including the governor system and the PSS-G for a single machine model, is shown.

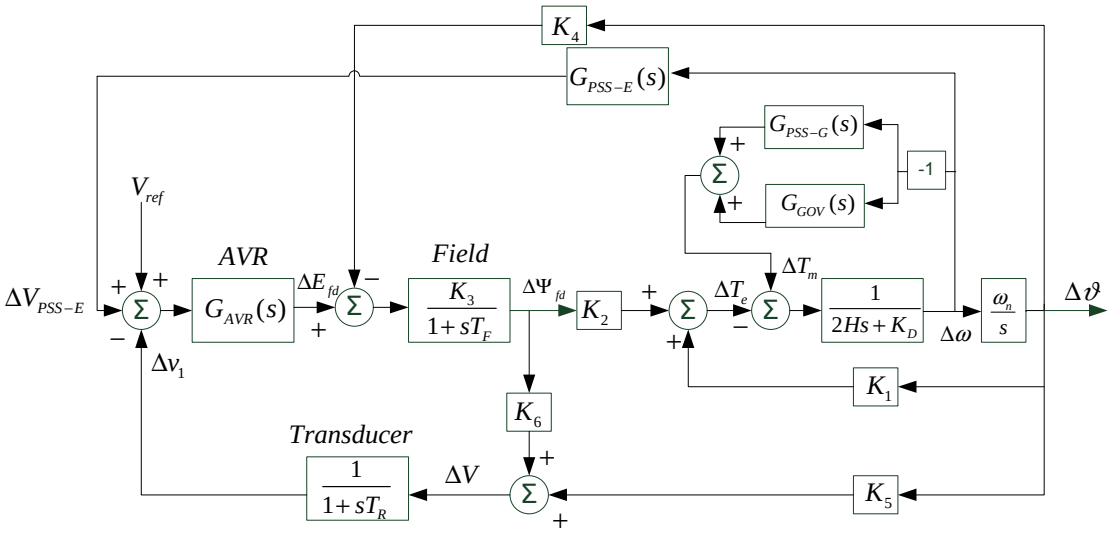

Figure 18: Block diagram of complete Heffron-Philipps model, including changes in field flux linkage variation, AVR realized as excitation system ST1A[6], the effect of the PSS-E, governor and PSS-G in K-constant representation

The input signal for the PSS-G is exemplary realized with the speed deviation. Also commonly used input signals are the accelerating power [34] or signals, provided by WAMS [35]. More detailed investigations, regarding the signal selection for the PSS-G, are given in section 6.4.2.

From Figure 18 one can see that the influence of the transfer function of the governor as well as of the PSS-G is decoupled from the voltage regulation. This is a clear advantage of the PSS-G compared to the PSS-E. The configuration in parallel to the governor system, in combination with the appropriate parameterized wash out transfer function, also implies the separation from the primary control path.

According to the settings of the single machine input system the general complex transfer function for the governor from $\Delta\omega$ to ΔT_m, assuming a general real and imaginary part (Real, Imag), gives

$$\begin{aligned}\Delta T_{m(G_{Mechanical}(s))} &= \Delta\omega \cdot G_{Mechanical}(s) \\ &= \Delta\omega \cdot (\pm Real\{G_{Mechanical}(s)\} \pm j \cdot Imag\{G_{Mechanical}(s)\}) = \\ &= \pm Real\{G_{Mechanical}(s)\} \cdot \Delta\omega \pm Imag\{G_{Mechanical}(s)\} \cdot \Delta\vartheta\end{aligned} \qquad \textbf{4-10}$$

In 4-10 one can see that for the configuration in Figure 18, similar to the considerations described for the excitation system, the governor and the PSS-G add either a positive or a negative damping and synchronizing term to the system. The control target is therefore to increase the damping torque component in the frequency range of interest.

Simplifying Figure 18 by summarizing the mechanical and the electrical loop, the following Figure 19 is obtained. The transfer function $G_{Mechanical}(s)$ contains the governor and its

[6] Static excitation system, for further details see [7]

actuators as well as the activated or deactivated PSS-G whereas the electrical system is summarized in $G_{Electrical}(s)$ also containing the optional PSS-E. Based on this compact illustration the transfer functions can be analyzed and the real and imaginary parts can be converted into damping and synchronizing terms.

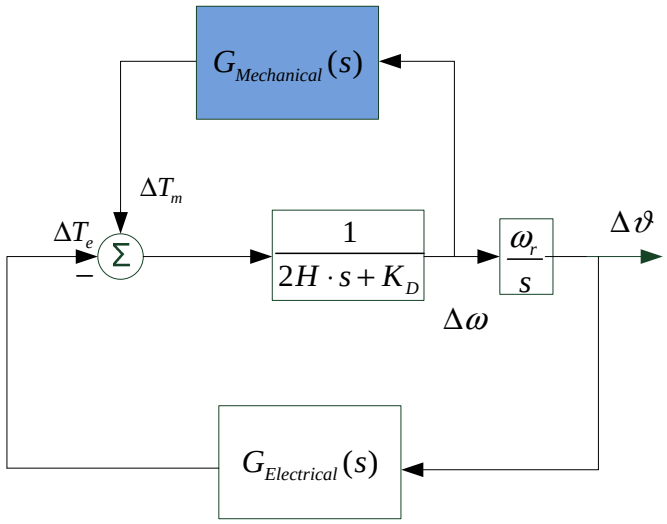

Figure 19: Summarized Heffron-Phillips model for the electrical and the mechanical control path, including PSS-E and PSS-G

The perturbation of the mechanical torque ΔT_m is a function of the mechanical system at a general frequency s and the speed deviation. Splitting $G_{Mechanical}(s)$ in real and imaginary part and following 4-10 the generalized transfer function for the mechanical system is given by

$$\Delta T_m = G_{Mechanical}(s) \cdot \Delta\omega = \\ = \text{Real}\{G_{Mechanical}(s)\} \cdot \Delta\omega + j \cdot \Delta\omega \cdot \text{Imag}\{G_{Mechanical}(s)\} \qquad \textbf{4-11}$$

The first term in phase with $\Delta\omega$ is dedicated to the damping term $K_{D\ \Delta Tm}$. The second term $j \cdot \Delta\omega \cdot$ Imag needs to be rearranged. From Figure 19 it is clear that

$$\Delta\vartheta = \frac{\omega_r}{s} \cdot \Delta\omega \qquad \textbf{4-12}$$

$$j \cdot \Delta\omega = j \cdot \frac{s \cdot \Delta\vartheta}{\omega_r} \qquad \textbf{4-13}$$

Substituting for $j \cdot \Delta\omega$ in 4-11 for an oscillatory mode given by the general eigenvalue $s = \lambda = \text{Real}\{\lambda\} + j \cdot \text{Imag}\{\lambda\}$ leads to

$$j \cdot \Delta\omega = j \cdot \frac{s \cdot \Delta\vartheta}{\omega_r} = j \cdot \frac{\text{Real}\{\lambda\} + j \cdot \text{Imag}\{\lambda\}}{\omega_r} \cdot \Delta\vartheta = \quad \textbf{4-14}$$
$$= -\frac{\text{Imag}\{\lambda\}}{\omega_r} \cdot \Delta\vartheta + \frac{\text{Real}\{\lambda\}}{\omega_r} \cdot j \cdot \Delta\vartheta.$$

Finding a substitute for $j \cdot \Delta\vartheta$ by rearranging 4-12 gets

$$\Delta\omega = \frac{s}{\omega_r} \cdot \Delta\vartheta = \frac{\text{Real}\{\lambda\}}{\omega_r} \cdot \Delta\vartheta + j \cdot \Delta\vartheta \cdot \frac{\text{Imag}\{\lambda\}}{\omega_r} \cdot, \quad \textbf{4-15}$$

and hence

$$j \cdot \Delta\vartheta = \frac{\omega_r}{\text{Imag}\{\lambda\}} \cdot \Delta\omega - \frac{\text{Real}\{\lambda\}}{\text{Imag}\{\lambda\}} \cdot \Delta\vartheta\,. \quad \textbf{4-16}$$

Substituting 4-16 in 4-14 leads to

$$j \cdot \Delta\omega = -\frac{\text{Imag}\{\lambda\}}{\omega_r} \cdot \Delta\vartheta + \frac{\text{Real}\{\lambda\}}{\omega_r} \cdot \left[\frac{\omega_r}{\text{Imag}\{\lambda\}} \cdot \Delta\omega - \frac{\text{Real}\{\lambda\}}{\text{Imag}\{\lambda\}} \cdot \Delta\vartheta\right] = \quad \textbf{4-17}$$
$$= -\left[\frac{\text{Imag}\{\lambda\}}{\omega_r} + \frac{\text{Real}\{\lambda\}^2}{\omega_r \cdot \text{Imag}\{\lambda\}}\right] \cdot \Delta\vartheta + \frac{\text{Real}\{\lambda\}}{\text{Imag}\{\lambda\}} \cdot \Delta\omega\,.$$

Substituting 4-17 into 4-11 gives the general transfers factors for the contribution of $G_{Mechanical}(s)$ to the damping torque $K_{D\,\Delta Tm}$ and synchronizing torque $K_{S\,\Delta Tm}$.

$$\Delta T_m = \text{Real}\{G_{Mechanical}(s)\} \cdot \Delta\omega - \text{Imag}\{G_{Mechanical}(s)\} \cdot \quad \textbf{4-18}$$
$$\cdot \left\{\left[\frac{\text{Imag}\{\lambda\}}{\omega_r} + \frac{\text{Re}al\{\lambda\}^2}{\omega_r \cdot \text{Imag}\{\lambda\}}\right] \cdot \Delta\vartheta + \frac{\text{Real}\{\lambda\}}{\text{Imag}\{\lambda\}} \cdot \Delta\omega\right\}$$

$$\Delta T_m = \underbrace{\left[\text{Real}\{G_{Mechanical}(s)\} + \frac{\text{Imag}\{G_{Mechanical}(s)\} \cdot \text{Real}\{\lambda\}}{\text{Imag}\{\lambda\}}\right]}_{K_{D\,\Delta Tm}} \cdot \Delta\omega - \quad \textbf{4-19}$$
$$- \underbrace{\left[\frac{\text{Imag}\{G_{Mechanical}(s)\} \cdot \text{Imag}\{\lambda\}}{\omega_r} + \frac{\text{Imag}\{G_{Mechanical}(s)\} \cdot \text{Real}\{\lambda\}^2}{\omega_r \cdot \text{Imag}\{\lambda\}}\right]}_{K_{S\,\Delta Tm}} \cdot \Delta\vartheta$$

For any given eigenvalue λ the damping torque in phase with $\Delta\omega$ and synchronizing torque component in phase with $\Delta\vartheta$ for the mechanical system can be determined.

From 4-19 and 4-6 the contributions from the mechanical system, respectively the governor system, as well as from the electrical part of the generator to the overall

damping and synchronizing torque, can be separated and thus be analyzed and compared for different oscillatory modes of interest.
For a multi machine system and using the speed deviation as an input signal, the principle considerations derived above remain unchanged. This is not valid for the PSS-E as mentioned in chapter 4.2.2.
The mutual coupling of the transfer functions for the governor path is not relevant in this regard, leading to a good basis for the local synthetisation of the governor and PSS-G settings.
Assuming that the PSS devices (PSS-E or PSS-G) on the generator i introduce a pure damping into the system, the eigenvalue shift of the target mode in the complex plain is horizontal to the left and is given by [30]

$$\Delta\lambda = \frac{\Delta K_D}{4 \cdot H_i} \qquad \textit{4-20}$$

where ΔK_D is the additional damping introduced by a PSS device. For utilization of the transfer functions in Figure 19 this means the summation of the damping torque deviations from the mechanical and the electrical transfer function resulting in ΔK_D. Applying on equation 4-20 leads to the shift of the eigenvalue of interest due to ΔK_D.

4.3.3. **Components of the Active Power Control Path and their Characteristics**

In the following the impact of the components of the governor to the phase and amplitude characteristic of the governor system is investigated.

Controller
The setpoint controller for hydro power plants is usually realized with a PID feedback controller, acting on a computed signal error. This error is calculated out of the setpoint and the respective actual governor output signals, such as accelerating power or speed difference.
For normal operation, the active power control path is operating on a signal processed by an adjustable deadband, for example +/- 10 mHz, to prevent the governor and its actuators from immanent movement.
The controller settings are adjusted to the wanted dynamic behavior of the system.

Actuators
The actuators are the connection between the controller output and the controlled unit, e.g. the hydro turbine. Depending on the type of hydro turbine and the needed detail of the simulation model, the mechanical actuators can provide different degrees of complexity.
Following [15], actuators can be subdivided in

- Mechanical
- Mechanical hydraulic
- Electromechanical

- Electrohydraulic

Impulse turbines (Pelton wheels) are usually equipped with a various number of servo motors, depending on the number of needle valves. In parallel, an actuator is used to control the deflector system which, in principal, can be controlled or regulated. Usually, the deflectors are used to rapidly reduce the mechanical torque from the generator shaft, in order to prevent the generator from high rotor speed in case of emergency situations. Additionally, they can also be controlled by a (digital) controller and thus be an element for frequency control for very fast actions. For example, during islanded operation it has been used to reproach fast controlled active power for load switching actions. The controlled deflector system can also be used as a damping device with the advantage of a weak coupling of the change in active power to the hydraulic system. Also for dual regulated reaction turbines, like Kaplan- or Francis, separate servo motors are used to independently control wicket gates and runner blades.

Frequency Domain

Concerning the phase behavior, the actuators typically introduce a phase lag behavior to the system. Depending on the actuator type, parameters and complexity the phase lag can be modeled due to the implementation of various combinations of first and second order lag blocks.

Time Domain

The actuators with their respective speed limits define the theoretical limits for the governor system to provide a damping torque. Depending on the values, the governing system is able to react on oscillations.

In Figure 20 the maximum active power change of the governing system, limited by the speed limits for different oscillation frequencies (abscissa) and various speed limits, is shown for a principal understanding. The speed limits are representing exemplary values of very fast acting actuators like deflector systems for Pelton wheels down to slow movements of, for example, Francis turbine driven governing systems with considerable vertical heights.

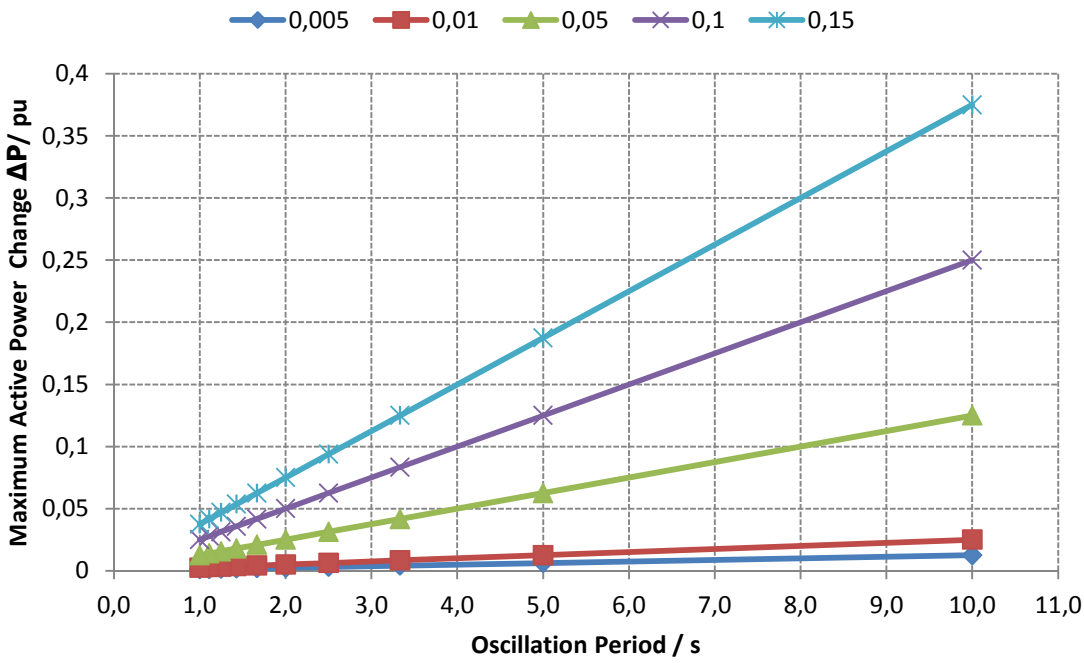

Figure 20: Theoretical potential ΔP of the governing system limited by the actuator speed for different actuator speed limits (0.005 pu/s – 0.15 pu/s), nonlinearities neglected

The maximum active power change corresponds to the theoretical active power, limited by the actuator speed during the first quarter period of the oscillation.
In this sense it is obvious that the theoretical potential of governor systems acting as a damping device is only relevant in the range of low and very low oscillation frequencies.
Furthermore the nonlinear relationship between the controller output and the actuator position is relevant to the sensitivity of the device towards small movements. Especially in lower operating points, for example during grid restoration, these nonlinearities can lead to instable behavior of the governing system. Around the rated operating point the influence is comparatively small; nevertheless the nonlinearities can be taken into account in the time domain simulations.
In most cases, such detailed information is not easily available for the evaluation of the simulation model. By measuring the controller output and the actuator positions the nonlinear relationships can be determined and implemented into the simulation model. An exemplary model is given in [36].

4.3.4. Turbines and Hydraulic Systems

The turbine and hydraulic system components, such as penstock, surge tank and reservoir, are modeled in various software representations. Depending on the aim of the study, e.g. transient stability, small signal stability, system restoration in islanded operation or water hammer effects, the model implicating the respective accuracy is used. Simplified models take into account a lossless turbine and a simplified representation of the conduct system with an inelastic water column. For more detailed investigations regarding traveling water

waves, more advanced models are used, taking into account the impact of surge tanks, conducts and turbine dynamics. According to [25] and [14] the following nonlinear models cover most of the requirements for transient stability and, after linearization, small signal stability issues:

- Simplified nonlinear model
- Nonlinear model without surge tank, inelastic water column
- Nonlinear model without surge tank, elastic water column
- Nonlinear model with surge tank, inelastic water column
- Nonlinear model with surge tank, elastic water column in penstock
- Linear turbine model, with surge tank, inelastic water column
- Linear turbine model, with surge tank, elastic water column in penstock

Following the recommendation in [14], in this work nonlinear models for small signal stability concerns are used and linearized about the operating point. Fixed time constant linear models constrain the flexibility of the analyzed model since some time constants can vary with the operating point of the generator and are therefore not implemented.
The complete block diagram for the hydraulic system relationships, including the rotor dynamics and the electrical system, is shown in Figure 21.

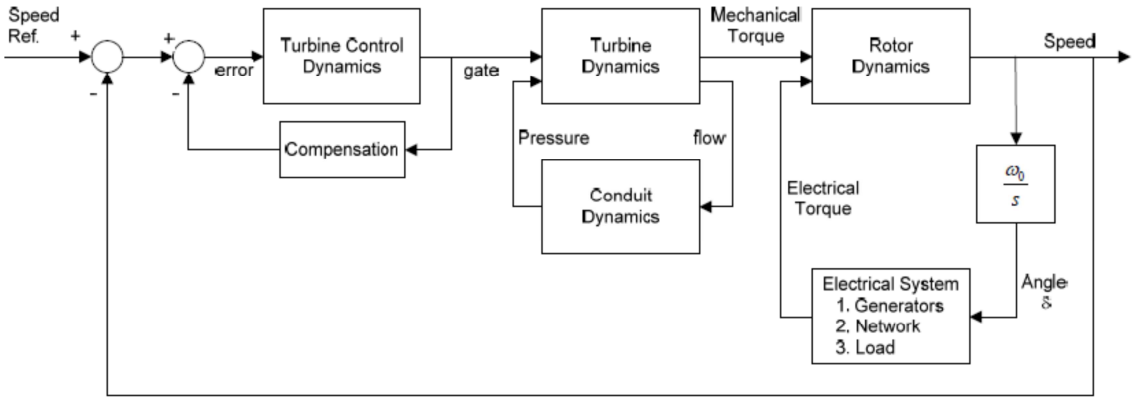

Figure 21: Block diagram of the hydraulic couplings including the mechanical and electrical components [25]

For the principal investigations, regarding the feasibility of the governor system to act as a damping device in chapters 6.3 and 6.4, the simplified nonlinear model, including a Francis turbine as shown in Figure 22, is used.

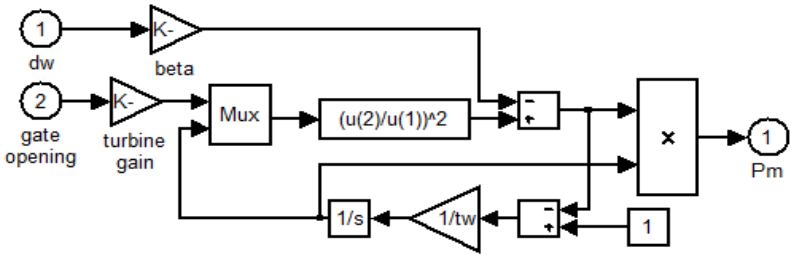

Figure 22: Simplified nonlinear model of Francis-turbine, non-elastic water column, turbine damping beta, water starting time t_w, mechanical output power P_m, [14]

The level of detail of the hydraulic system, shown in Figure 22, is stepwise expanded, implementing the impact of the surge tank and the elastic water column, representing the traveling water waves.

The hydraulic models without surge tank are shown in Figure 22, Figure 23 and Figure 24, whereas the models with surge tank are pictured in Figure 25 and Figure 26.

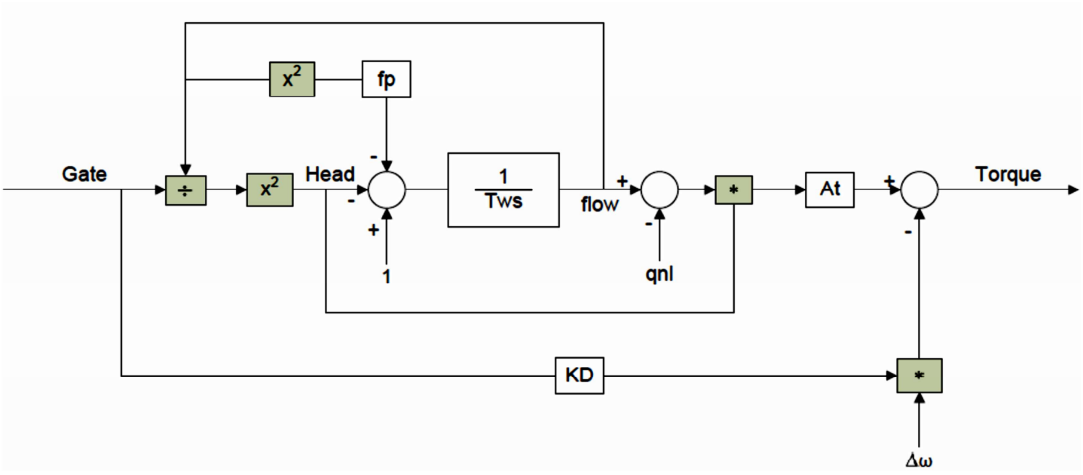

Figure 23: Nonlinear turbine model, without surge tank, inelastic water column [25]

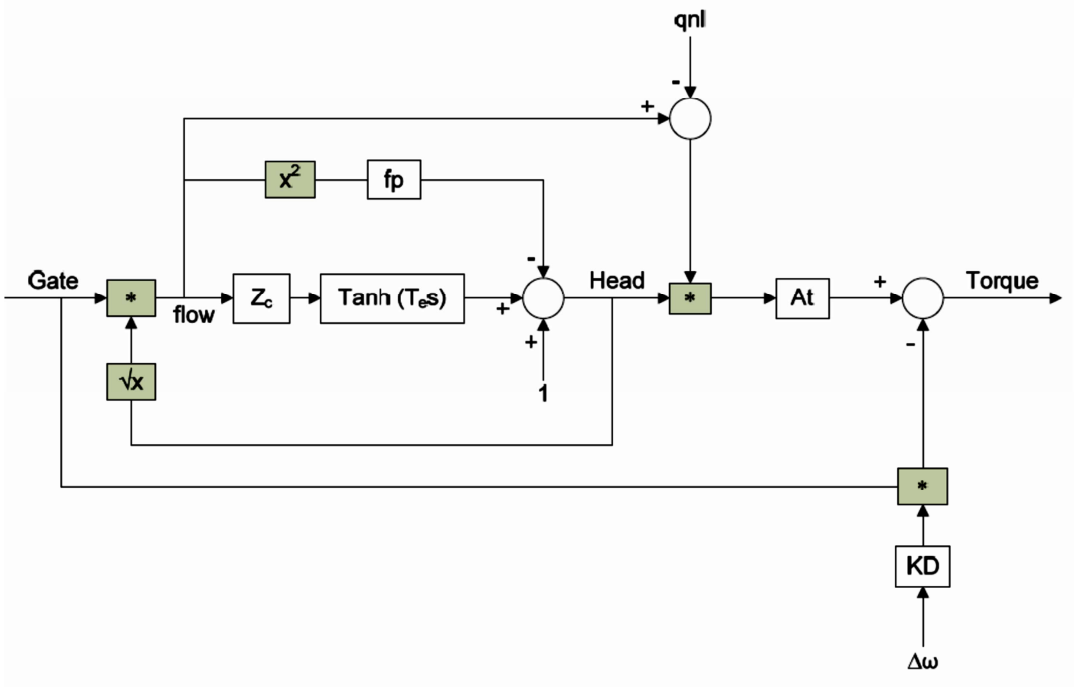

Figure 24: Nonlinear turbine model without surge tank, elastic water column [25]

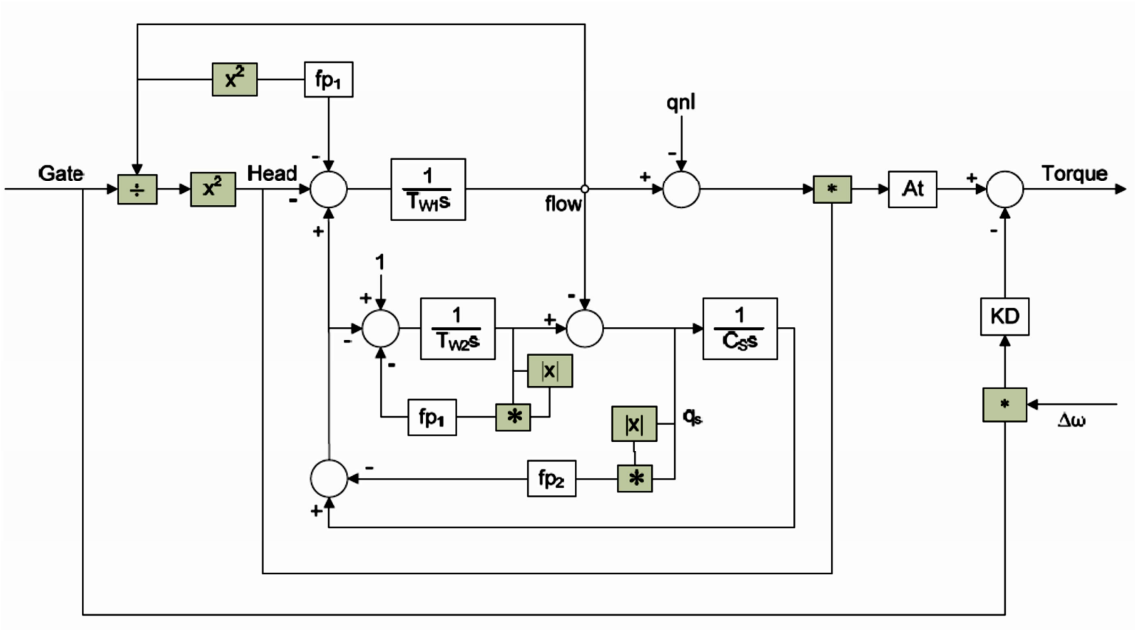

Figure 25: Nonlinear turbine model, with surge tank, inelastic water column [25]

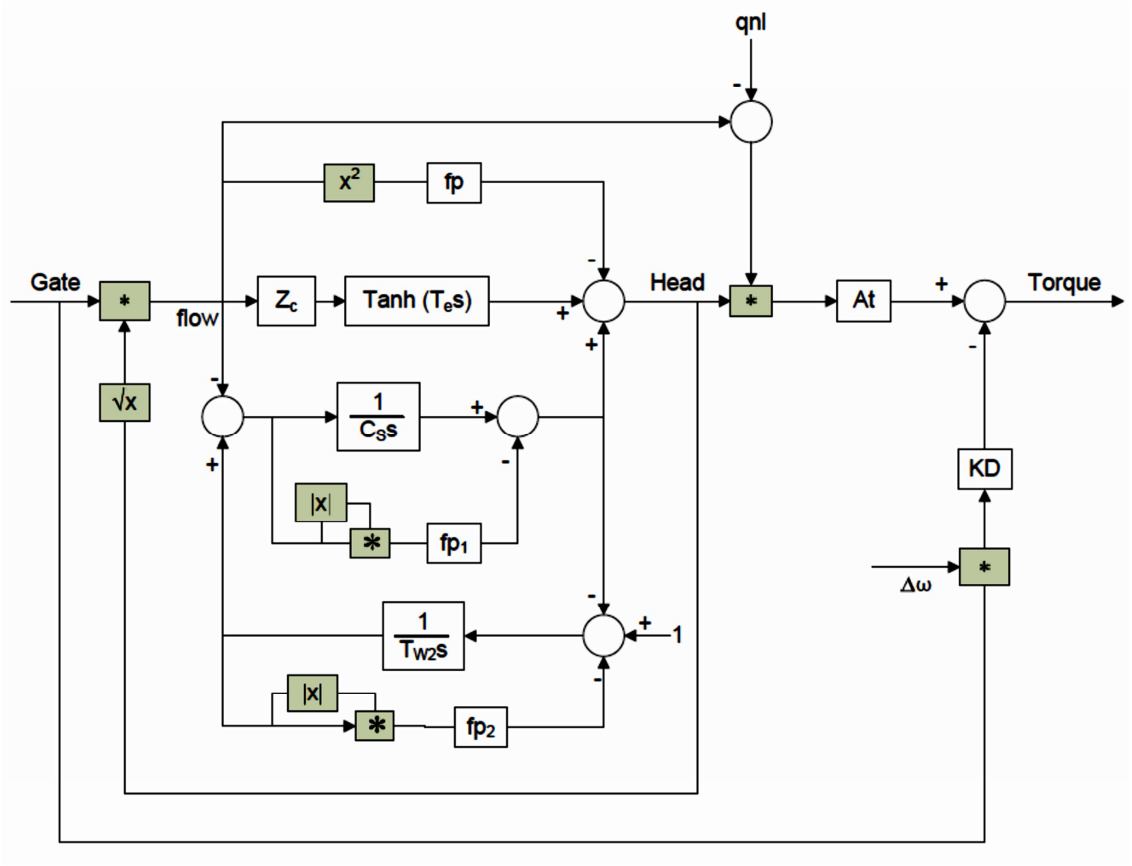

Figure 26: Nonlinear turbine model, with surge tank, elastic water column [25]

For stability studies, the factor for turbine damping is represented by a factor, proportional to the speed deviation (beta in Figure 22, KD in Figure 23 until Figure 26). The value is given in terms of per unit and is between 0.5 and 2 for hydraulic turbines [37].

Turbine damping is proportional to the speed deviation of the rotor shaft from the steady state rated sped. For small signal stability analysis, the impact of hydro turbine damping is thus commonly neglected. The reason is the small deviation of the turbine-generator unit from the rated speed. Transient stability studies, characterized by locally great excursions from the rated speed, the factor for turbine damping is taken into account, depending on the respective type of hydro power plant.

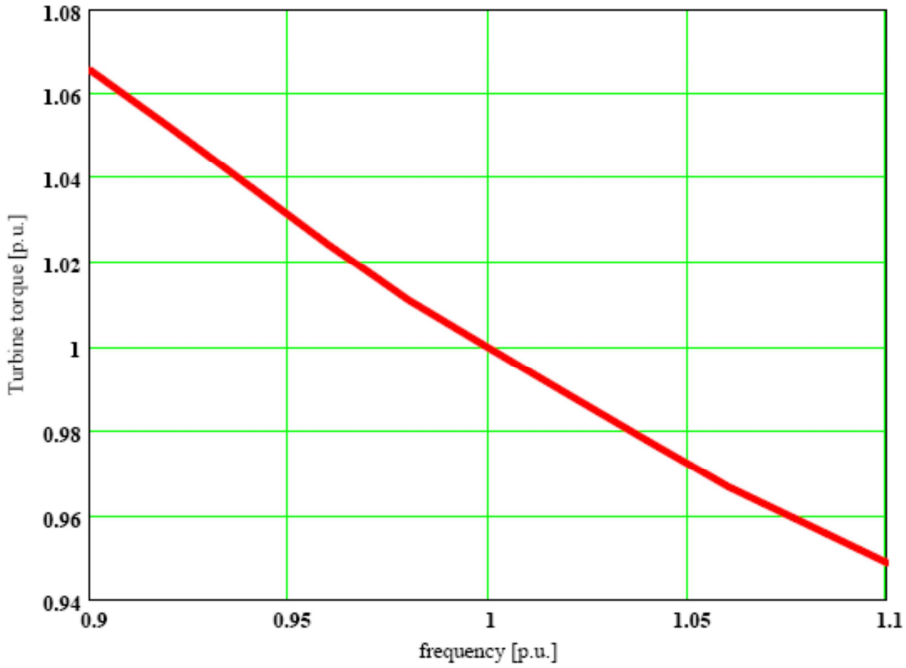

Figure 27: Exemplary torque-speed characteristic of a hydro turbine [37]

In [37] turbine damping of hydro turbines is described as the gradient of the characteristic speed-torque curve of the turbine, shown in Figure 27.

4.4. Amortisseurs

In case that the disturbance in torque balance leads to a relative movement of the rotor compared to the synchronously rotating field, the electrical power of the salient pole synchronous machine gets

$$P_e = \frac{E' \cdot V}{X_d'} \cdot \sin(\theta) + \frac{V^2}{2} \cdot \left(\frac{1}{X_q'} - \frac{1}{X_d'}\right) \sin(2\theta) + D \cdot \dot{\theta} \,. \qquad \textbf{4-21}$$

The synchronous reactance is substituted by the transient values as well the internal voltage E is turning to E'.
The damping coefficient D gives respect to the mechanical losses of the rotor movement and predominately to the induced currents in the amortisseur windings due to relative movement of the rotor compared to the synchronous speed of the rotating stator field. Usually the mechanical losses are accounted to friction and are neglected for most practical considerations.
Following the explanations in [38], the damping power P_D is introduced and can also be written as:

$$P_D = D \cdot \dot{\theta} \,. \qquad \textbf{4-22}$$

The amortisseur windings provide a similar effect as the short-circuit cage in an induction motor. Relative rotor movements to the synchronous circulating field induce currents, which try to restore the synchronous speed. Thus the resulting torque component is given as asynchronous torque. The base of the action of force is Lenz's law.
In principal, amortisseur windings can be mounted in direct or quadrature axis or in direct axis only. The equivalent circuit for the synchronous machine, operating as an induction machine on an infinite bus system, is shown in Figure 28.

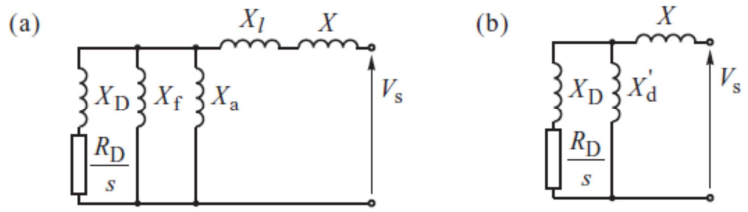

Figure 28: The equivalent circuit of the synchronous generator operating as an induction machine: (a) with leakage reactances included; (b) with leakage reactances neglected [38]

Following the derivations in [38] and Figure 28, the damping power P_D is given by

$$P_D = {I_D}^2 \cdot \frac{R_D}{s}. \qquad \textbf{4-23}$$

For small values of rotor deviations $\frac{R_D}{s}$ is large and I_D can be derived by the series connection of X and X_d', treated as a voltage divider.
Thus the current in the amortisseur windings can be written as

$${I_D}^2 \cong {V_s}^2 \cdot \left(\frac{X_d{}'}{X + X_d{}'}\right)^2 \cdot \frac{1}{\left(\frac{R_D}{s}\right)^2 + X_D^2} \qquad \textbf{4-24}$$

From Figure 28 the amortisseur winding leakage reactance is simplified given by

$$X_D \cong \frac{X_d{}' \cdot X_d{}''}{X_d' - X_d{}''}, \qquad \textbf{4-25}$$

where $X_d'' \cong \frac{1}{X_f + X_a + X_D}$.

For the expression $\frac{R_D}{s}$ to substitute in 4-23, the subtransient time constant $T_d'' = \frac{X_D}{\omega_s \cdot R_D}$ is rearranged using 4-25.

$$\frac{R_D}{s} = \frac{X_d{}' \cdot X_d{}''}{X_d' - X_d{}''} \cdot \frac{1}{T_d'' \cdot \omega_s \cdot s} \qquad \textbf{4-26}$$

Equation 4-23 turns into

$$P_D \cong {V_s}^2 \cdot \frac{X'_d - X''_d}{\left(X \quad + {X_d}'\right)^2} \cdot \frac{X'_d}{X''_d} \cdot \frac{T''_d \cdot \omega_s \cdot s}{1 + \left(T''_d \cdot \omega_s \cdot s\right)^2}. \qquad \textbf{4-27}$$

For salient pole synchronous machines similar considerations can be applied for the quadrature axis. The resulting damping power for small speed deviations ($s = \frac{\Delta\omega}{\omega_s} \ll 1$, neglecting $(T''_d \cdot \omega_s \cdot s)^2$ and $V_d = -V_s \cdot \sin\theta, V_q = V_s \cdot \cos\theta$) in equation 4-27 gets

$$P_D = {V_s}^2 \cdot \left[\frac{X'_d - X''_d}{\left(X \quad + {X_d}'\right)^2} \cdot \frac{X'_d}{X''_d} \cdot T''_d \cdot sin^2\theta + \frac{X'_q - X''_q}{\left(X \quad + {X_q}'\right)^2} \cdot \frac{X'_q}{X''_q} \cdot T''_q \cdot cos^2\theta \right] \cdot \Delta\omega \,. \qquad \textbf{4-28}$$

For large rotor angels θ, the damping in direct axis is therefore strongest, whereas for small rotor angles the damping is strongest on quadrature axis. From 4-28 it can also be seen that the grid connection impedance X has a significant impact on both damping axis, as it is squared in the denominator. For increasing connection impedances, the damping power P_D and thus the damping effect of the amortisseur windings is decreasing.
For large rotor excursions the damping contributions in both axes reach a critical maximum which will most likely be not the same (see Figure 29).

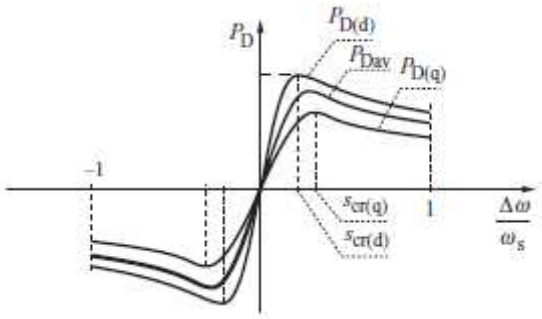

Figure 29: Average value of the damping power as a function of speed deviation [38]

Another possible derivation and comparison to other commonly used damping factors, representing the impact amortisseur windings in various simulation models, is given in [39].

4.5. Doubly Fed Induction Generator

The role of doubly fed induction machines (DFIG) to damp low frequency oscillations is under of investigations in industry and academia at that time.

Their numbers and especially rated powers for pump storage hydro power plants increased continuously in the last years. Large scale plants with rated active powers of 300 MW, like in Goldisthal, Germany are predominately installed because of their economic advantages of variable speed and convertor sizing. Rated powers up to 500 MVA with a speed range of ±10 %, corresponding to a power variation of ±30 %, are seen to be the maximum unit power at the present. Besides this, the advantage of variable speed DFIM features a set of beneficial characteristics, regarding power grid control and stability. In [40] the major advantages of DFIM, such as instantaneous active and reactive power control and non-oscillatory behavior in case of transient failures are issued based on simulations. Other expected benefits of the DFIM by using adjustable speed pumped storage plans are listed in [41]. An enhancement of grid stability by the additional contribution to small signal stability and other fields of grid stability are achieved due to the utilization of multilevel GTO converters. However, the quantification in terms of investment compared to conventional synchronous machines is still in evaluation in academia and industry. The most attractive feature regarding small signal stability is the ability inject or absorb energy with the rotating masses by varying the introduced rotor frequency [42]

Furthermore, the number of installed DFIM has increased due to the massive implementation in wind turbines. As the total amount of installed capacity grew to a significant range, many efforts have been undertaken to further improve the stability characteristics of DFIM regarding the grid inertia. In [43] possible negative effects of increased wind generation on the oscillation damping on the overall grid behavior has been shown based on case studies. A modal analysis investigation based on several DFIM dynamic models has been proposed in [44].

4.6. Load

The dynamic characteristic of the load can have a significant impact on power system stability and can result in small signal instability [4]. The author investigates root loci of mechanical oscillation modes at varying time constants of the dynamic load model. The dynamic modeling of loads is mostly determined by the emulation of motors. This is based on the penetration of motors in the overall energy consumed by loads of 60 to 70 % [5].

4.7. FACTS

Besides the application of generator side PSS-E, the application of PSS controllers on FACTS devices, have experienced great attention as well. The advantage of such oscillation damping devices is the flexible location, providing a high controllability of the mode of concern. Combined with signals with a high observability, e.g. allocated by WAMS, promising results have been carried out in simulations in [44]and [9]. Nevertheless, there

is still a demand for research, regarding the mutual interaction of PSS devices with different control targets, retrieving great risk of severe system upsets.
Many FACTS devices, like SVCs, have been introduced not only as a voltage and reactive power control device but also as a damping control device. Although their geographical flexibility is a great advantage, any additional device in the power grid is afflicted with certain reliability. Besides this, the optimum of the control action of one or more FACTS devices in one region does not automatically mean the optimum for FACTS operating in several interconnected regions of the system. Therefore the interaction of multiple FACTS damping controllers is still of concern in academia and industry.

5. Parameterization Methods of PSS-E and PSS-G

To investigate the impact of the governor and excitation control path on the damping behavior of the system to a certain mode of interest, different method-based parameterizations are used.
For the calculation of the PSS-G parameters bode diagrams as well as the residue method are applied, for the PSS-E parameters the residue method, as well as two standard parameterizations of the PSS-E (Kundur parameterization, Simulink-Multiband parameterization).
In the following, the different standard parameterizations are discussed and the parameterization methods are described.

5.1. Standard Parameter Sets

Two generic parameterizations PSS-E setups, using the speed deviation as input signal, are used in the simulations as a reference. One setup is taken from the common Kundur model and the other one is a multiband stabilizer with recommended parameters.

5.1.1. **Kundur**

The Kundur parameterization is a generic standard parameterization for system stability studies, especially for the investigation of low frequency inter area oscillations [5]. Table 1 contains the parameters for the compensator.

K	T_s	T_w	$T_{lead(1)}$	$T_{lag(1)}$	$T_{lead(2)}$	$T_{lag(2)}$	V_{min}/V_{max}
p.u.	s	s	s	s	s	s	p.u.
20	0.01	10	0.05	0.02	3	5.4	-0.15/0.15

Table 1: Parameters of the Kundur-type; K Gain, T_s transducer time constant, T_w wash-out time constant, T_{lead} lead time constant, T_{lag} lag time constant, $V_{min/max}$ output limits [5]

In Figure 30 one can see that the magnitude plot is kept flat in the frequency range from 0.1 Hz to 1 Hz. In the area of low frequencies below 0.05 Hz, the DC rejection due to the wash out function is weak. This attribute could have an unwanted effect on the voltage regulation behavior of the excitation system in case of reference voltage changes. The phase shape is kept flat in the range of 0.1 Hz to 1 Hz region as well as the low frequency shaping provides sufficient lead behavior.
This characteristic describes the Kundur parameterization as generic power system stabilizer with wide application spectrum.

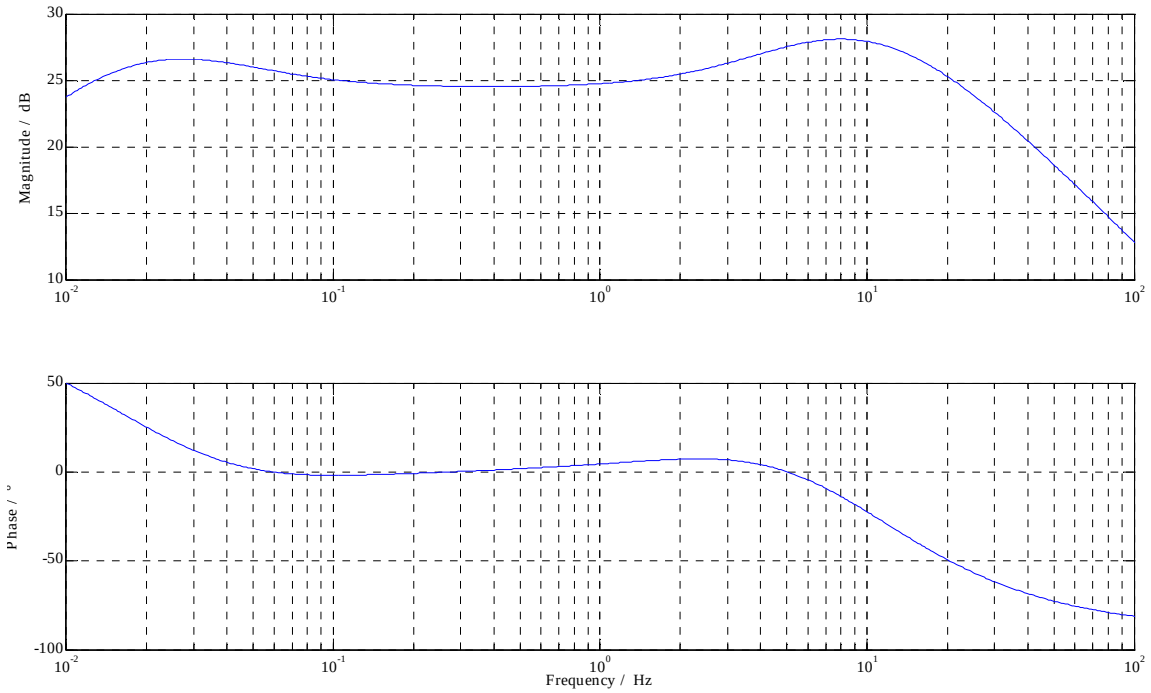

Figure 30: Bode plot of the Kundur type

5.1.2. **Multiband**

The Multiband PSS structure and parameters are based on the IEEE Std 421.5™-2005 [7]. The conceptual representation implies three center frequencies. The low-, intermediate- and high frequency range.

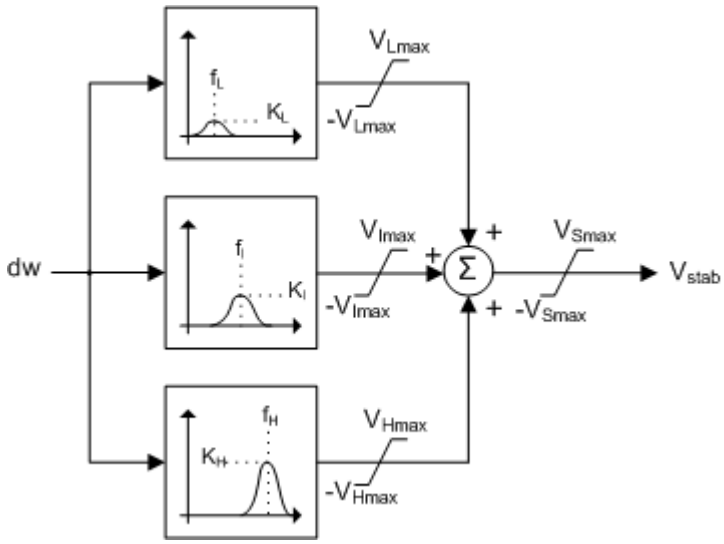

Figure 31: Conceptual representation of the Multiband PSS; f_L f_I f_H low, intermediate and high range center frequency, K_L K_I K_H low, intermediate and high peak gain, V_{xmax} band- and controller limitations, d_w rotor speed deviation, V_{stab} stabilizing signal to voltage regulator

Figure 31 gives an overview of the principal block diagram. The three frequency ranges are defined by the respective center frequency and peak gain.

Band	K	CF	V_{Lmax}	V_{Imax}	V_{Hmax}	V_{Smax}
	p.u.	Hz	p.u.	p.u.	p.u.	p.u.
Low Frequency	7.5	0.07	0.075	0.6	0.6	0.15
Intermediate Frequency	30	0.7				
High Frequency	120	8				

Table 2: Parameters of Standard Multiband PSS [7]; K gain, CF center frequency, V_{Lmax} output limit low frequency, V_{Imax} output limit intermediate frequency, V_{Hmax} output limit high frequency, V_{Smax} output limit stabilizer

Figure 32 shows the magnitude and phase plot. The global shaping performs the specification of a moderate phase advance up to 4 Hz.

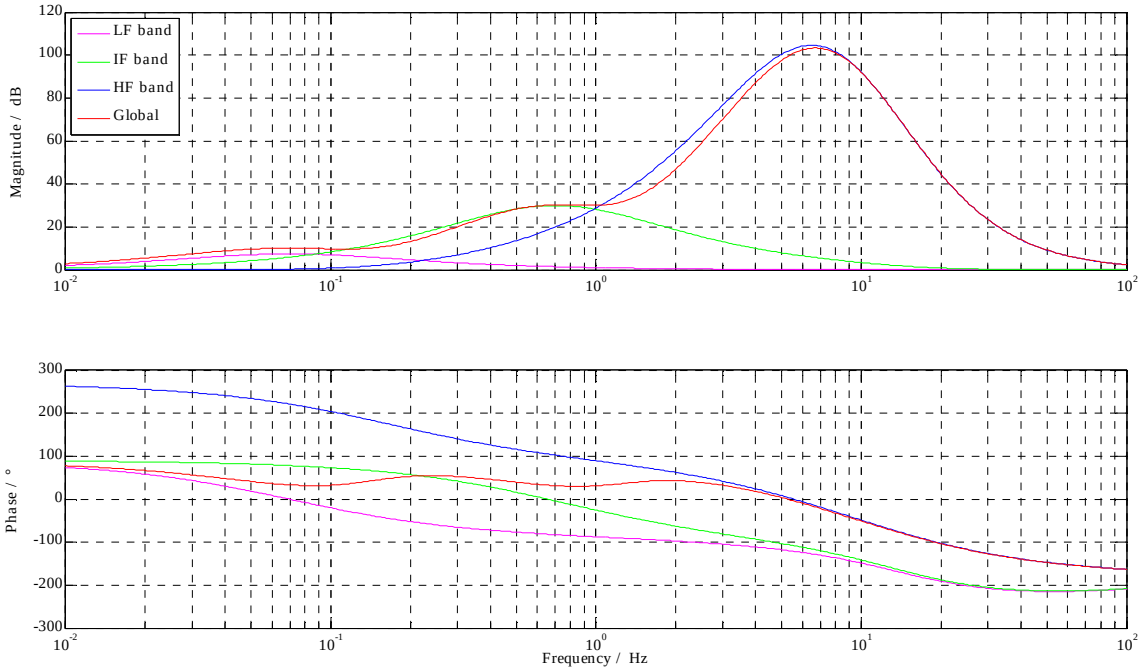

Figure 32: Bode plot of a Standard Multiband PSS

5.2. Bode Plots

In order to achieve a damping effect of the governor, in the event of low frequency oscillations, phase opposition between the input signal $\Delta\omega$ and the output signal P_m of the governor is required. For the PSS-E the control target is to achieve an output signal in phase with the rotor speed deviation $\Delta\omega$. Due to the characteristic of the respective elements of the governor or excitation system a phase lag between the input and output signal occurs, depending on the signal frequency.

In Figure 33 the principal conditions for the determination of an adequate phase compensation for the governor control path is shown.

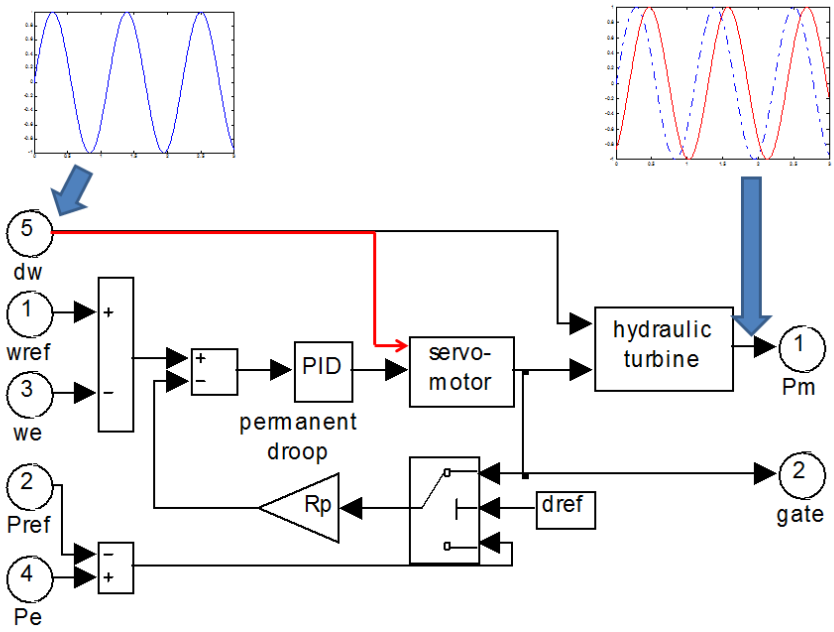

Figure 33: Principle schema of the phase shift between input d_w (blue) and output P_m of the governor (red)

The determination of the phase difference between the input and output variables is done via the analysis of the bode plots of the open-loop transfer function from $\Delta\omega$ to P_m. Looking at Figure 34, the phase difference needed for the compensator design can be directly retrieved for the target frequency of the respective electromechanical oscillation mode.

The phase shift is compensated subsequently by inserting a suitable lead/lag compensator.

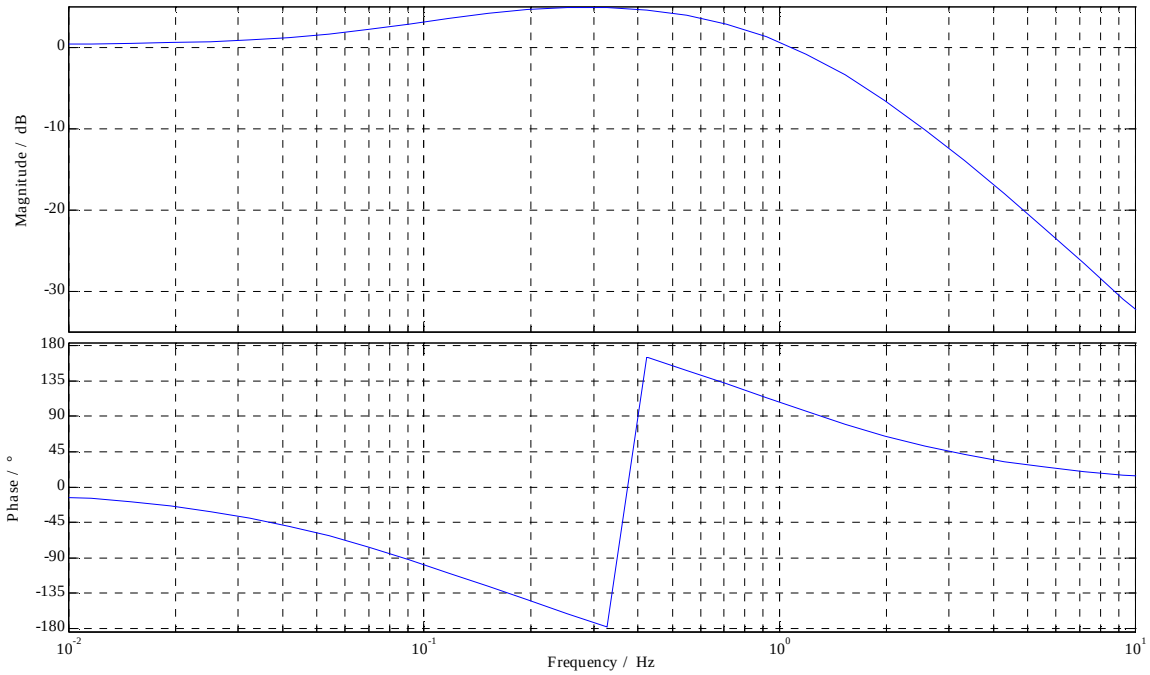

Figure 34: Bode plot of the open control loop from d_w to P_m to determine the phase difference

At the exemplary target frequency of approximately 1 Hz (oscillation frequency excited in the SMIB-system) in Figure 34, the estimated phase lead is about 110°.
As seen from Figure 35, the phase behavior is predominately determined by the influence of the servo motor and the hydro turbine model.

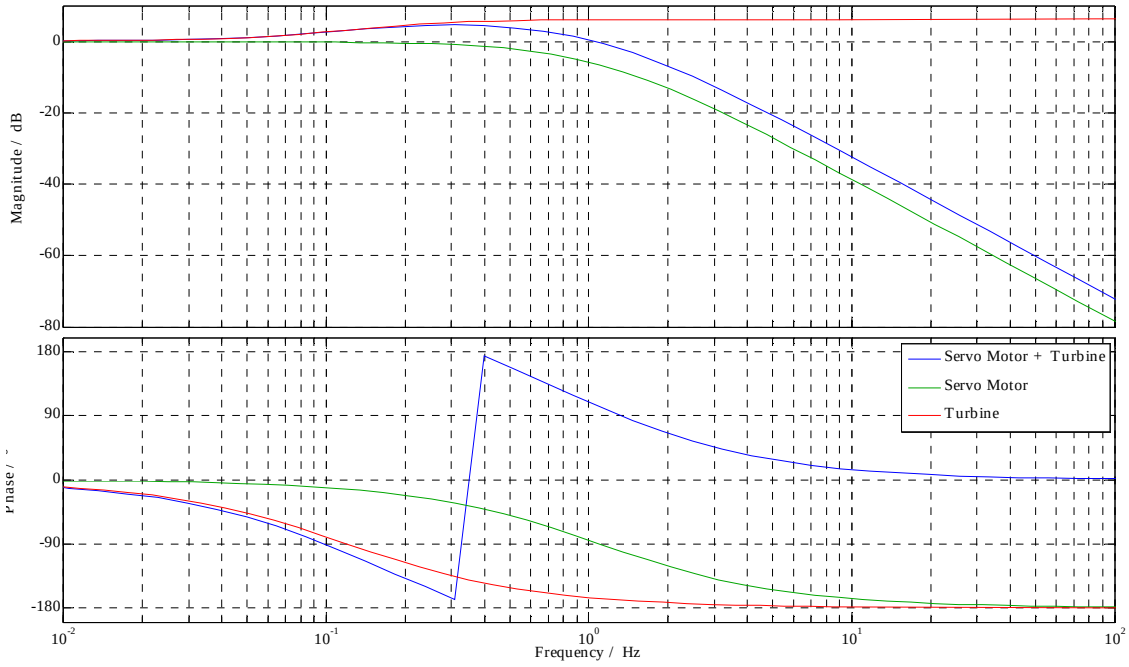

Figure 35: Bode blots of servo, turbine (simplified nonlinear model) PID controller and the overall governor from input signal d_w to output signal P_m

Inserting an additional phase lead of approximately 65° to Δω, in parallel to the primary controller, fulfills the requirement of the phase difference between d_w and P_m of about 180 °.

The bode plot of the lead lag compensator is shown in Figure 36.

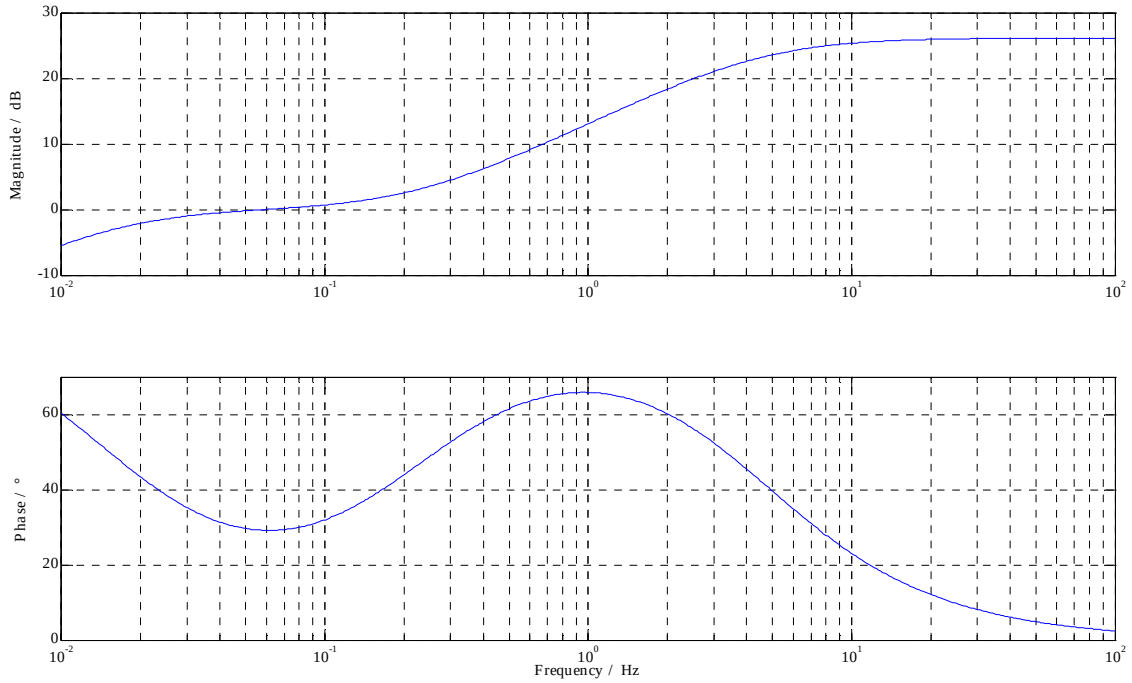

Figure 36: Bode plot of lead compensator of the PSS-G

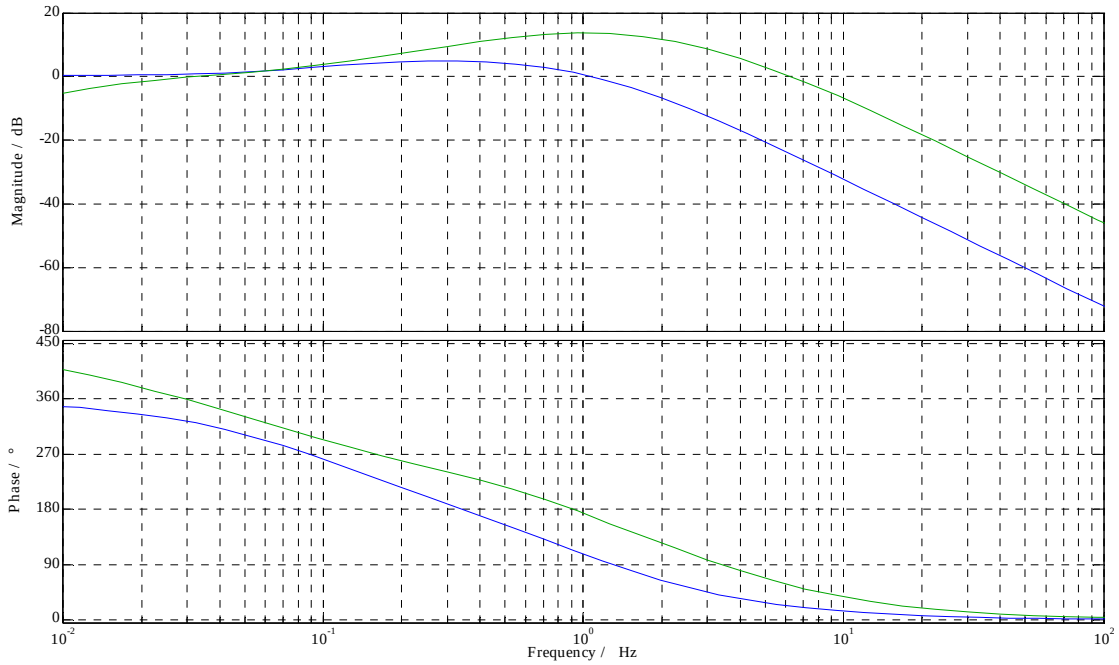

Figure 37: Bode plot of the open loop transfer function from Δω to P_m with phase compensation due to PSS-G (green) and without phase compensation (blue)

The resulting closed loop bode diagram with and without the PSS-G is shown in Figure 37.

5.3. Residues of Transfer Functions

The second applied method to derive an optimized set of parameters for the PSS-G is the calculation of the residues of the open loop transfer function from the PSS-G input signal to the speed deviation Δω (see Figure 33).
The method is described in detail in [34]. Only the most important facts are repeated here, to draw a principle picture of the method.
Based on the transfer function of a SISO (single input-single output) system

$$G(s) = \frac{y(s)}{u(s)}, \qquad \textbf{5-1}$$

the partial fractions can be derived in the following form:

$$G(s) = \frac{y(s)}{u(s)} = \sum_{i=1}^{N} \frac{Ri}{(s - \lambda i)}. \qquad \textbf{5-2}$$

Each nominator R_i is a scalar called residue.
Every complex eigenvalue λ_i corresponds to a certain mode of the mode spectrum of the system. One can see that each residue R_i contains a measure of sensitivity of a certain mode in the transfer function.
Due to the implementation of a feedback loop H(s) to the SISO system, a selected mode can be influenced. The respective eigenvalue can be shifted towards the left half plane to improve the damping of the target mode.

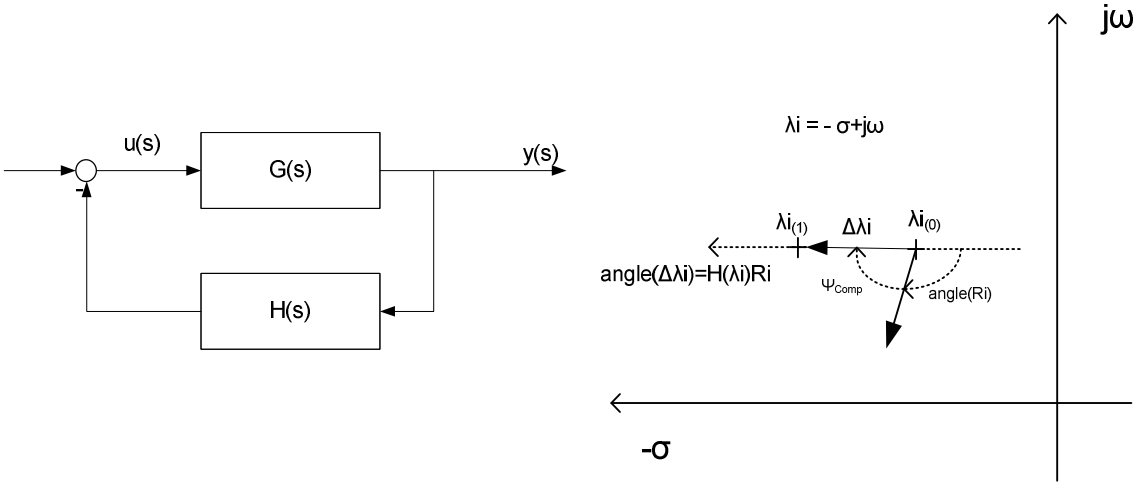

Figure 38: Shift of the eigenvalue λi due to the implementation of a feedback loop H(s), shift of eigenvalue from λi(0) to λi(1)

The transfer function of the damping controller can be written as

$$H(s) = K\frac{1}{1+s\cdot T_s}\cdot\frac{s\cdot T_w}{1+s\cdot T_w}\cdot\left[\frac{1+s\cdot T_{lead}}{1+s\cdot T_{lag}}\right]^m, \qquad \textbf{5-3}$$

where K is the controller gain, T_s represents the delay of the signal measurement, T_w is the washout-time constant and T_{lead} and T_{lag} are the time constants of the compensator. Seen from the following equation, $\Delta\lambda i$ must be a real negative scalar.

$$\Delta\lambda i = Ri\cdot H(\lambda i) \qquad \textbf{5-4}$$

The residues of the system's transfer functions also implies information about the best position for the stabilizing device to act on a certain mode, as well as a recommendation of the best input signal for the PSS.
To visualize the eigenvalue shift, the feedback gain K is varied as well as the angle of departure at the point $\lambda_{i(0)}$ (see Figure 38) is varied. In Figure 39 an exemplary root locus of a closed loop PSS for a target mode of approximately 1 Hz is shown. The values in the legend of this figure are the various angles of departure representing the respective lines. The lines are furthermore obtained by varying the controller gain K. The blue arrow indicates the direction of the eigenvalue drift from the starting point $\lambda_{i(0)}$.

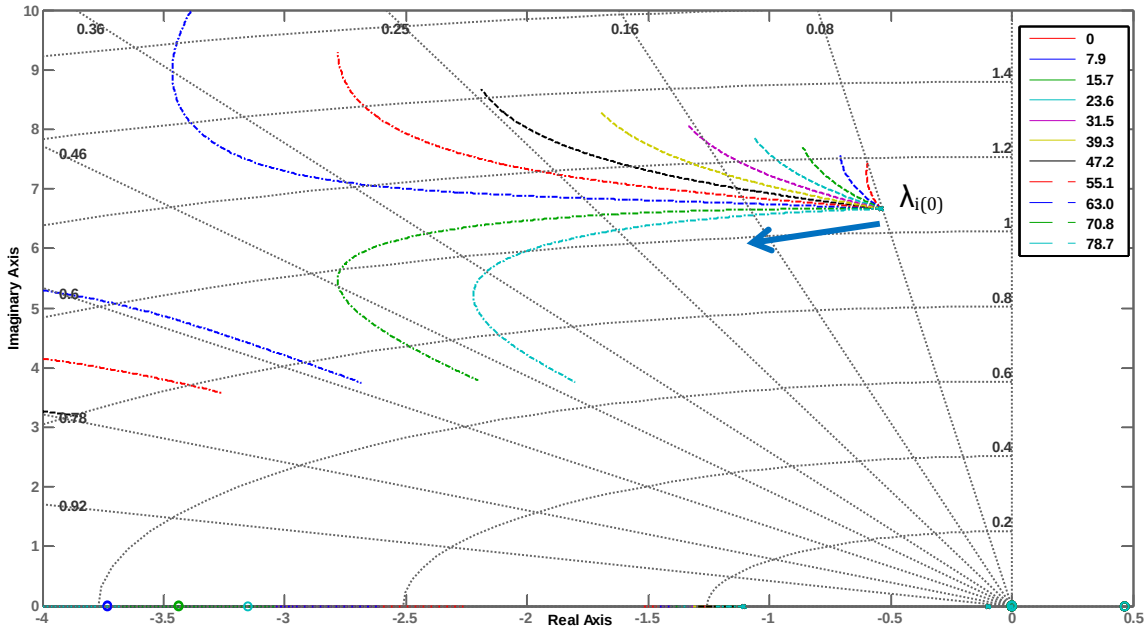

Figure 39: Root locus of an exemplary closed loop PSS controller for the SMIB system, target frequency at approximately 1 Hz

Under the consideration that $\Delta\lambda i$ is shifted horizontally towards the left half plain, a pure damping is induced in the system and so the oscillation frequency in the closed loop system remains unchanged. If the root locus deviates from the horizontal axis, also the synchronizing torque is varied, resulting in an oscillation frequency drift compared to the system without PSS.

5.4. Design of Lead/Lag Compensators

Once the required phase compensation is ascertained, the calculation of the associated lead/lag compensators is following a standard routine. A detailed description is given in [34].
Basically the procedure is based on the following equations.

$$\alpha_c = \frac{T_{lead}}{T_{lag}} = \frac{1 - \sin\left(\frac{\beta_{comp}}{m}\right)}{1 + \sin\left(\frac{\beta_{comp}}{m}\right)}$$

$$T_{lead} = \frac{1}{\omega_i \cdot \sqrt{\alpha_c}}$$

$$T_{lag} = \alpha_c \cdot T_{lead}$$

5-5

6. Modal Analysis and Nonlinear Simulations

6.1. Introduction to Simulation Models and Investigation Method

In general, the investigation platform consists of two different simulation models and therefore two stages of investigation. A Single Machine Model as a first stage and a Multi Machine Model as a second stage. The aim of this stepwise approach is to start the investigation with a simple and straightforward model and test the principle method in a system without influences from surrounding grid elements before the extension to an improved multi machine Model. All dynamic components of both models are basically implemented as nonlinear elements.

The **Single Machine Infinite Bus Model** consists of a generator, equipped with an AVR and a governor, connected to an infinite bus via a power line. It can be seen as the first stage of the investigations where principle relationships and governor system behavior in case of oscillations is illuminated. The structures of the controllers are similar to standard models, whereas the parameters of the governor and the PSS-G are optimized, according to the respective case of investigation. The advantage of this model is the absence of mutual coupling among generators and controllers or other damping devices and the isolation of the dynamic characteristics of the hydro governor as a damping device. Although the expected mechanical oscillation frequency of the generator, swinging against an infinite bus system (around 1 Hz for a salient pole hydro generator), is out of the oscillation frequency range, where the PSS-G is believed to have the optimal operational range, principle characteristics of the mechanical system can be derived. Also this simple model is the basis for the development and plausibility check of the applied analysis tools, such as the modal tool, the calculation for PSS parameters, or the tool for the graphical representation of the results.

Due to the extension of the generator and controllers of the Single Machine Model by three more generators and interconnection lines, the second stage **Multi Machine Model** is deployed. The topology is related to the well-known Kundur two-area system, described in [5], which is in many cases used in small signal studies. The controllers of the additional generators, respectively the dynamic model structures and parameters, basically rely on the recommendations in the respective IEEE documents in [7], [15] and [45]. On basis of this configuration, the interaction of the controllers is of central concern. Furthermore the damping devices are subjected to an inter area mode, occurring on the tie lines between the two areas and their effectiveness is compared.

The focus in this work is to assess the contribution of the hydro governor to system damping during the occurrence of low frequency oscillations. An appropriate approach is to make use of small signal stability analysis, described in chapter 3.3. The linearized models are firstly used to determine the optimal parameter sets for the PSS-G and the PSS-E, taking into account various comparative scenarios. For the analysis and the comparison of the impact of the devices (PSS-G and PSS-E) on system damping, the models are linearized around the current point of operation. Root locus plots are used to analyze the movement of the system eigenvalues and to determine the additional damping, introduced by the respective PSS devices. Furthermore the evaluation of the results from

the closed loop transfer functions, according to the setup of the Heffron-Phillips model (see chapter 4.2.1 and 4.2.2), quantifies the contribution of the governor and voltage control loop in terms of damping and synchronizing torques.
As mentioned in chapter 3.3, the utilization of small signal stability analysis assumes the linearity of the system. Depending on the degree deflection from the stationary operational point, this assumption leads to reasonable results. Outgoing from small deviations, the results from linear and nonlinear analysis provide coincide results. The higher the contribution from nonlinear elements- such as the mechanical actuators- is, the bigger is the deviation of linear from nonlinear results.
Thus, the aim of time simulations is to prove the results from small signal stability analysis under consideration of nonlinearities and speed limitations of actuators. Time courses of selected signals, such as governor output or actuator position are used to assess the impact of the hydro governor on the mode damping for the operational conditions, where linear analysis is insufficient.

6.2. Dynamic Components of the Models

6.2.1. Generator

The synchronous generators are salient pole types and are represented by subtransient models. According to the IEEE Standard 1110-1991 in [45], the implemented generator model, utilized in the simulations, is based on the structure of Model 2.2. This type is characterized by two equivalent damper windings in the q-axis and is commonly used for hydro generator representations. The machine parameters, such as reactances and time constants, are chosen from typical value ranges for hydro generators according to [5].

6.2.2. Excitation System Models

The excitation system is implemented, following the IEEE-type ST1A shown in Figure 40. The parameters are taken from the exemplary data in [7].

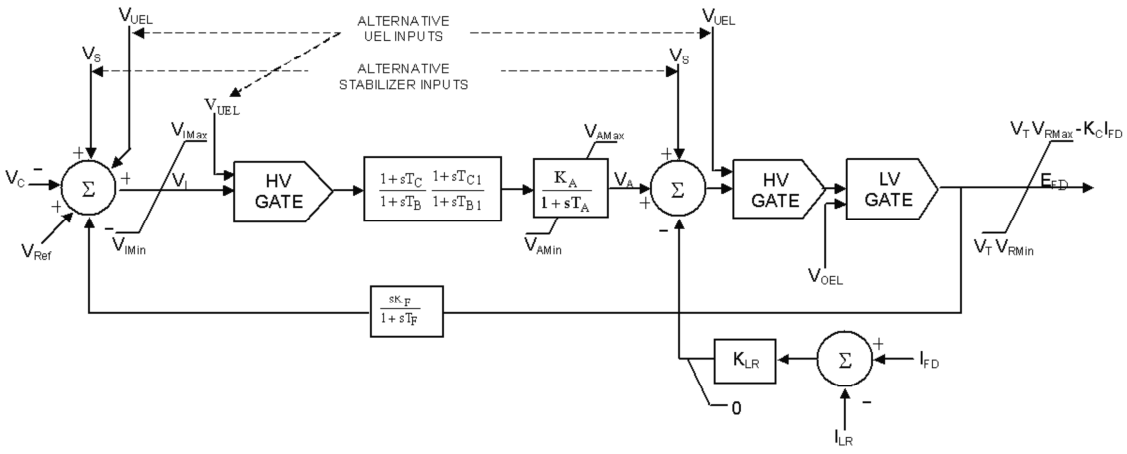

Figure 40: Block diagram of the static excitation system, IEEE-type ST1A

T_C	0	Lead Lag Compensation
T_B	0	
T_A	0	Regulator
K_A	210	
T_F	0	Damping filter
K_F	0	
K_{LR}	0	Gain field current limiter
V_{Rmax}	6.43	Limits
V_{RMin}	-6.0	

Table 3: Relevant controller settings, based on the example data for ST1A excitation systems, recommended in [7]

6.2.3. **Common PSS-E Representations in Stability Studies**

In Figure 41 the principle structure of the IEEE-standard types PSS1A with one single input and PSS2B with two inputs is shown.

The wash out blocks (T_5, T_{w1}-T_{w4}) filter signals with very low frequencies to prevent changes in the terminal voltage due to steady state rotor speed changes.

A first order term for each input signal represents the sensor time constants (T_6, T_7). Depending on the required phase compensation, the block diagrams contain one or more first order lag terms (T_1-T_4, T_{10}, T_{11}). The gains (K_s, K_{s1}, K_{s2}) are proportional to the damping, provided to the system.

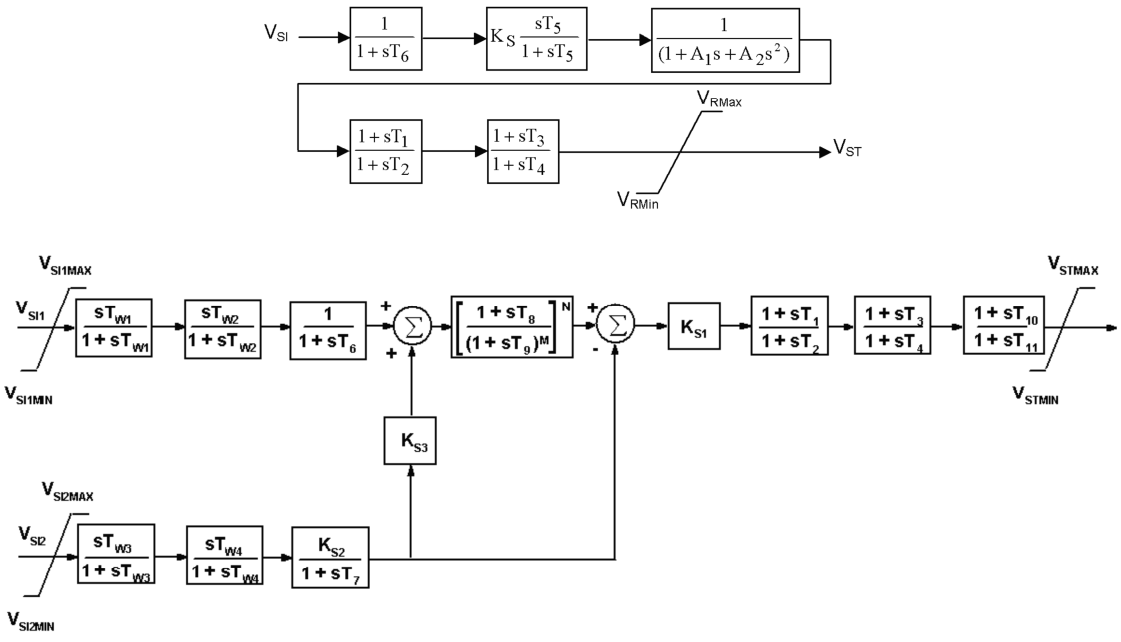

Figure 41: Block diagram of IEEE-PSS-E types PSS1A and PSS2B [7]

As common input signal speed, frequency or power is used for the single input structure, whereas for the two input structure usually speed and electrical power is used. Limitations of the output signals (V_{RMax}, V_{RMin}, V_{STMAX} V_{STMIN}) are implemented to limit the

interaction with the voltage control mechanism which has commonly inverse control targets.
Further possible inputs can be signals driven from WAMS. For example, voltage phase deviations or tie line active power, are possible choices depending on the observability of the respective target mode.

6.2.4. **Dynamic Governor Models**

A generic hydro governor model, often used in dynamic studies, is shown in Figure 42. This type is valid for older, mechanical-hydraulic, as well as newer electrohydraulic governor systems.
The feedback loop with the permanent droop R_P is responsible for a high forward gain in or close to steady state operation.
Temporary droop compensation, represented by the gain R_T and the reset time constant T_R in the feedback loop, fulfill the requirement for a large transient droop, resulting in a low transient gain combined with a with a long reset time. This control target gives respect to the effect of the water hammer effect and ensures the water column to be able to follow the gate changes in case of high transient controller action.

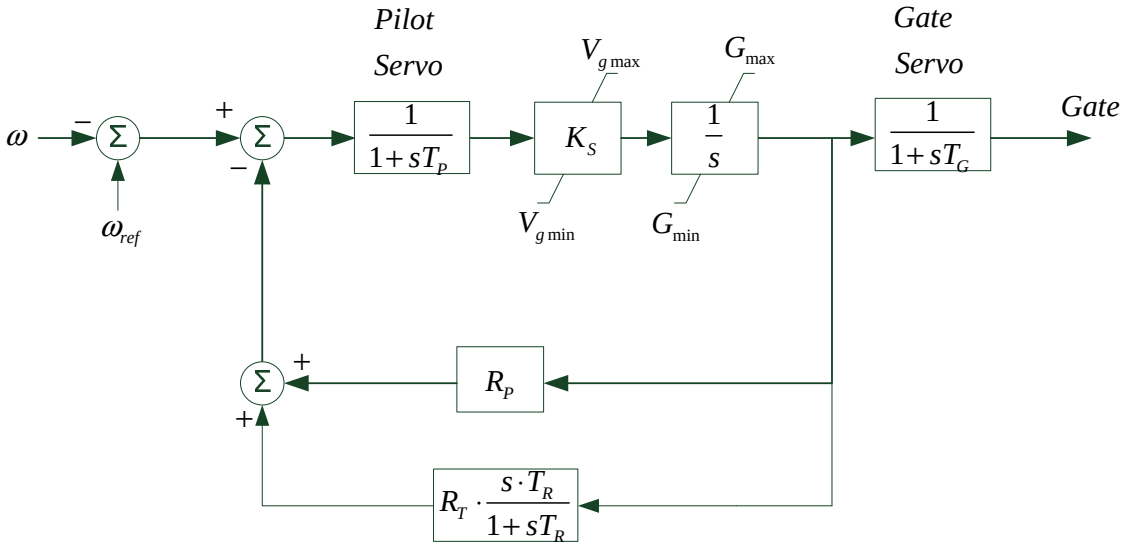

Figure 42: Electromechanical hydro governor [5]

The parameterization of the controller is provided following [14]. Based on the typical hydro governor realization with temporary droop compensation, the parameters R_T and T_R are given by

$$R_T = \frac{T_W}{H} \cdot (1.15 - (T_W - 1) \cdot 0.075) \qquad \textbf{6-1}$$

$$T_R = T_W \cdot (5 - (T_W - 1) \cdot 0.5) \qquad \textbf{6-2}$$

The hydro governors in the simulation models are controlling electrohydraulic actuators and are equipped with a PID controller. Most of the modern hydro power plants are equipped with this type of controller.

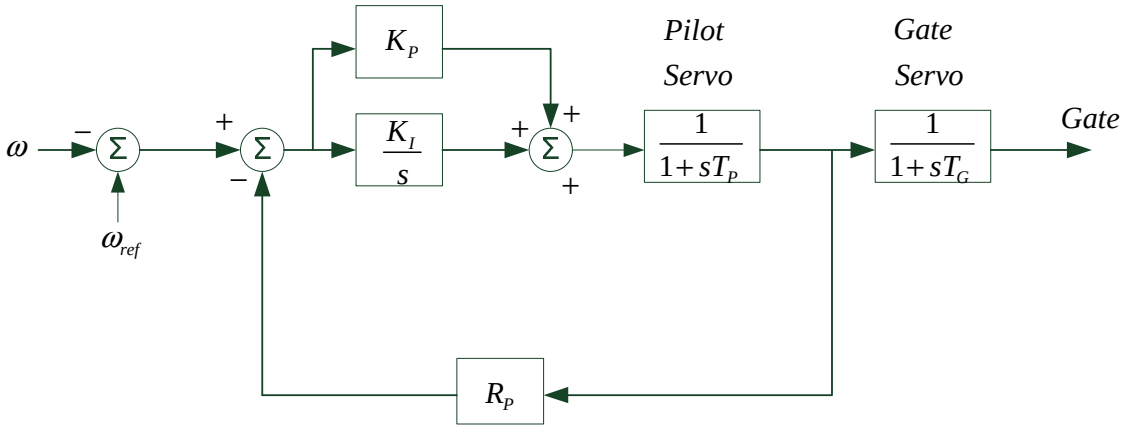

Figure 43: Block diagram of the governor model, PI controller, pilot servo and gate servo

The derivative term, typically parameterized for power plants in islanded operation with large water starting time constants [5], is set to zero resulting in a PI controller. The controller output is connected to a pilot servo, followed by the main gate servo as shown in the block diagram in Figure 43.
According to the calculated temporary droop compensation, the tuning guidelines described in [14] are applied.

$$K_P = \frac{1}{R_T} \qquad K_I = \frac{K_P}{T_R} \tag{6-3}$$

The resulting parameters of the governor system are given in Table 4. For the servo time constants T_P and T_G, typical values from sample data in [5] are used.

T_P	0.05	s	Servos
T_G	0.2	s	
Gmin	0	p.u.	Limits
Gmax	0.97	p.u.	
Vgmin	-0.05	p.u./s	
Vgmax	0.05	p.u./s	
Rp	0.04		Permanent Droop
Kp	2		Proportional(PID)
Ki	0.27		Integral (PID)
Kd	0		Differential (PID)
Td	0.01	s	Differential (PID)
T_W	2.67	s	Water starting time

Table 4: Governor settings and simplified hydro turbine parameters

For the investigations done in this work, the effect of unwanted, or wanted dead bands of mechanical systems are not considered.

Unwanted dead bands of the mechanical governor system are usually difficult to identify and thus to represent in a simulation model. Also the degree of detail of common hydraulically governors do not imply dead bands and are therefore usually not modeled in system studies [5].
Programmed dead bands offer varying parameter ranges, depending on the requests of the respective TSO or the aim of the control action (e.g. primary frequency control).

6.2.5. **Performance Indices of the Governor**

Figure 44 shows the simplified governor control loop for the verification of the calculated controller parameters. Connecting the gate of the governor to the hydraulic turbine (see chapter 4.3.4) and taking into account the linear representation of the rotating masses, the speed deviation for the feedback of the governor control loop is determined.

a)

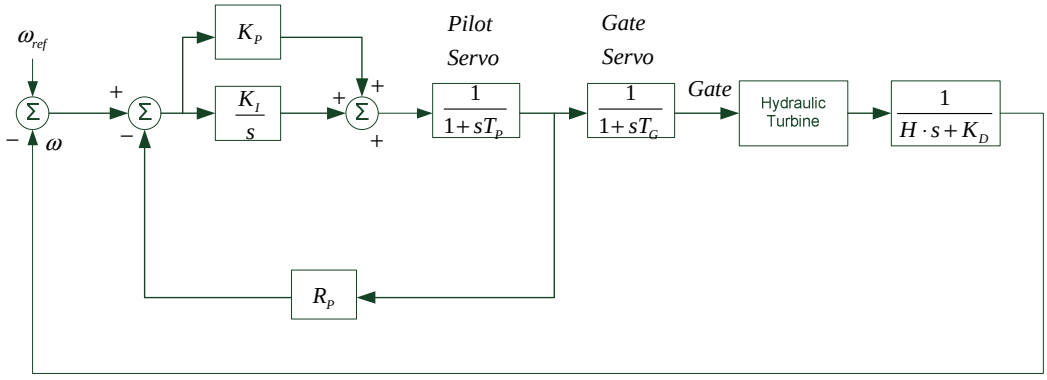

b)

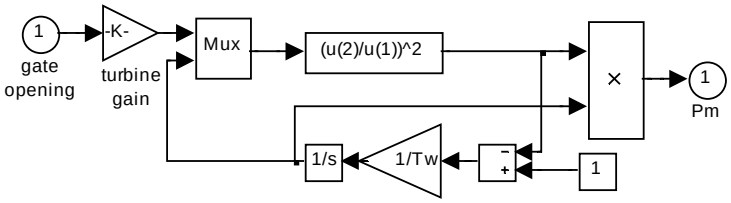

Figure 44: a)Simplified governor control loop, generator feeding an isolated load b) Hydro turbine model [46]

According to the stability tests in [15], Annex F, Table F.2, the open loop transfer function of the governor control path including the rotor behavior, should have a gain margin between 2 dB and 20 dB and a phase margin between 20 ° and 80 ° for a satisfying small signal performance. Negative gain or phase margins result in unstable control behavior of the closed control loop.
In Figure 45 one can see that the resulting gain margin is 7.24dB and the phase margin is 30.9 °. The values are satisfying the stability criterion, according to [15]. In the phase plot of the closed loop system in Figure 46, the bandwidth given in Hz and the peak value M_P in dB are marked.

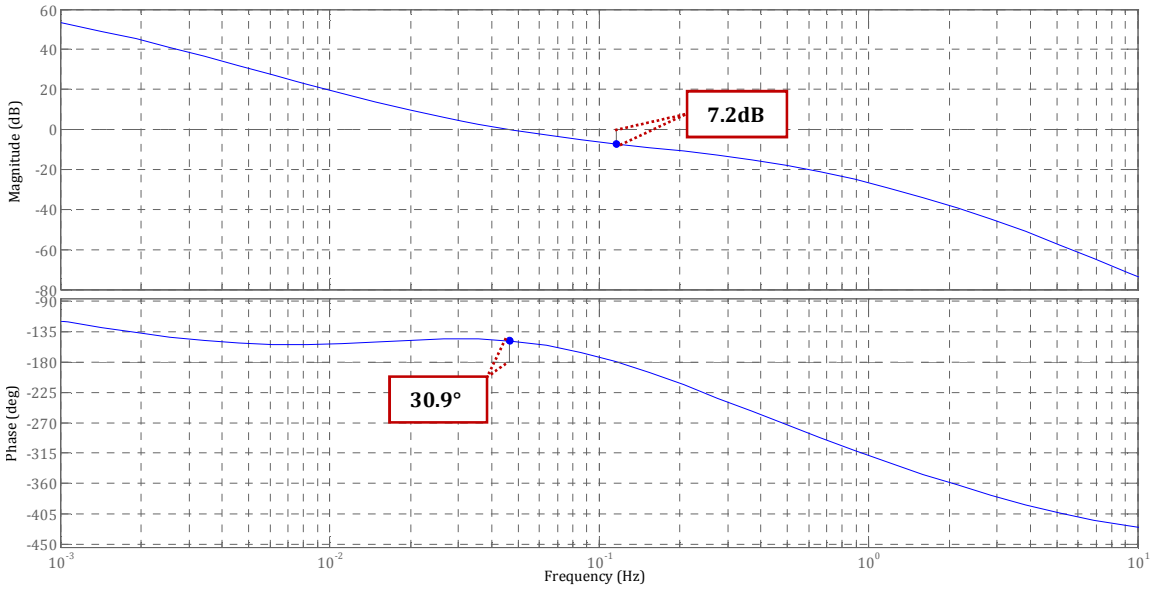

Figure 45: Bode plot of the simplified open loop governor control loop

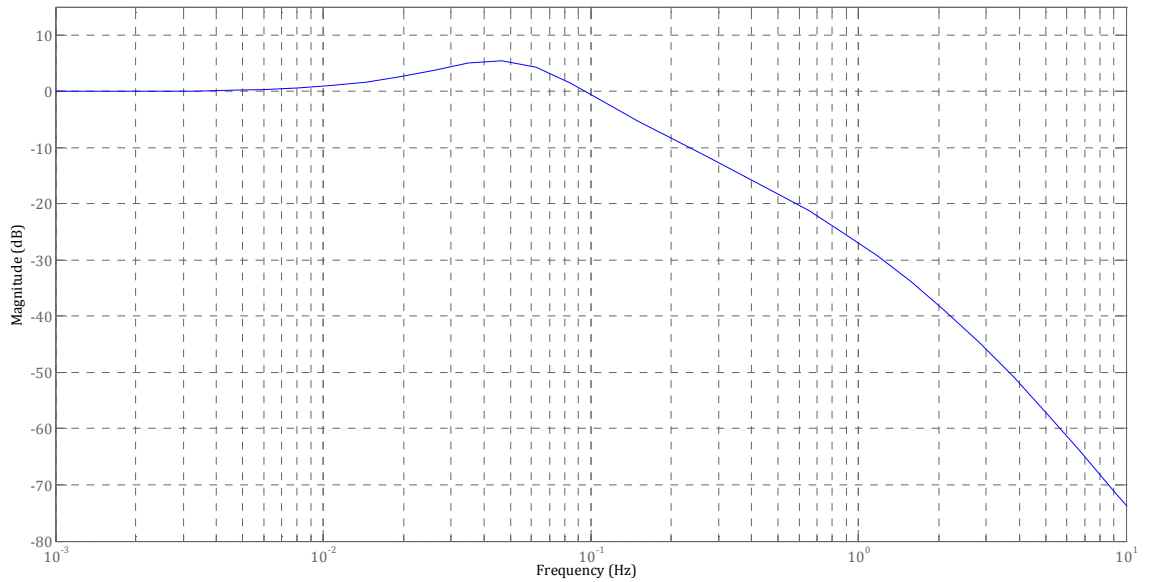

Figure 46: Magnitude of the simplified closed loop governor control loop

In Table 5 the summary of the governor stability indicators is given. Performance indices, given by [15], are not generally applicable and cannot be optimized simultaneously. Optimization for the control loop performance can be done, regarding the respective application. For this work the indices give a good orientation of the range of the calculated parameters, since the simulation model should be a general representation of the typical characteristics of a hydro power plant and is not the modeling of a real power plant.

Performance Index	IEEE Std 1207-2004	Governor Model
Gain Margin	2 dB – 20 dB	7.2 dB
Phase Margin	20 ° - 80 °	30.9 °
M_p	0 dB – 12 dB	6.1 dB
Bandwidth	0.03 Hz – 1 Hz	0.15 Hz
Rise Time	1 s – 25 s	1.93 s
Settling Time	2 s – 200 s	21 s

Table 5: Typical range of performance indices following [15] and comparison to the used governor model

6.3. Single Machine Infinite Bus Model

This chapter contains the comparison of the two standard parameter sets Kundur and Multiband, originally used for PSS-E devices, described in chapter 5.1 against a parameter set, derived by the bode plots and the residue method. For the derivation of the conclusions in the following subchapters only the PSS-G is applied.

Hence, the PSS-G device is variously adapted with

- Bode plot / Residue method
- Kundur parameterization (Standard)
- Multiband parameterization (Standard)

In chapter 6.3.1 the base case is described, whereas in 6.3.2 the bode method and the residue method are applied to the target mode. In chapter 6.3.3 basic linear characteristics of the voltage and governor control path are derived due to the utilization of transfer functions in the Heffron-Phillips model.
After a modal analysis is performed in chapter 6.3.4, in chapter 6.3.5 the model is exposed to changes in grid impedance to estimate the potential of the PSS-G impact for various grid conditions. The robustness of the PSS-G against changes in grid impedance is investigated in 6.3.5. The following nonlinear time domain simulation in chapter 6.3.6 is used to prove the results from modal analysis.

As described in the general introduction in 6.1, the single machine infinite bus system is used as a tool to investigate the principle feasibility of the governor control path to act on mechanical oscillations. The mechanical oscillation frequency is expected near the natural frequency of the hydraulic unit and thus in the range of around 1 Hz. Although the most effective operational range for the PSS-G is expected to be below oscillation frequencies of 1 Hz the single machine system is used as a basis to investigate the general functionality. The excitation of the oscillations in time domain is provided by a three-phase short circuit fault, connected via an impedance.

Figure 47 shows the structure of the single machine unit. The block 'GOV+AVR' contains the governor and voltage regulator. The small load is an auxiliary element in the very low value range, requested for the numerical stability of the initialization process in MATLAB.

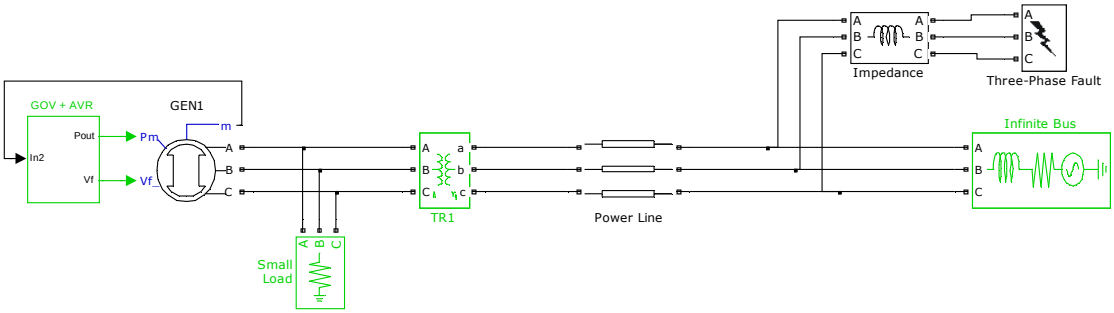

Figure 47: Singe Machine Infinite Bus (SMIB) model in MATLAB/Simulink for principle investigations

The three-phase source is represented by a short circuit impedance respectively short circuit power.

6.3.1. **Characteristics of the Base Case**

The base case characteristics are described separately in a linear investigation, utilizing the Heffron-Phillips model and the nonlinear time domain simulation.

Linear Characteristics

Figure 48 shows the modal plot of the base case. The mechanical oscillation is in the region of the estimated natural frequency of the generator at about 1.1 Hz with a damping of 5.8 %. The second mode at a frequency at about 1.9 Hz is assigned to the electrical model of the generator, as determined by the participation factors listed in Table 6.

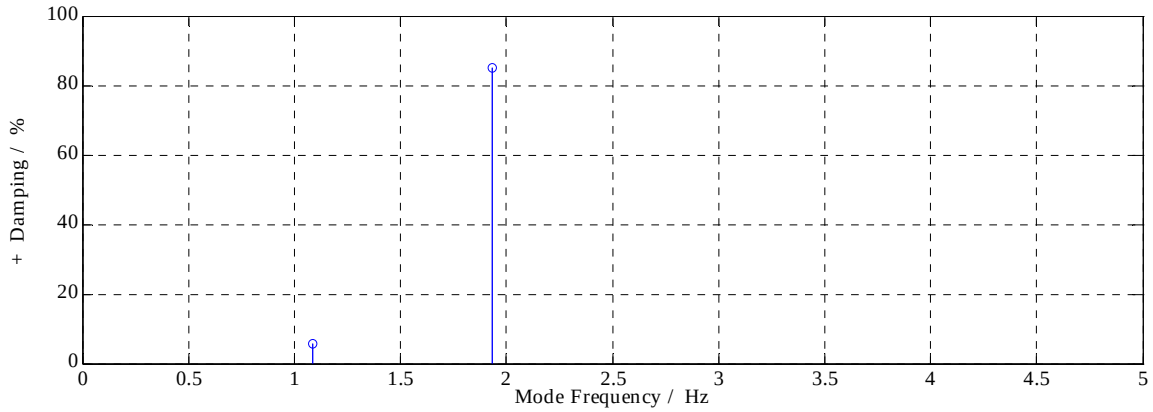

Figure 48: Modal spectrum of the base case

Number	Eigenvalue λ	Damping	Frequency	Natural Frequency	Dominant states
		%	Hz	rad/s	
1	-0.40 ± j6.82	5.8	1.09	6.84	ω, d_w
2	-19.67 ± j12.14	85.09	1.93	23.11	Ψ_{fd}, Ψ_{kd}

Table 6: Poles, damping, frequency and dominant states of the base case

The target mode for the parameterization of the PSS-G device is the mechanical mode at the frequency of 1.1 Hz with a damping of 5.8 %. The oscillation frequency is, as expected, near the natural frequency of the generator, swinging against an infinite bus.
The overall synchronizing and damping torque components K_S and K_D for the electromechanical target mode can be calculated from the eigenvalue representing the mechanical oscillation by rearranging 3-42 and 3-43.

$$K_S = \frac{{\omega_n}^2 \cdot 2 \cdot H}{\omega_r} = \frac{6.84^2 \cdot 2 \cdot 3.5}{314.16} = 1.04 \ \frac{\text{p. u. torque}}{\text{p. u. speed change}} \qquad \textbf{6-4}$$

$$K_D = 2 \cdot \zeta \cdot \sqrt{K_S \cdot 2 \cdot H \cdot \omega_r} = 2 \cdot 0.0582 \cdot \sqrt{1.04 \cdot 2 \cdot 3.5 \cdot 314.16} = \qquad \textbf{6-5}$$

$$= 5.57 \frac{\text{p. u. torque}}{\text{p. u. speed change}}$$

K_D and K_S are the sum of the damping and synchronizing torques from the voltage control path and the governor path. Considering the formulas 4-6 and 4-19, the quantification of each contribution results in a complex transfer function, based on the descriptions of the Heffron-Phillips equivalent.
For the mechanical oscillatory mode of the base case with the eigenvalue $\lambda_2 = -0.4 \pm j6.8$ the frequency responses of the transfer functions $G_{Mechanical}(s)$ and $G_{Electrical}(s)$ yield in

$$G_{Mechanical(s=\lambda_2)} = -1.31 + j2$$

$$G_{Electrical(s=\lambda_2)} = 1.09 + j0.15 \ .$$

Applying 4-19 and 4-6 results in

$$\Delta T_m = -1.43 \cdot \Delta\omega - 0.04 \cdot \Delta\vartheta$$

$$\Delta T_e = \ 7.12 \cdot \Delta\omega + \ 1.1 \cdot \Delta\vartheta \ .$$

The sum of the damping torques and the synchronizing torques, based on the analysis of the transfer functions, agree with the terms calculated from the respective eigenvalue with satisfying accuracy.

It is also obvious that the contribution of the governor to the system damping is thus to reduce the damping torque component by nearly 1.4 and slightly reduce the synchronizing torque. It should be noted that this behavior is resulting from the applied base configuration without the use of a damping device.

Figure 49 shows the above calculated damping and synchronizing components of ΔT_m and ΔT_e drawn in the $\Delta\vartheta/\ \Delta\omega$ plane.
It is worth to mention that the scale of abscissa and ordinate differ by factor 10 and hence, the angle of the drawn vectors is near to 90 °, which indicates a predominant damping torque component.

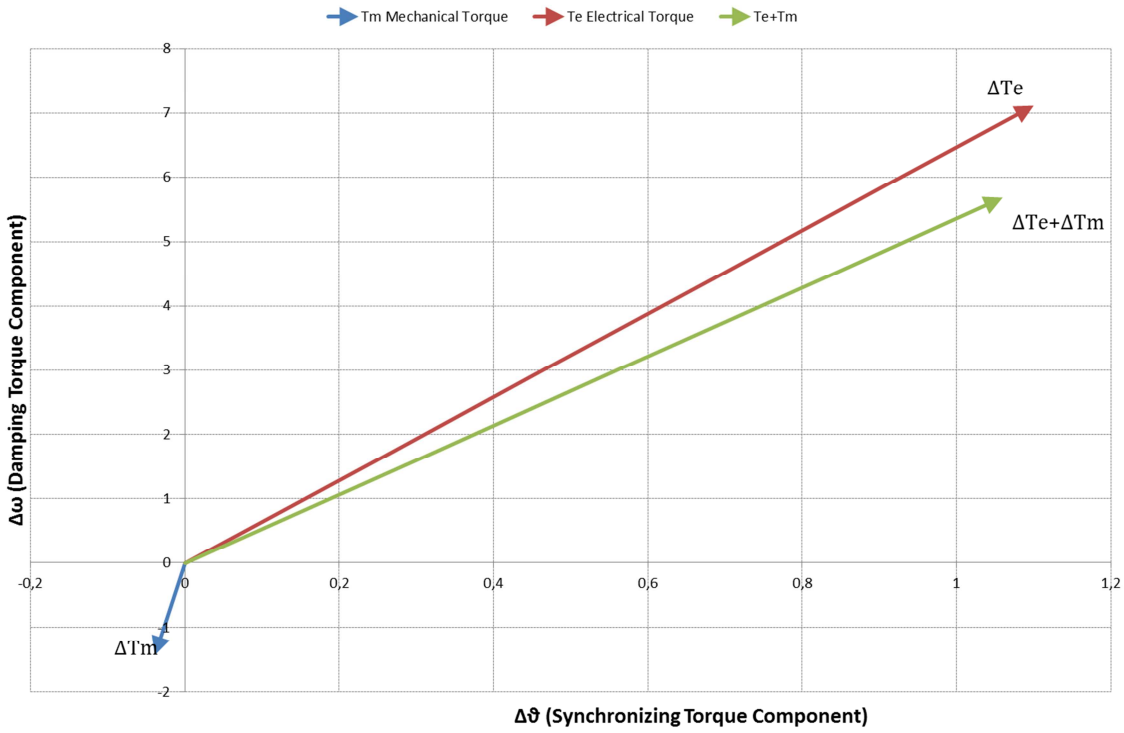

Figure 49: Damping and synchronizing torque component resulting from the governor system and from the electrical system for the target mode of the base case

The damping and synchronizing torque is dominated by the electrical system of the generator, including the excitation system. This is the reason why governor contributions and thus changes in mechanical torques for small signal studies are usually neglected. For cases with poor damped modes, respectively damping torques ΔT_e in the range of the negative components provided by the governor this assumption is not valid without restrictions.

Nonlinear Characteristics

To compare the results from the Heffron-Phillips equivalent with the nonlinear model, a time domain simulation is performed. Thus, the time course of the generator's speed

deviation is exemplary evaluated as shown in Figure 50 by comparing the decay time constant T_{decay} from [5], calculated from the real part of the eigenvalue with the decay of the amplitude.

$$T_{decay} = \frac{1}{|Real\{\lambda_2\}|} = \frac{1}{0.3985} = 2.5s \qquad \textit{6-6}$$

During time period T_{decay} the amplitude decays to 37 % of its initial value, marked red in Figure 50.
The mechanical mode is excited with a short circuit with the current, limited by an inductance.
The maximum amplitude reaches approximately 8.5 mHz. After the excitation the rotor oscillates near the natural frequency. From the time course, the rotor oscillation frequency is estimated with f = 1.09Hz.

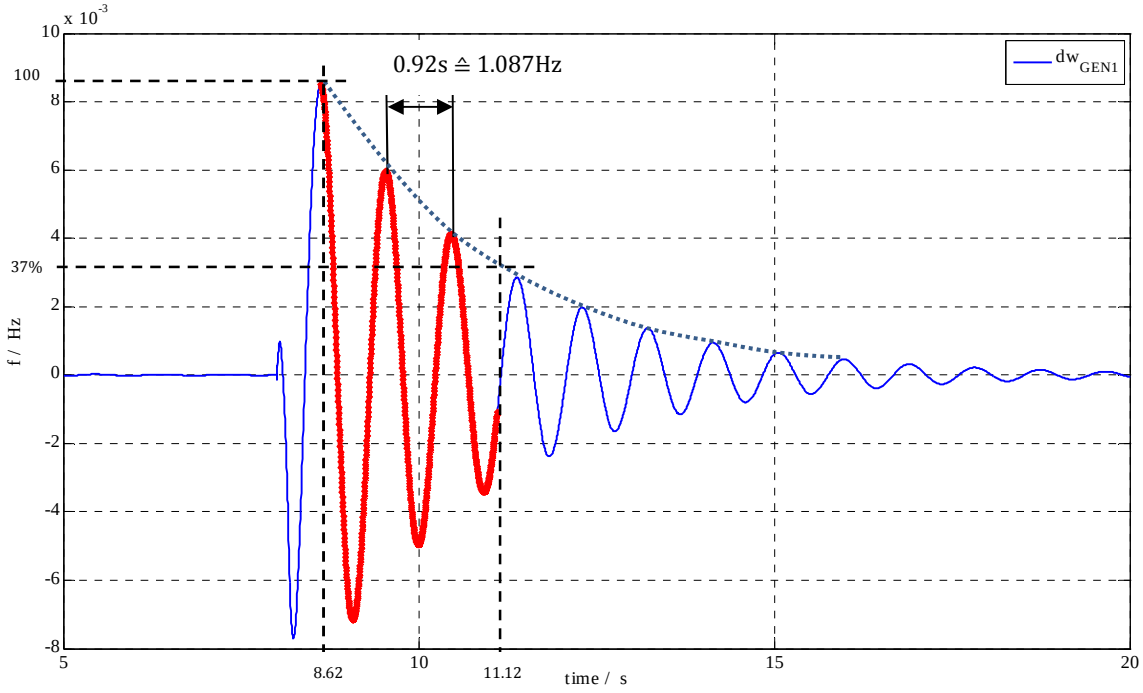

Figure 50: Speed deviation of the generator, oscillation frequency and decay parameter

Taken from the amplitude in Figure 50, the decay after the decay time constant T_{dec} = 2.5 s passed from the start value at 11.39 s is approximately 37.5 % and thus satisfying in accuracy compared to the values, calculated from the eigenvalue in 6-6.
Figure 51 shows the electrical and mechanical power on left side and the phase between mechanical power output of the generator and the rotor speed deviation as a consequence of the short circuit.
Subtracting mechanical and electrical power on the left side leads to the accelerating power responsible for the occurring rotor oscillations. The magnitude of the mechanical power and thus the impact of the governor is comparatively small.

On the right side of Figure 51 this governor contribution is zoomed and opposed to the governor input d_w. Especially after the first oscillations the phase shift is clearly observable.

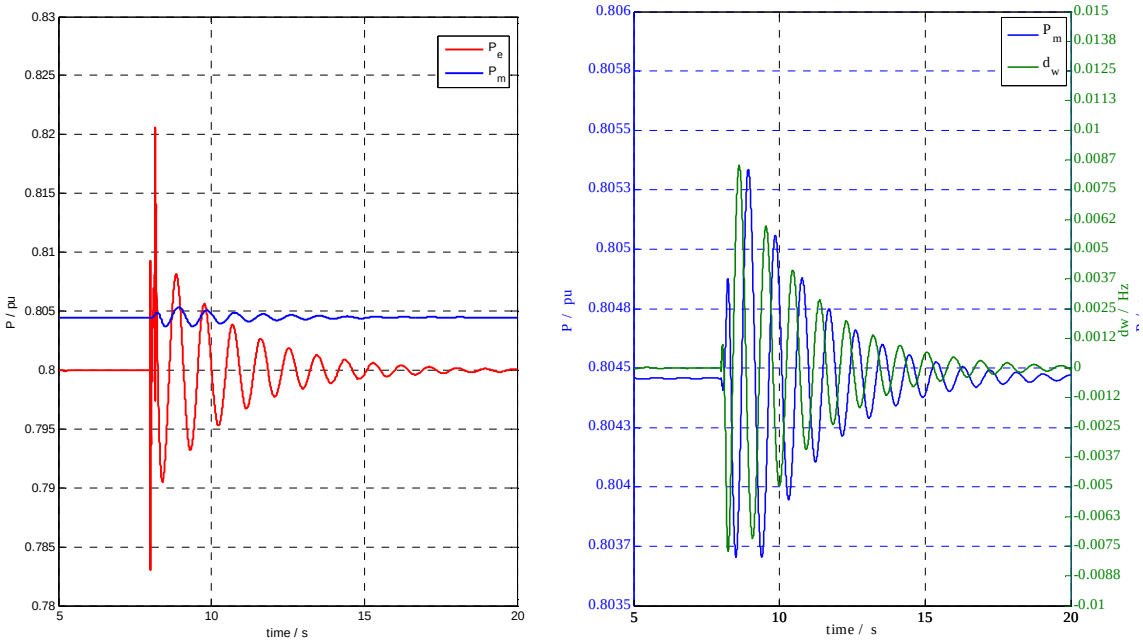

Figure 51: Mechanical power P_m and electrical power P_e (left) and mechanical power P_m and speed deviation d_w (right)

6.3.2. **Parameterizations of the PSS-G**

The aim for the damping device, parameterized in the following, is to add ideally a pure damping torque to the system and thus a contribution in phase with Δω. Therefore bode plots and the residue methods are demonstrated to be valuable tools. The standard parameterizations as well as the methods for derivation of an optimal set to introduce a pure damping torque, have been discussed in detail in chapter 5. Here, the bode plot parameterization and the residue method are executed for the occurring mechanical oscillation.

Bode Plot

For the analysis of the bode plot the transfer function from the speed deviation to the output signal of the governor ΔT_m, shown in Figure 33, is determined from the MATLAB model. In Figure 52 the respective magnitude and phase plot is shown.

For the target frequency of the mechanical oscillation at f = 1.1 Hz, the investigated transfer function produces a lag behavior of nearly -233 °. A pure damping component is induced at phase opposition of -180 ° resulting in a required additional lead of 53 °.

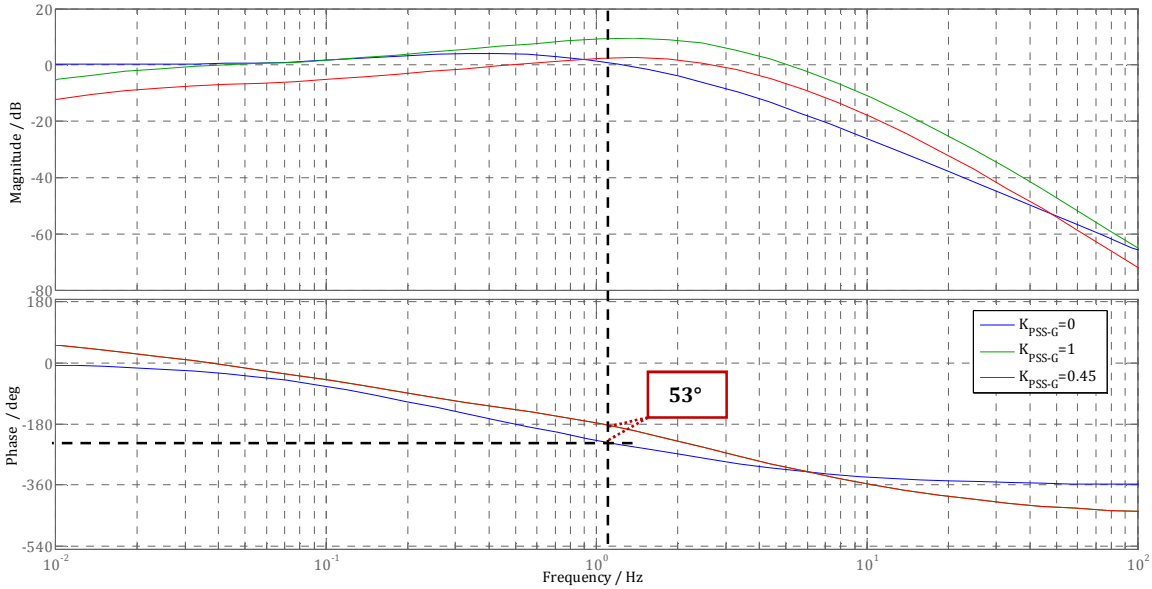

Figure 52: Bode response plot of the governor system, speed deviation as input point, mechanical power as closed loop output point

Figure 52 shows the bode plot of the transfer function from speed deviation to mechanical power for the base case without PSS-G active (blue), with PSS-G gain $K_{PSS\text{-}G}$=0.45 equal to the base case (red) and with $K_{PSS\text{-}G}$ = 1 (green). The phase behavior is unchanged for the two gains. Table 7 lists the parameters for both stabilizer gains.

$K_{PSS\text{-}G}$	T_s	T_w	$T_{lead(1)}$	$T_{lag(1)}$	$T_{lead(2)}$	$T_{lag(2)}$
p.u.	s	s	s	s	s	s
0.45	0.01	10	0.2371	0.0899	0.2371	0.0899
1	0.01	10	0.2371	0.0899	0.2371	0.0899

Table 7: Parameters of the PSS-G with stabilizer gain $K_{PSS\text{-}G}$ = 0.45 (green) and $K_{PSS\text{-}G}$ = 1 (red); K gain, T_s transducer time constant, T_w wash-out time constant, T_{lead} lead time constant, T_{lag} lag time constant

Residues

The detailed method of the parameterization due to the investigation of the factorized transfer function and the corresponding residues is described in detail in chapter 5.3.

The open loop transfer function, taking into account Figure 43 without the PSS-G, is derived defining the input signal right before the pilot to the speed deviation as an output signal.

The calculated parameters for the target mode λ_2 are listed below in Table 8. Based on the angle of the corresponding residue R_2 of 128 ° the angle difference to achieve a vertical shift of the eigenvalue towards the left half of the complex plane is 52 °. This angle β_{comp} is hence to be added by the controller and agrees with the result from the bode plot parameterization in sufficient accurateness.

Eigenvalue	Residue	Angle	Magnitude	Compensation
λ_2	R_2	angle(R_2)	abs(R_2)	β_{comp}
		°		°
-0.39848 ± j6.8245	0.054 ± j0.07	128	0.089	52

Table 8: Parameters of eigenvalue λ_2 without PSS-G

The optimal PSS-G gain $K_{PSS\text{-}G}$ is determined from the following root locus plot in Figure 53. Therein the controller gain $K_{PSS\text{-}G}$ is varied from 0 to 10. The angle of departure is altered by adapting the lead/lag compensation of the PSS-G. The respective angles are ±50 ° from the optimal compensation angle β_{comp}. One can see that the resulting mode frequency, which is 6.82 rad/s for the base case, varies with increasing controller gain.
The maximum damping can thus be determined with an angle of departure of 42.3 °and a gain close to $K_{PSS\text{-}G}$ = 10.
The damping of the mode can thus be increased by nearly 5 %, without influencing the oscillation frequency, respectively the synchronizing torque, which is desired for the controller design. The respective controller gain is therefore found at $K_{PSS\text{-}G}$ = 1.36, highlighted by markers in Figure 53 .

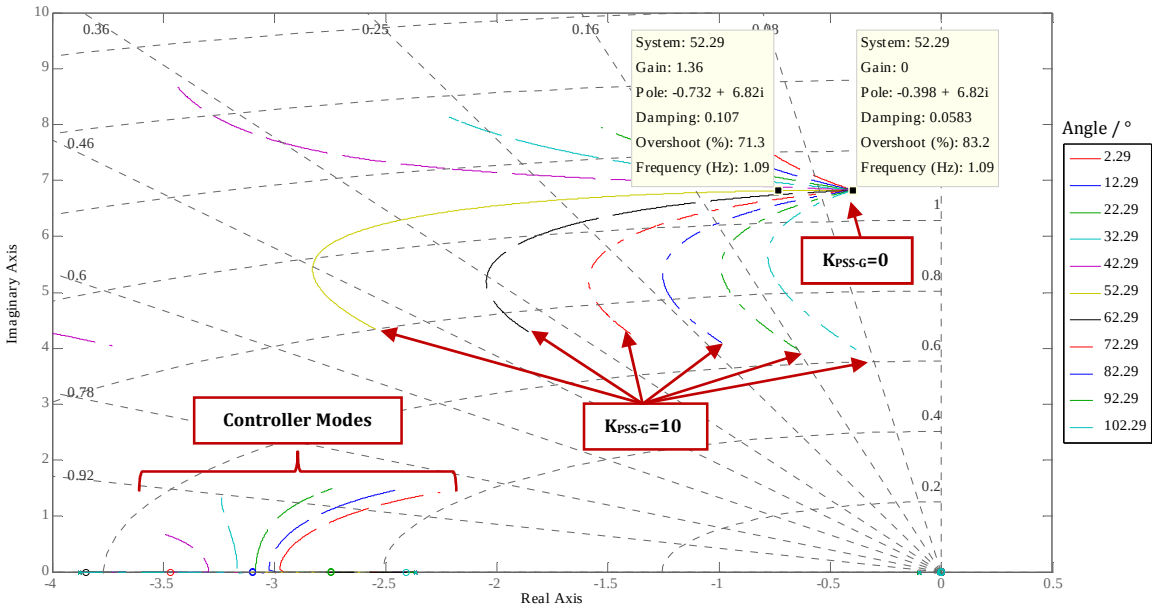

Figure 53: Root locus of the target eigenvalue λ_2 for varying angles of departure (from 2 ° to 102°), and varying gain $K_{PSS\text{-}G}$ (from 0 to 10)

From Figure 53 it can also be seen that non oscillatory modes change into oscillatory modes, when the PSS-G is active, although the damping of these modes is comparatively high. In the lower left corner the influence of the PSS-G on previous non-oscillatory mode can be seen. However damping is still satisfying.

Table 9 summarizes the parameters of the PSS-G derived from the manipulation of the residue of the target mode.

K_{PSS-G}	T_s	T_w	$T_{lead(1)}$	$T_{lag(1)}$	$T_{lead(2)}$	$T_{lag(2)}$
p.u.	s	s	s	s	s	s
1.36	0.01	10	0.2343	0.091	0.2343	0.091

Table 9: Parameters of the PSS-G, K_{PSS-G} Controller Gain, T_s transducer time constant, T_w wash-out time constant, T_{lead} lead time constant, T_{lag} lag time constant

6.3.3. **Linear Characteristics of the Voltage and Governor Control Path**

This chapter gives a principal overview of the characteristics of the voltage and governor control path, respectively the transfer functions $G_{Electrical}$ and $G_{Mechanical}$. The plotted figures show bode diagrams and frequency responses over a wide range of signal frequencies without the use of a PSS-E or PSS-G. This allows quite a general statement about the trends of impact of the voltage and governor control path. The underlying scenario originates from the base case.

Figure 54 shows the bode plot of the transfer functions $G_{Electrical}$ and $G_{Mechanical}$, derived from the simplified Heffron-Phillips model, illustrated in Figure 19. In case of $G_{Mechanical}$ one can observe a flat magnitude shaping with positive values up to 2 Hz. Further increasing frequencies are attenuated with a decaying magnitude of approximately 30 dB/decade. The phase is shaped flat from very low frequencies of about 0.02 Hz up to 0.15 Hz, above 0.3 Hz a lag behavior is observable.

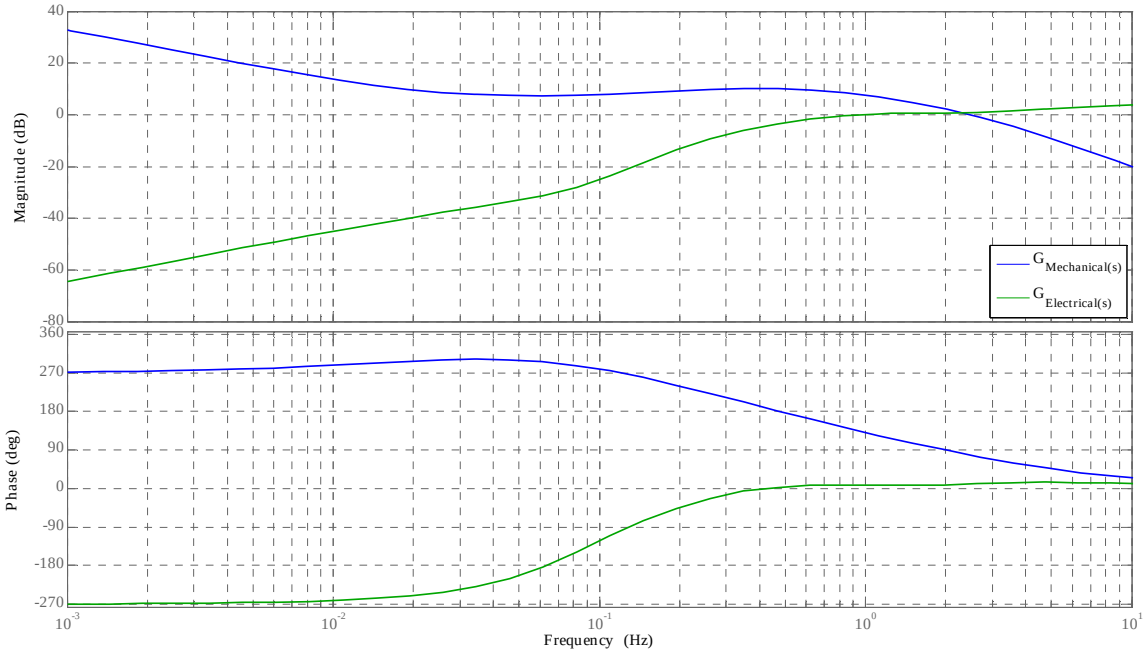

Figure 54: Bode plot of $G_{Electrical}$ and $G_{Mechanical}$

For the transfer function $G_{Electrical}$ the magnitude for frequencies below 0.8 Hz is negative and thus modes in this frequency range are attenuated. The behavior is from the characteristic of a high pass filter. The phase curve gets to 0 ° at a frequency of 0.4 Hz. Further increasing frequencies lead to a slight phase lead.

The interpretation of Figure 54 leads to the conclusion that the two control paths show a flat phase shape for frequencies above 0.8 Hz in case of $G_{Electrical}$ and below 0.2 Hz in case of $G_{Mechanical}$. In these value ranges the parameterization of damping devices is therefore expected to be robust.

Furthermore the governor control path $G_{Mechanical}$ provides favorable magnitude behavior below 1 Hz, compared to the attenuating trend of the excitation control path $G_{Electrical}$. This leads to the conclusion that the potential governor operational range is at frequencies below 1Hz, depending on the limiting actuator speed. Fast acting actuators, like deflector systems of impulse turbine systems, can theoretically provide around 0.05 p.u. of maximum active power output change at 0.9 Figure 20

From further interest is the contribution of $G_{Mechanical}$ to the overall damping and synchronizing torque for various frequencies. Therefore the respective frequency response is identified and converted into damping and synchronizing torque components, based on the derivations 4-6 and 4-10.

The respective frequency responses and courses of the damping and synchronizing torques are calculated by the determination of the transfer function from $\Delta\omega$ to ΔT_m, based on the representations in the complete Heffron-Phillips Modell in Figure 18. The frequency response of $G_{Mechanical}(s)$ is derived in the oscillation frequency of interest from 0.01 Hz up to 1.2 Hz.

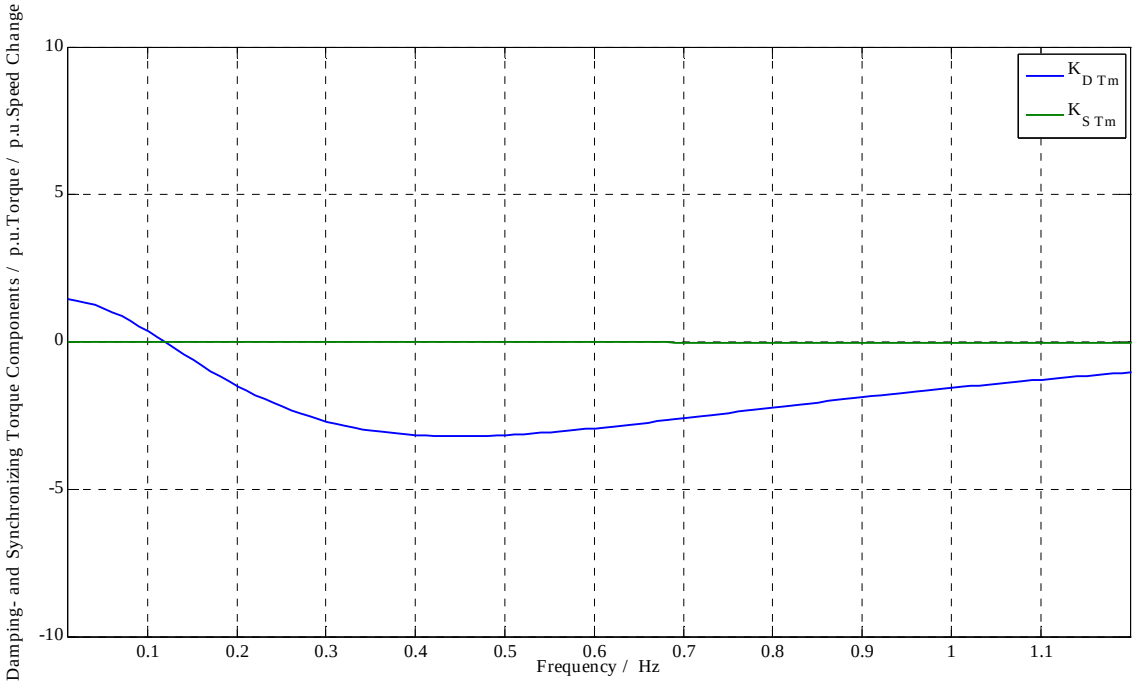

Figure 55: Damping and synchronizing torque, provided by the governor, frequency response of $G_{Mechanical}$

Figure 55 shows the results. It can be observed that the governor system provides negative damping to the system in the frequency range from 0.05 Hz to 0.7 Hz. Similar behavior has been observed already in [4] and [19] for governors of steam turbine systems. The synchronizing torque component $K_{S\ TM}$ is slightly negative but almost constant over the whole range.

For various grid impedances the respective damping and synchronizing torques of the mechanical oscillation are drawn in scatterplots in Figure 56 and Figure 57 by analyzing the transfer function responses. In Figure 56 and Figure 57 the connection line impedance changes in length from 10 km to 230 km.
In Figure 56 the damping torque components $K_{D\ Te}$ and $K_{D\ Tm}$, as well their sum, are shown. The damping torque component $K_{D\ Te}$ is decreasing with increasing grid impedance. As already shown in Figure 55, the contribution from the mechanical transfer function is negative but almost constant for the various grid impedances. Thus, the decay in the damping torque from the electrical side is superposed by a constant decrease from the mechanical side, leading to the resulting damping torque $K_{D\ sum}$.

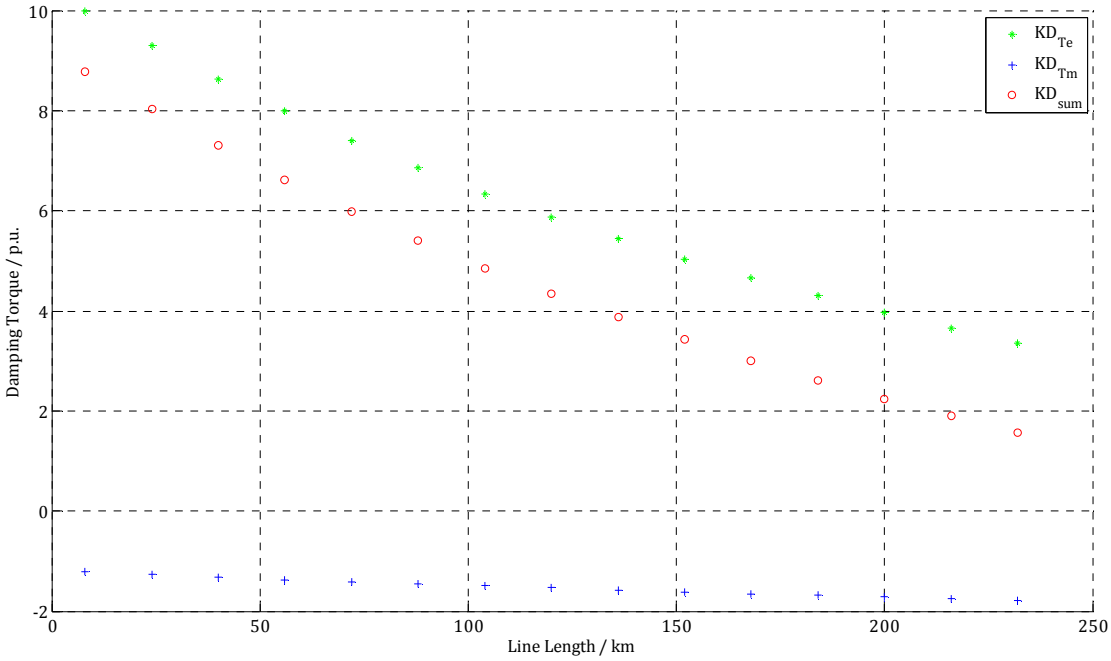

Figure 56: Damping torque components of $G_{Electrical}$ and $G_{Mechanical}$, variation of connection line length

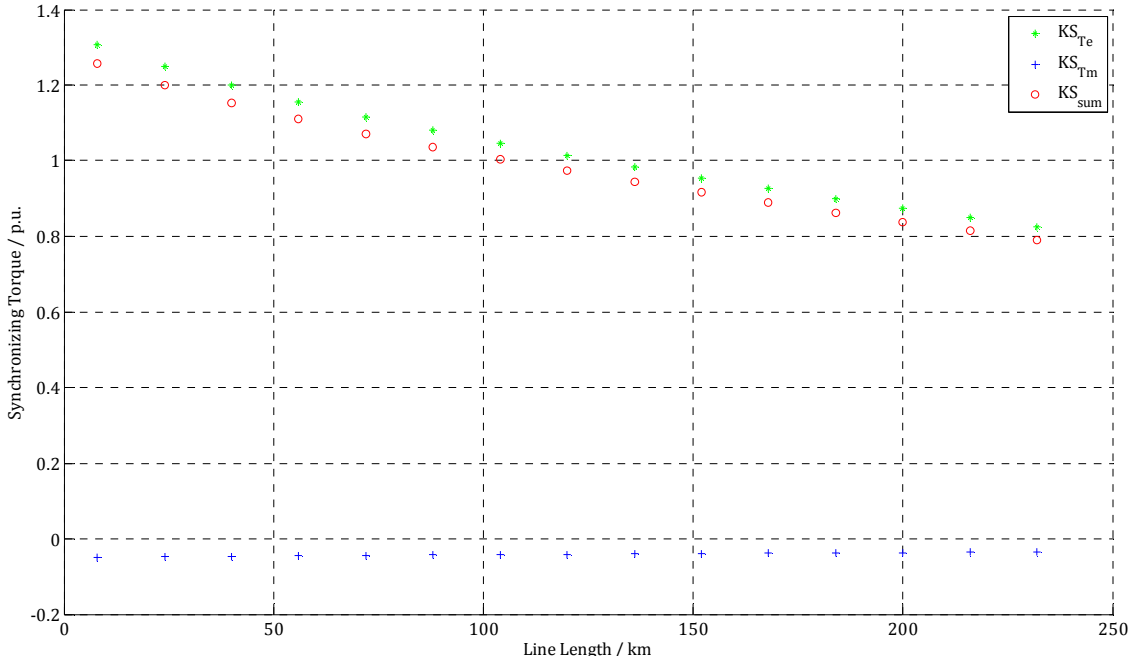

Figure 57: Synchronizing torque components of $G_{Electrical}$ and $G_{Mechanical}$, variation of connection line length

The same procedure has been applied in the following, investigating the respective damping and synchronizing torque components for the variation of the infinite bus voltage. For the variation from 0.9.p.u. to 1.1 p.u. the damping torque, provided by the excitation system, increases, whereas the synchronizing term remains almost constant. Concerning the contributions from the governor control path both, the damping and the synchronizing term remain almost constant. The associated scatterplots are displayed in Figure 58 and Figure 59.

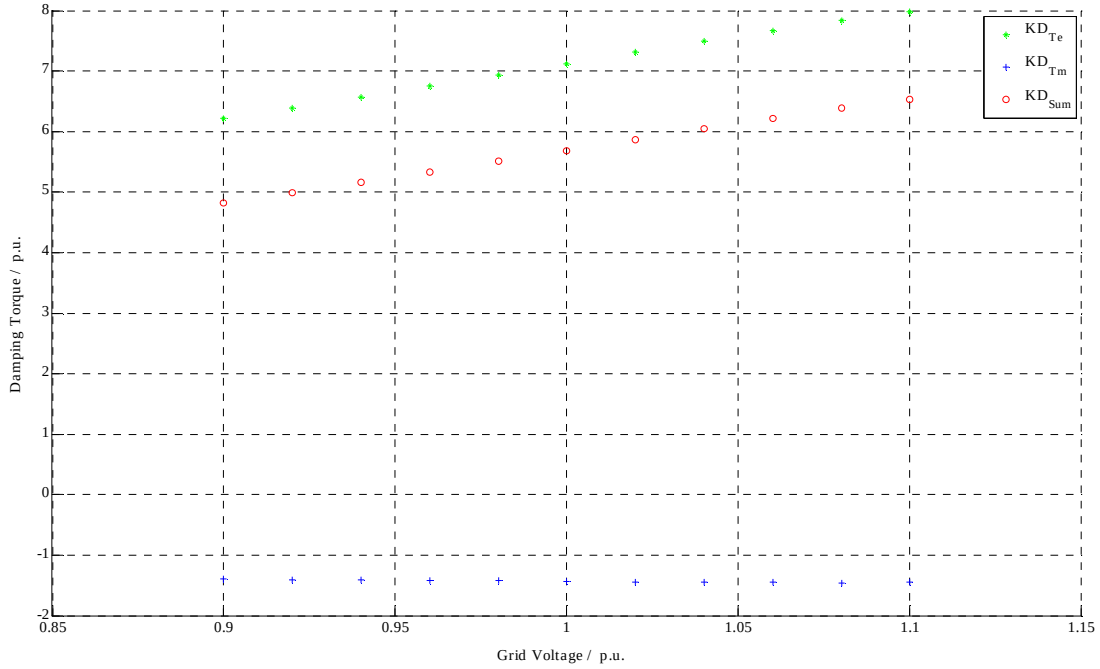

Figure 58: Damping torque components of $G_{Electrical}$ and $G_{Mechanical}$, variation of grid voltage

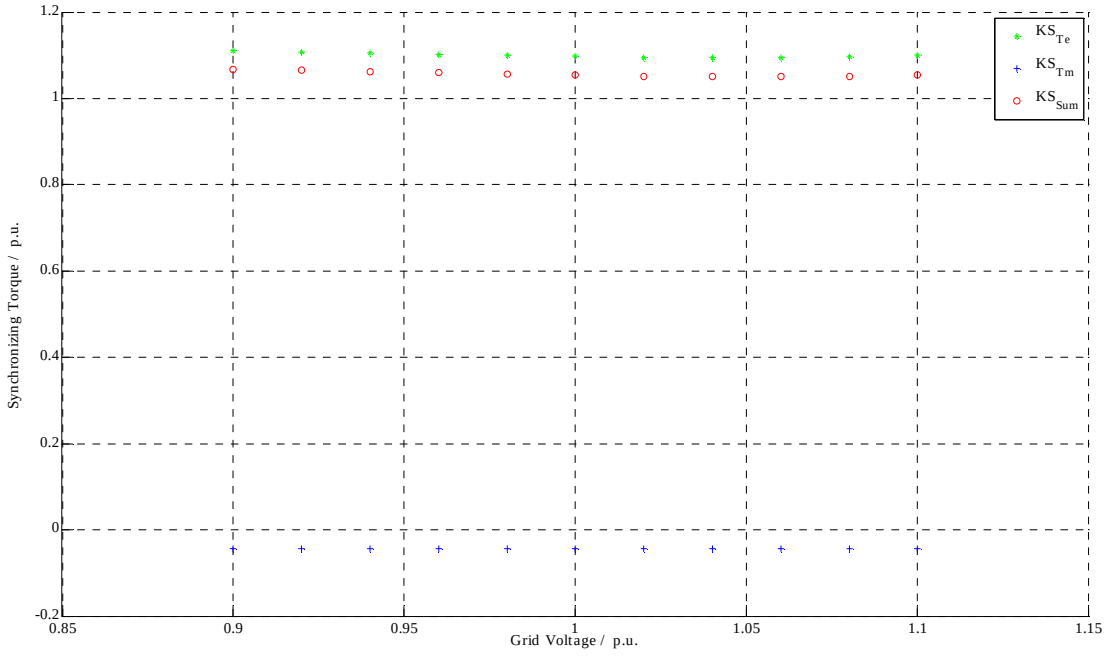

Figure 59: Synchronizing torque components of $G_{Electrical}$ and $G_{Mechanical}$, variation of grid voltage

6.3.4. **Modal Analysis and Torque Components**

Based on the modal analysis, the impact of the different PSS-G structures and parameterizations is investigated. The base case is compared with an individual parameter set, derived with the residue method, the generic Kundur-parameterization and a generic Multiband-approach.
The operating point is at rated active power of the generator at P_r = 0.8 p.u., controlling the stator voltage to V_S = 1 p.u.
The advantage of linear analysis is the straightforward mathematical problem formulation and the extensive controller design possibilities. A drawback is the fact that the solution is developed for a time snapshot, respectively a single operating point. This implies the suppression of the time domain limitation blocks, for example the actuator speed restrictions in the mechanical system of the governor.

	Eigenvalue λ_2	Damping	Frequency
	1/s ± 1/s	%	Hz
Base Case	-0.4 ± 6.8i	5.8	1.09
Residue	-0.7 ± 6.8i	10.7	1.08
Kundur	-1.0 ± 7.7i	13.2	1.22
Multiband	-2.7 ± 7.8i	33.0	1.24

Table 10: Eigenvalue of the mechanical oscillation of the base case, PSS-G activated

Table 8 gives an overview of the eigenvalue of the mechanical mode λ_2 for the base case and for the applied parameterization methods.
In Figure 60 the mode spectra of the investigated PSS-G devices, compared to the base case (blue), are shown. The controller modes arise in closed loop system with activated PSS-G and have to be considered, especially in the parameterization process.

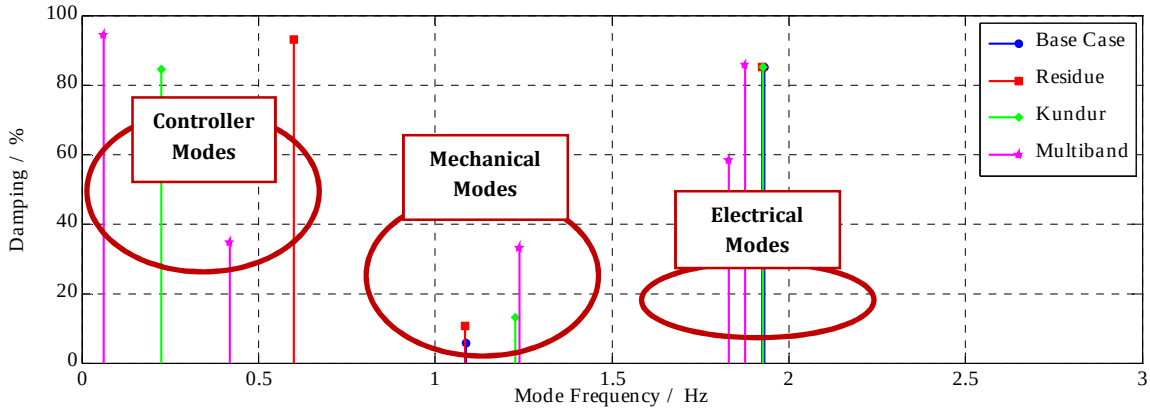

Figure 60: Mode spectrum for three PSS-G parameter sets, parameters derived from residue method, Kundur and generic multiband PSS

The base case situation in Figure 60 reflects the target mode at a frequency of 1.09 Hz and a damping of 5.8 %.
With the action of the PSS-G- parameterized with the use of residues- the mode damping can be increased to 10.7 % without changing the original oscillation frequency. This is achieved by the choice of the PSS-G gain as shown in chapter 6.3.1. As mentioned before, a former non-oscillatory mode gets to an oscillatory mode at a mode frequency of 0.6 Hz. The damping of this controller mode is comparatively high at 93 %.
The Kundur parameterization results in a damping of the mechanical oscillation of 13.2 % with a shift in oscillation frequency to 1.22 Hz. The controller mode occurs at a frequency of 0.22 Hz, again with a high damping of 84 %.
The generic multiband device increases the damping of the oscillatory mode to 33 %, shifting the resulting mode frequency to 1.24 Hz. This behavior can be attributed to the intermediate band and the high frequency band. The controller mode occurs at 0.41 Hz with a damping of 34.5 %. Furthermore highly damped modes, resulting from the low frequency and the high frequency band are induced as well.
Figure 61 shows the scatter plot of the poles for the base case and the three parameterization methods. The impact of the various damping devices is highlighted by the light blue frame. This view allows an insight to the movement of the mechanical mode of the base case towards the left half plain.

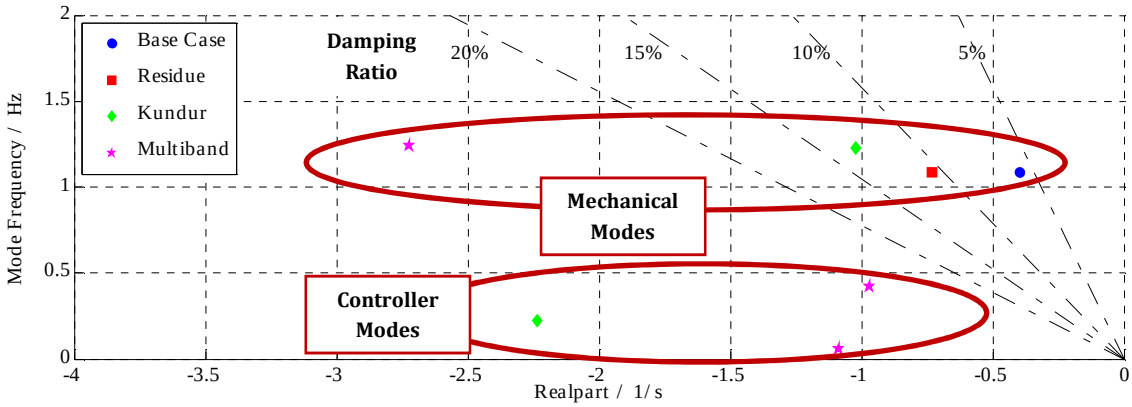

Figure 61: Scatter plot of the poles for the base case and the three PSS-G parameter sets, parameters derived from residue method, Kundur and generic multiband PSS

The marked area highlights the movement of the target mode. One can see that due to the choice of the controller gain $K_{PSS\text{-}G}$, the eigenvalue is shifted vertically only, whereas the other parameterizations increase the damping of the target mode at higher frequencies.
In Table 11 the dominant states of the mechanical and electrical modes are listed. Detailed values and scales are given in Appendix.

	Dominant System States	
	Mechanical Mode	Controller Mode
Residue	ω, d_w, Main Servo	ω, Main Servo, Pilot Servo, PSS-G
Kundur		ω, d_w, Main Servo, Pilot Servo
Multiband	IF1, IF4, HF1, HF4	d_w, IF1, IF4, HF1, HF4

Table 11: Dominant system states for various PSS-G parameterizations, mechanical modes and controller modes

Figure 62 depicts the damping and synchronizing torque components for the base case (no active PSS-G) and the three PSS-G configurations, provided by the electrical and the mechanical transfer function. Similar to the descriptions in Figure 49, the respective contributions as well as the resulting sum of the single components are drawn into the Δϑ/ Δω plane. The scaling of the axis is thereby similar in all four subfigures.
The residue parameterization adds a pure damping, resulting in a vertical shift of the sum vector (red) compared to the base case (blue). The resulting synchronizing torque component remains almost unchanged. This is congruent with the results from the modal analysis, respectively the modal spectrum in Figure 60. In contrast, the contribution from the governor side, respectively the PSS-G, adds a vertical damping component, resulting in a rotated vector of the torque components from the mechanical transfer function ΔT_m.

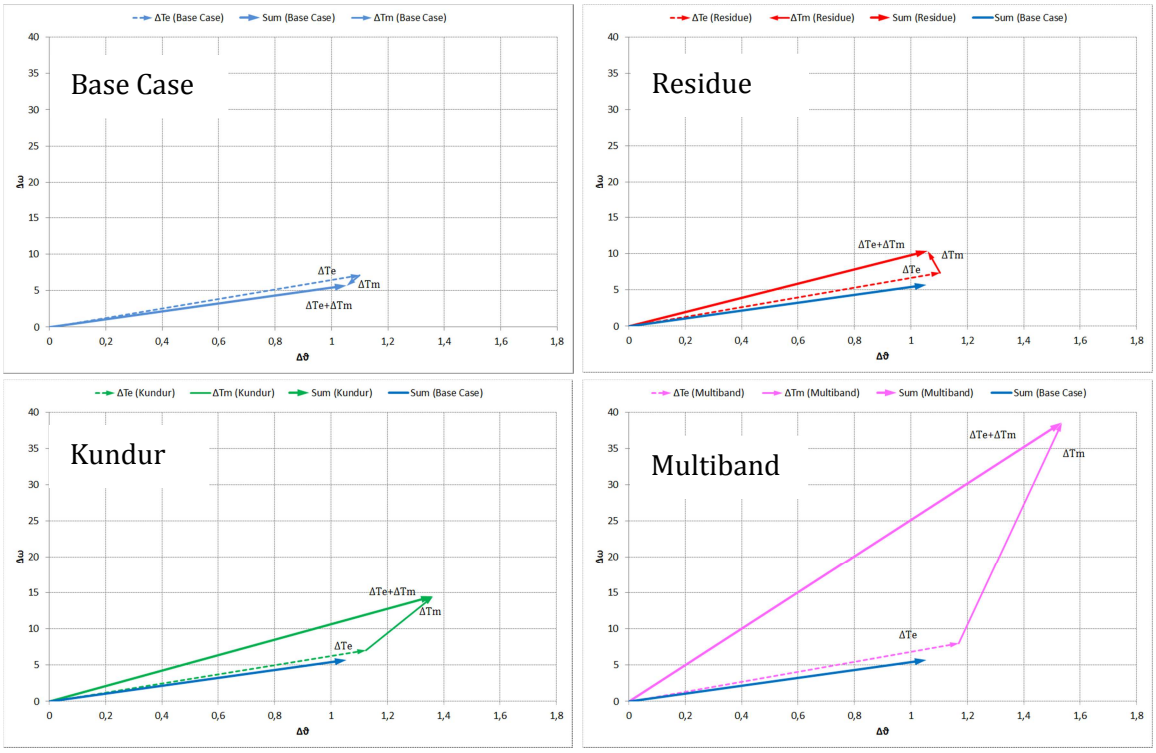

Figure 62: Damping and synchronizing torque components provided by the electrical and the mechanical transfer function for three parameterization methods Residue, Kundur and Multiband, compared to the base case(blue)

The Kundur and the Multiband parameterizations additionally add a synchronizing torque via the governor control path, resulting in a change of the mode oscillation frequency, as described in the modal analysis before.

Based on the same PSS-G structure, the contribution of the electrical transfer function ΔT_e remains constant for the residue and the Kundur parameterization. The structural difference of the Multiband PSS-G also introduces a slight increase of the damping and synchronizing torque of ΔT_e.
Despite this, it can be generally concluded from Figure 62 that the voltage control path is largely unaffected by a damping device, utilized in the governor control path.

6.3.5. **Robustness of PSS-G to Changes in Grid Impedance**

To get a picture of the robustness of the PSS-G, the three parameterizations are tested under varying grid conditions, respectively for varying grid impedance. The varying grid conditions can be referred to smaller changes in grid impedances due to changes in grid topology or larger changes due to line connections or disconnection in instant surroundings of the generator.
The variation is done from 0.4 to 0.04 p.u. in terms of generator base. The results are shown in Figure 63.
The base case without the use of a PSS is colored in blue, whereas the arrow represents the change of the grid impedance in descending order. The smaller the grid impedance gets, the higher is the damping, dominated by the contribution from the voltage control path. These characteristic has already been observed in the investigations of the linear characteristics of the voltage and the governor control path in chapter 6.3.3.
For the residue parameterization it is obvious that the amount of damping, provided by the PSS-G, is constant, compared to the base case. This leads to a parallel shift of the roots compared to the base case. Also the eigenvalue shift of the electromechanical mode is horizontal towards the left half plain, in accordance with the tuning target to introduce a pure damping.
The Kundur parameterization in general introduces additional synchronizing torque, resulting in an increased mechanical oscillation frequency. For high grid impedances the performances introduce a slight increment in damping, as shown by the green markers.
The multiband PSS-G provides almost constant damping over the whole scatter of grid impedances.
The occurring controller modes of all three variants of PSS-G show a generally satisfying damping with consistently increasing damping for lower values of grid impedances.

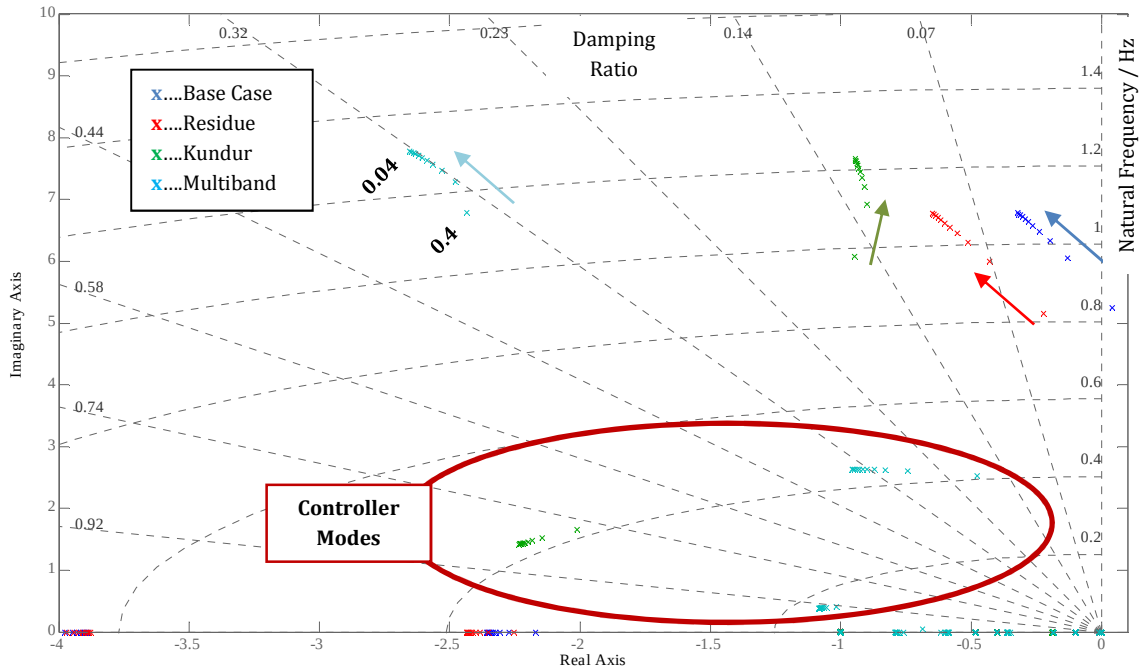

Figure 63: Comparison of the root loci for three PSS-G parameterizations (Residue, Kundur Multiband) and the base case, variation of grid impedance from 0.4 to 0.04 p.u., generator base

Concluding Figure 63 it can be summarized that these results confirm the observations from chapter 6.3.3, regarding the weak coupling and therefore a robust behavior of the governor control path against changes in grid conditions earlier in this chapter. The behavior of the structural different PSS-G standard parameter sets Kundur and Multiband is similar with constant damping in good approximation. The residue parameter set provides a constant amount of damping, compared to each base case scenario.

To visualize the impact of a change in grid conditions on the damping behavior of the excitation and governor control path, the Kundur parameterization is applied alternately as a PSS-E as well as a PSS-G. Figure 64 provides the results from the comparison, based on the variation of grid impedance from 1 p.u. to 0.1 p.u. This value range shows an obvious difference in the damping behavior.

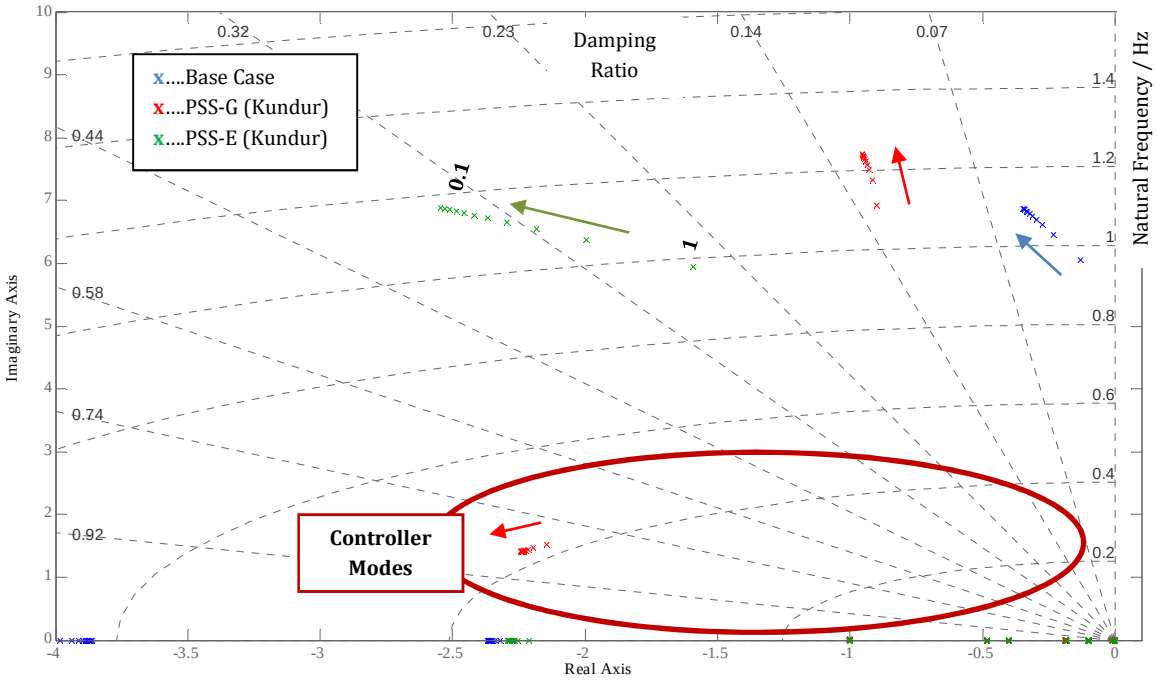

Figure 64: Comparison of the root loci for Kundur parameterization applied as PSS-E and PSS-G compared to the base case, variation of grid impedance from 1 p.u. to 0.1 p.u., generator base

At constant damping with good approximation in the governor path (red), the scatter of the damping in the excitation path varies in scale of more than 60 % (green), although the provided damping is higher for all cases.

Summarizing the results from Figure 63 and Figure 64, the robustness of the governor control path, including the alternately utilization of the three PSS-G devices, is shown based on the root shifts. The impact of the governor is predominately depending on the respective parameterization but hardly on the prevalent grid conditions. This favors the optimization of PSS-G parameter sets and increases the robustness in cases of varying grid conditions.

6.3.6. **Time Domain Simulation**

In the following the results of the time domain are examined using the nonlinear simulation model. The diagrams show the impact of the three parameterization methods described in 5.1 and 6.3.1 under the restrictions of the time domain, such as voltage output or governor speed limits.

A significant variable for the depictions in time domain is the accelerating power P_d (equation 6-7).

$$P_d = P_{mech} - P_{el} \qquad \textbf{6-7}$$

This variable has already been mentioned indirectly in the mathematical formulation of synchronous rotor oscillations 3-2 as the difference between mechanical and electrical power.

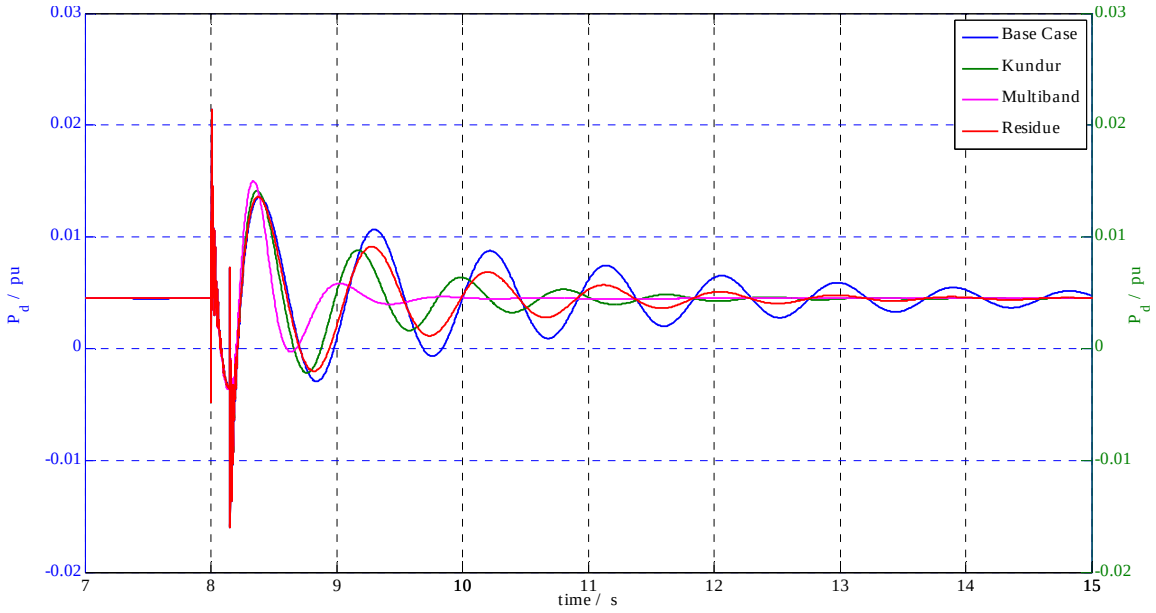

Figure 65: Accelerating power P_d, comparison of different controller configurations

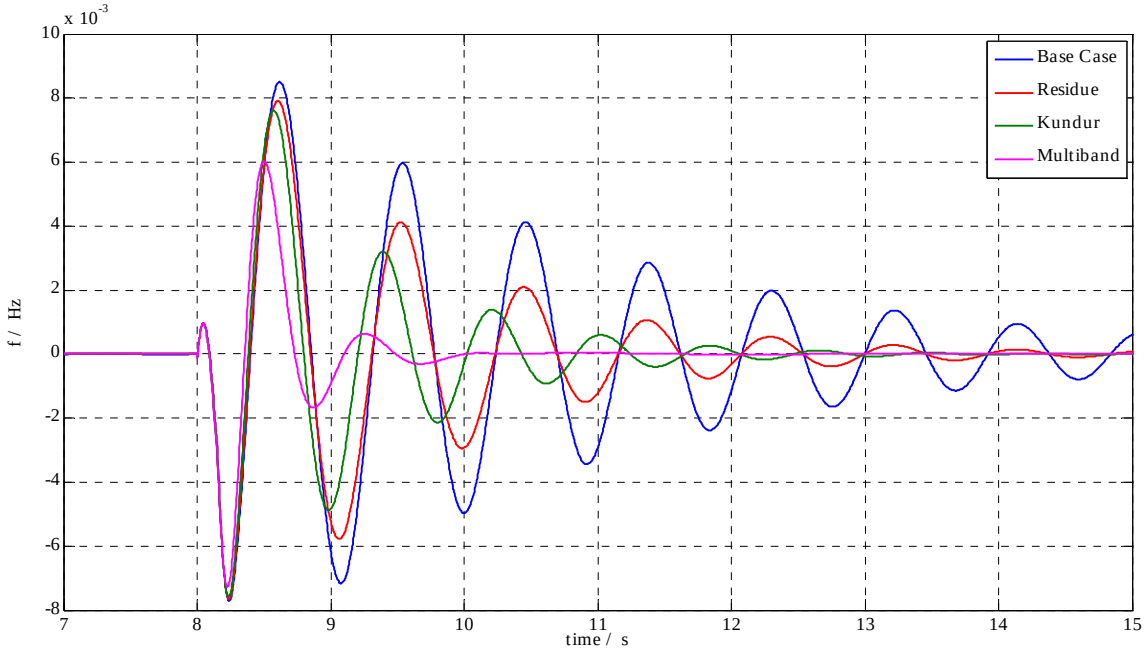

Figure 66: Speed deviation d_w, comparison of different controller configurations

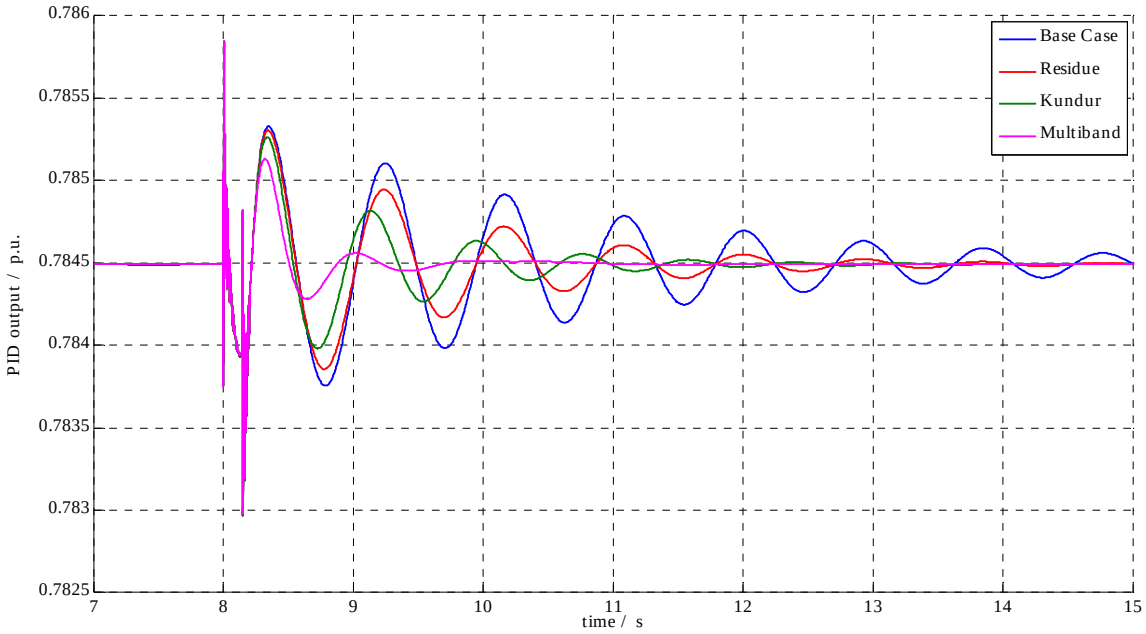

Figure 67: PID output of the governor, comparison of different controller configurations

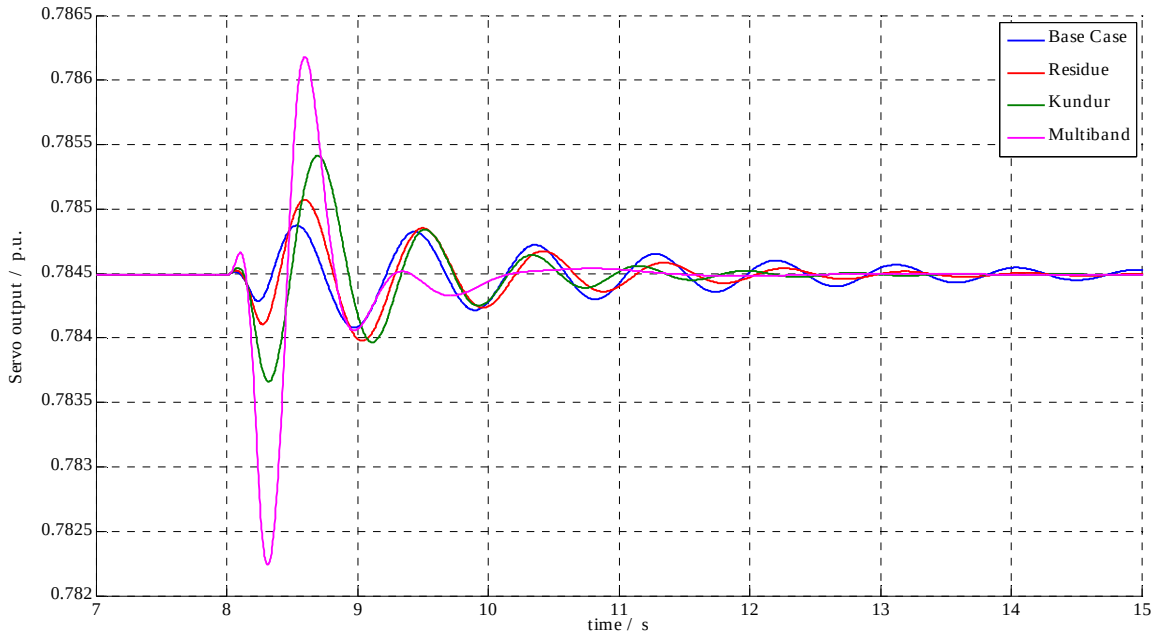

Figure 68: Main servo output, comparison of different controller configurations

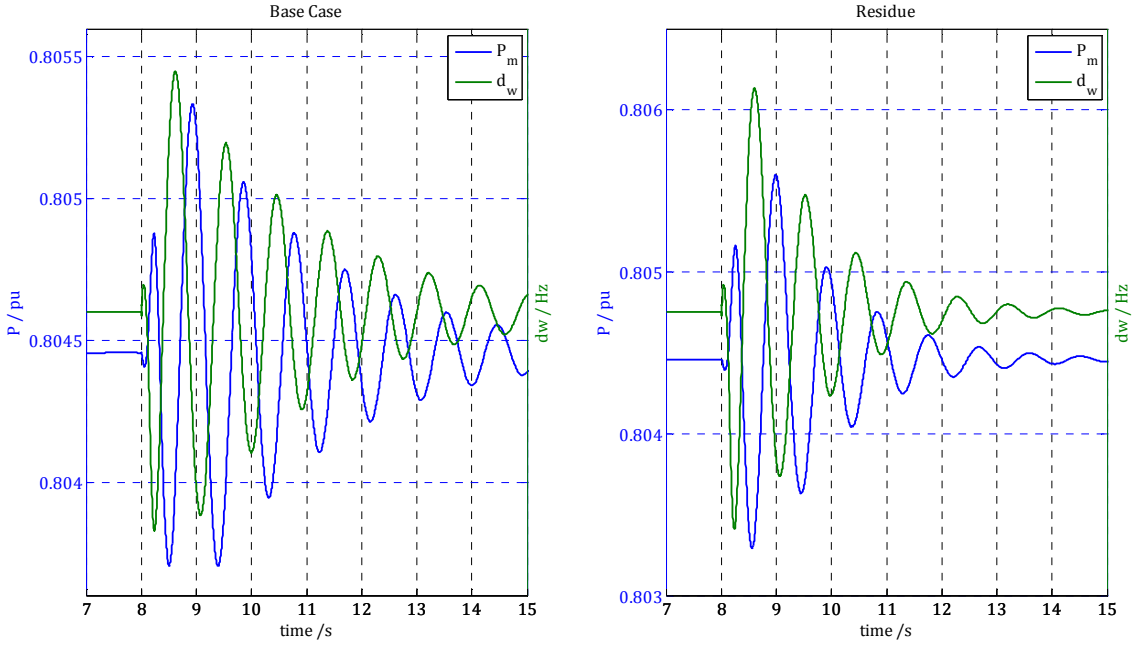

Figure 69: Mechanical power P_m and speed deviation base case (no PSS-G) and with PSS-G active (residue method)

6.3.7. **Summary of Results**

The single machine model, utilized in this chapter, is the first step to investigate the impact of the hydro governor to the system damping. Two standard parameterizations, respectively PSS structures (Kundur and Multiband) and a residue based parameterization are compared to a base case scenario. Regarding the residue parameterization, the focus is on the introduction of pure damping to the system. Basically the investigations are built upon a detailed linear analysis on the one hand and a nonlinear time domain simulation on the other hand.

The investigated base case implies an excited generator oscillation with a frequency close to 1 Hz. Although this scenario does not represent the optimal operational range of the PSS-G, it allows the derivation of principal characteristics of the governor control path as well as of the voltage control path.

From the analysis of the voltage and governor control path it is concluded that the governor control path is robust against changes in grid impedance and therefore against changes in grid conditions. In contrast the contribution of the voltage control path to system damping is varying for both, grid impedances and terminal voltage.

Similar characteristics have been observed when the three PSS-G parameterizations are applied. The amount of damping, provided by the PSS-G is constant for the investigated values of grid impedance. In contrast the application of the Kundur parameterization to the PSS-E indicates leads to a wide scatter of the additional damping.

The impact of the governor to system damping is thus predominately depending on the respective parameterization but hardly on the prevalent grid conditions. Therefore, the optimization of parameter sets for a target frequency is facilitated and more robust.

Furthermore, the governor control path provides negative damping over a wide range of oscillation frequencies. This contribution is commonly neglected in small signal stability for cases with dominating positive damping contributions from the voltage control path. However, especially for the investigated weak grid conditions this negative contribution of the governor needs to be taken into account.

The residue parameterizations have been designed to add pure damping without affecting the synchronizing torques and therefore the oscillation frequencies. In contrast, the standard parameterizations show a noticeable influence on the resulting mode spectrum of the mechanical mode. Thus, the residue parameterization method is the basis for the further work.

The modal analysis and the time domain simulations show the principle capability of the governor system to contribute to the enhancement of system damping. Depending on the respective parameters of the PSS-G and on the utilized PSS-G structure, a considerable impact on system damping has been identified. Additionally the implantation of a PSS-G remains without side effects on the voltage control.

The potential operational range of the governor to act as a damping device is at oscillation frequencies below 1 Hz down to very low frequencies from the linear point of view. In this range the governor control path shows favorable behavior compared to the excitation

control path. The factual operational range is given by the respective actuator speed limits and the type of governor, respectively hydro turbine.

6.4. Multi Machine Model

In contrast to the single machine infinite bus model in chapter 6.3 in this section the focus is on the interaction between the generators and the effectiveness of the damping devices on an inter area mode. Two areas, each containing two generators, are connected via inter tie lines. The substitute generators Grid 1 and Grid 2 represent the dynamics of the surrounding grid. Due to their values of apparent power they dominate the overall system inertia. Hence, the inter area mode, propagating along the tie lines is in the value range of interest close to 0.4 Hz.
The occurring inter area mode between area 1 and area 2 is thus the target mode for the parameterization of the respective damping devices.
To compare the contribution of the PSS-G with the effectiveness of the classical PSS-E, several parameterizations are implemented, using various input signals. Furthermore, the impact on system damping of the PSS-G and the PSS-E is opposed. The focus is thereby on the investigation of weak grid conditions, where the PSS-G shows promising results in the single machine infinite bus model in chapter 6.3.

The basement for the following investigations is the simulation model in Figure 70. The excitation of the inter area modes is again provided by a three phase fault of 150 ms duration.

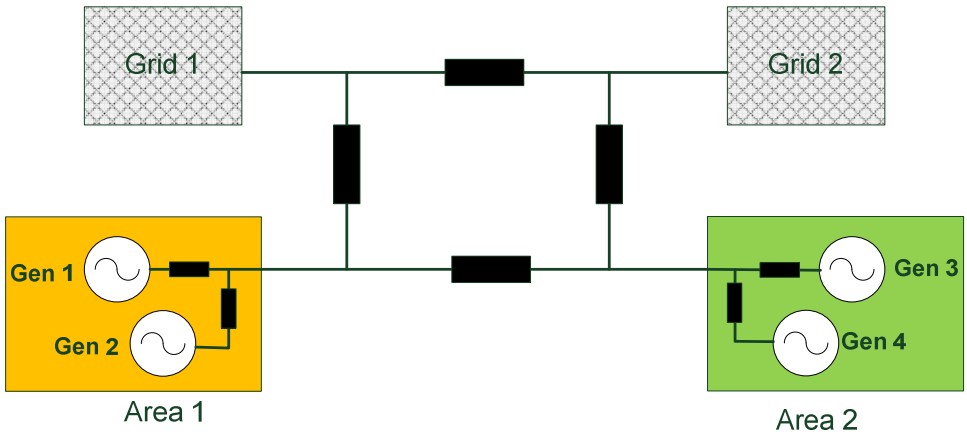

Figure 70: Principle block diagram of the multi machine simulation model, related to the Prabha Kundur two-area-system

To derive the best siting, respectively the most effective generator for the application of a PSS device, the participation factors of characteristic system states as well as the characteristics of transfer functions and the respective residues are analyzed. Hence, different remote signals for the damping devices are compared for the resulting generator site, regarding their effectiveness to damp the inter area mode.

6.4.1. **Characteristics of the Base Case**

The description of the base case characteristics is separated in a reflection of the linear characteristics of the system as well as a nonlinear simulation with the illustration of significant variables.

Linear Characteristics

In Figure 71 the modal spectrum of the first base case scenario is shown. The target mode is at 0.39 Hz with a poor damping of 1.48 %.

The mode Grid 1-2 refers to the substitute grid representations Grid 1 and Grid 2 and the damping is satisfying at more than 30 %. The mode Grid 1 represents the oscillation against the rest of the system, analogously valid also for Grid 2. The two local modes in area 1 and area 2 provide a damping of nearly 15 % respectively 10 % and occur in the typical range of local oscillations.

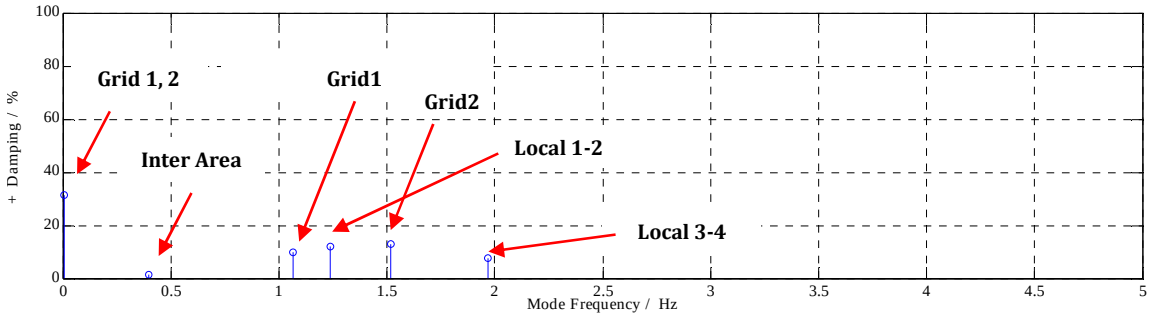

Figure 71: Modal spectrum of the Base Case

The dominant states listed in Figure 72 refer to the substitute grid representations Grid 1 and Grid 2.

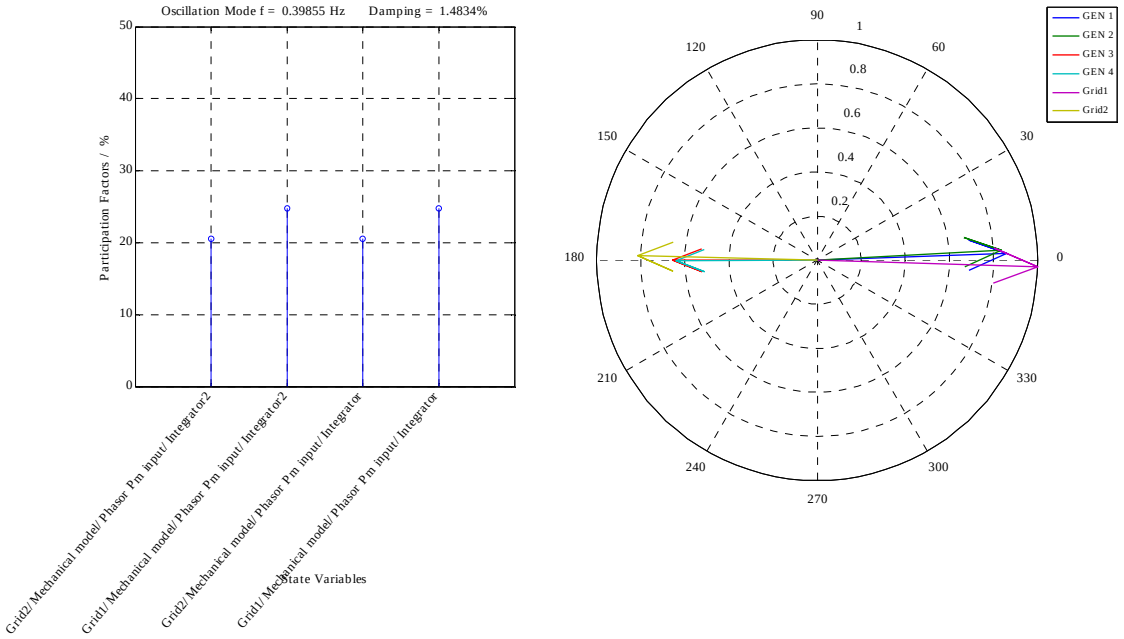

Figure 72: Participation factors and mode shape for the inter are mode

From the mode shape in the right half of Figure 72 is it obvious that its characteristic is from a classical inter area mode with the right eigenvectors of the speed deviations in phase opposition.

Table 12 lists the dominant poles of the modal analysis, complemented by the respective natural frequency of modes.

Number of λ	Eigenvalue λ		Damping	Frequency
	1/s ± 1/s		%	Hz
1	-0.950	12.360	7.66	1.967
2	-1.256	9.543	13.05	1.519
3	-0.938	7.784	11.96	1.239
4	-0.653	6.703	9.70	1.067
5	-0.037	2.504	1.48	0.399
6	-0.013	0.041	31.38	0.006

Table 12: Poles, damping, frequency and natural frequency of the base case

The target mode for the parameterization of PSS-G and later on PSS-E is therefore the inter area mode, represented by eigenvalue λ_5.
Exemplary applying 4-7 and 4-9 to generator 2, the damping contributions can be calculated for the target eigenvalue.

$K_{D\text{-}\Delta Te\_GEN2}$ = 3.61 p.u. torque / p.u. speed change
$K_{D\text{-}\Delta Tm\_GEN2}$ = -3.2 p.u. torque / p.u. speed change

The resulting damping torque provided by generator 2 is thus
K_{D_GEN2} = 0.41 p.u. torque / p.u. speed change

From the ratio of $K_{D\text{-}\Delta Te\_GEN2}$ and $K_{D\text{-}\Delta Tm\_GEN2}$ it obvious that the negative damping torque provided by the governor, should not be automatically neglected, especially for the predominant weakly damped modes.

Nonlinear Characteristics
The speed deviations of the four generators in area 1 and area 2 are derived from the time domain simulation and are represented in Figure 73. After the short circuit event at t=5 s the modes with higher frequencies decay within the first 6 s after the event. After t=11 s, the inter area mode can be clearly seen as two generators in each area swing in opposite phase. The initial amplitude of the inter area oscillation is around 25 mHz around t= 10 s.

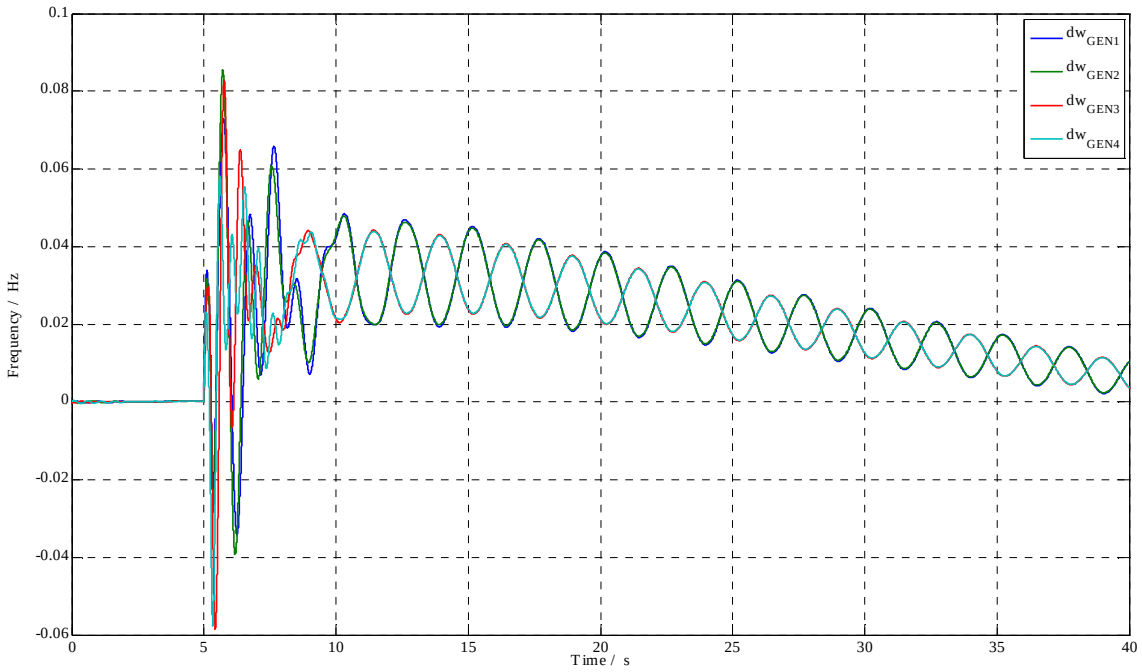

Figure 73: Speed deviations of the generators excited with a short circuit behind an inductance

Figure 74 shows the electrical and mechanical output power as well as the governor signals of generator 2. Even without active PSS one can see that the governor reacts to both, the fast decaying local oscillations, as well as to the inter area oscillation.

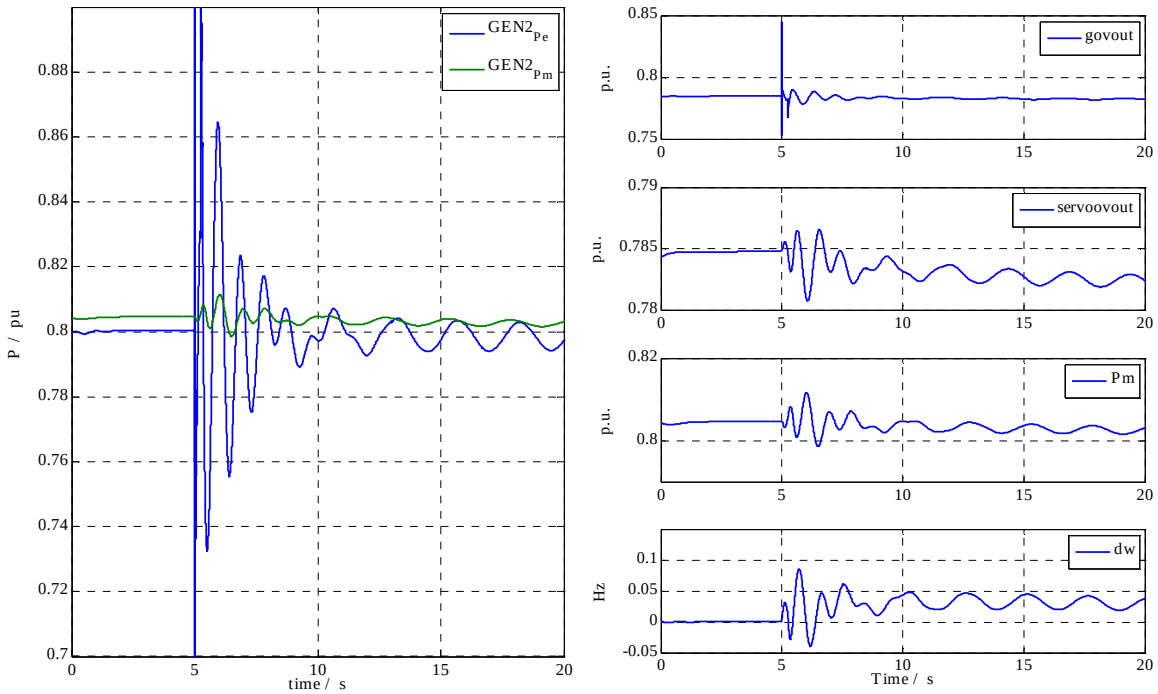

Figure 74: Electrical and mechanical power and governor signals of generator 2 for the base case

6.4.2. **Siting, Selection of Input Signals and Parameterization of PSS-E and PSS-G**

The proper positioning of damping devices, parameterized for the considered oscillation, is the fundament of an effective and reliable operation. Based thereon, a suitable input signal in accordance with a parameter set, derived for the oscillation mode of concern, needs to be selected to obtain sufficient results.

The participation factors of the speed deviation in Figure 75 contain the left and right eigenvector elements, respectively the modal observability and controllability of the state speed deviation to the target mode λ_5. The values are normalized to the highest participation, in this case generator 2. Although the participation factors give a good indication, which generator is a proper candidate the participation factors, they only rely on states and not on inputs and outputs of the transfer function of interest.

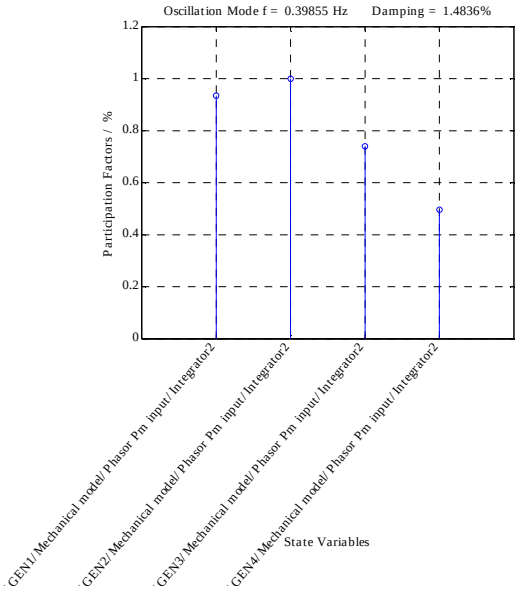

Figure 75: Participation factors of the speed deviations for the inter are mode, normed to the maximum value

Hence, the respective residue from the transfer function of the output of the future PSS-G device to the potential input signal is analyzed for the target mode. In Table 13 the residues and their angles are listed for the transfer functions obtained by the input signal of interest. The best siting, or rather the best candidate for the application of a PSS-G or a PSS-E, is done on the basis of the local signals speed deviation d_w, generator output power P and accelerating power P_d, as well as on the synthesized WAMS signals tie line active power P_{line} and angular difference $d_{theta\ line}$.

In this context it is important that only residues resulting from the same type of signals are compared with each other [9].

The local signal speed deviation d_w is scaled by the factor sca in 6-8. This allows the comparison with the local generator power P and P_d in case that mechanical damping of the generator is neglected and mechanical torque is assumed to be constant [9].

$$sca = H \cdot \lambda_i \qquad \textit{6-8}$$

The angles of the residues in Table 13 can be positive or negative, depending on the eigenvalue they belong to.

		Input Signals					
		Local			WAMS		
		d_w	P_d	P	P_{line}	$d_{theta\ line}$	
PSS-G	Gen1	0.0211	0.0418	**0.0389**	0.072	23.6	$abs(R_5)$
		±175.2	±94.2	±92.6	±85.4	±96.8	β_{comp}
	Gen2	**0.0221**	**0.0437**	0.0371	**0.089**	**29.0**	$abs(R_5)$
		±153.3	±62.8	±124.7	±55.1	±66.5	β_{comp}
	Gen3	0.0164	0.0326	0.0291	0.066	21.5	$abs(R_5)$
		±172.0	±97.3	±93.3	±93.3	±82.0	β_{comp}
	Gen4	0.0109	0.0217	0.0196	0.053	17.3	$abs(R_5)$
		±172.2	±97.1	±94.9	±93.3	±82.0	β_{comp}
PSS-E	Gen1	0.0052	0.0104	**0.0098**	0.018	5.9	$abs(R_5)$
		±175.4	±93.9	±92.6	±85.2	±96.5	β_{comp}
	Gen2	**0.0056**	**0.0111**	**0.0098**	**0.022**	**7.3**	$abs(R_5)$
		±175.7	±85.2	±102.7	±77.5	±88.9	β_{comp}
	Gen3	0.0034	0.0068	0.0065	0.014	4.5	$abs(R_5)$
		±147.5	±121.8	±68.5	±68.8	±57.4	β_{comp}
	Gen4	0.0022	0.0044	0.0043	0.011	3.5	$abs(R_5)$
		±158.8	±110.5	±81.4	±79.9	±68.6	β_{comp}

Table 13: Absolut values R_5 and angle β_{comp} of residues for local and WAMS Signals, PSS-G and PSS-E; the respective maximum is marked bold; speed deviation is scaled following 6-8

From the red marked magnitudes in Table 13, the best candidate for applying a PSS-G or PSS-E is area 1, respectively generator 2. The siting, based on the participation factors in Figure 75, is therefore confirmed. Due to the scaling of the speed deviation it is also obvious that the accelerating power P_d is the most promising local signal.

Based on the results in Table 13, the PSS-E and PSS-G devices were parameterized for the local input signals speed deviation d_w, accelerating power P_d as well as for the WAMS

signals of the interconnection tie line active power P and angular difference $d_{theta\ line}$ between the two areas. According to the control target for the single machine infinite bus system in chapter 6, the parameters of the PSS are derived to add pure damping to the system. The amount of synchronizing torque should therefore be unchanged.
The standard parameter sets from Kundur and Multiband parameterization, used for the single machine infinite bus system in chapter 6, are not considered any more.

The parameterizations have been derived by root locus plots similar to the process applied for the single machine infinite bus system in chapter 6.3.1. For varying angles of departures of the target root the PSS gain is varied. The respective phase compensation and controller gain are derived from the root position, where

- the controller shall **introduce** a **pure damping**, meaning no change in synchronizing torque components and
- the damping of other eigenvalues respectively modes (occurring controller modes) shall **not decrease below 10 %**

Representative for all parameterizations in Table 14, this process is shown in Figure 76 for the PSS-G, using the most effective local signal accelerating power P_d as an input signal.

Figure 76 provides the root locus plot, covering the shifts of the concerned eigenvalues, using the PSS-G with various parameterizations, respectively various angles of departure and various controller gains.
Outgoing from an angle of departure, the controller gain $K_{PSS\text{-}G}$ is varied from 0-20. The shown initial values of the root traces are pointed out with red arrows and are identical with the values in Table 12 and Figure 71. The result of the gain variation is one dashed line of a certain color.
One can see which roots are sensitive to the use of PSS-G and which roots do not shift at all.
Figure 77 gives a more detailed insight to the shift of the target inter area mode. For the angle of -130° the maximum (linear) damping can be given with 15.7 %, which is near the nose point of the dashed yellow line. The setting value for the PSS-G gain is therefore 13.3.

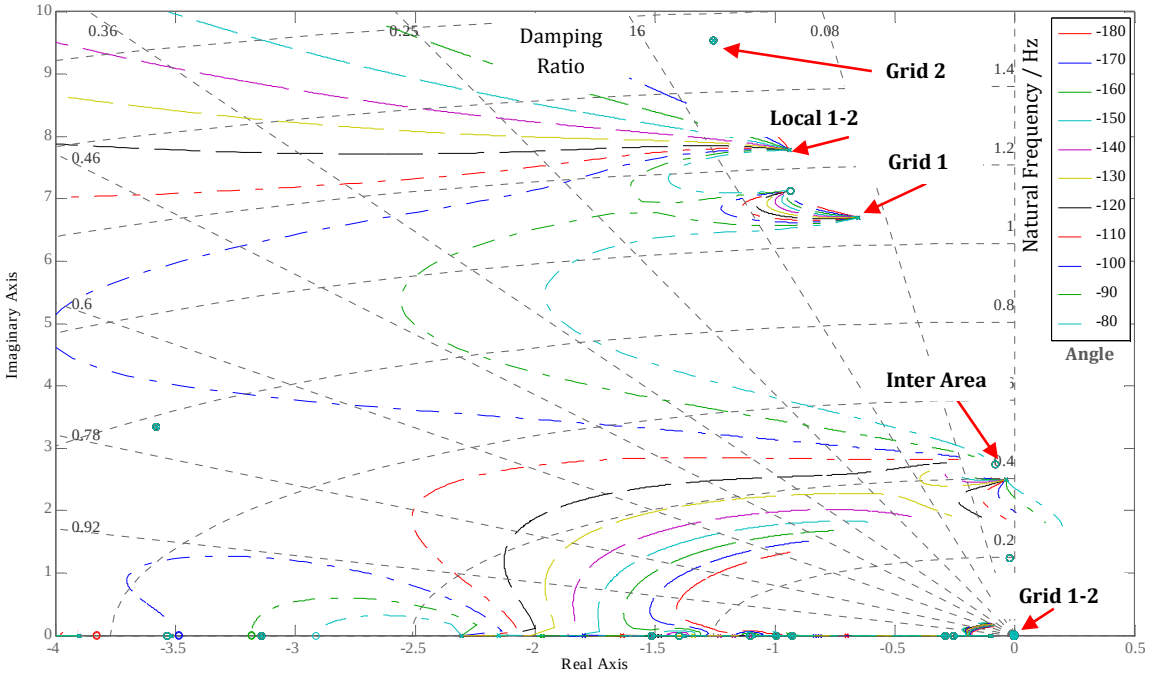

Figure 76: Root locus for varying angles of departure, and varying gain $K_{PSS\text{-}G}$ (from 0 to 20), local signal P_d as input signal

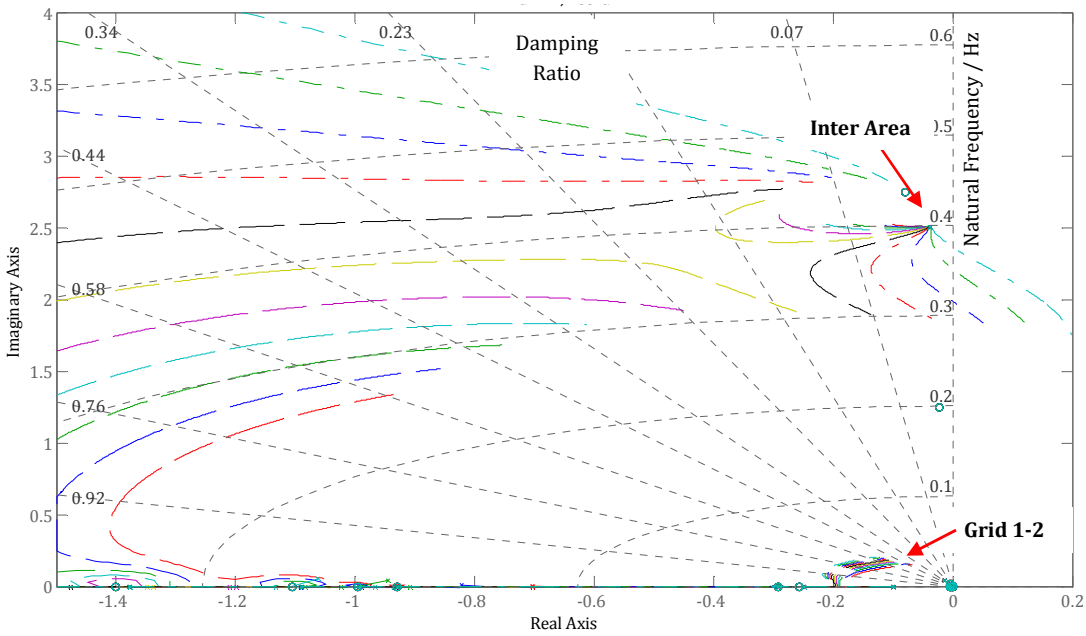

Figure 77: Root locus for varying angles of departure, varying gain $K_{PSS\text{-}G}$ (from 0 to 20), local signal P_d as input signal, zoom at inter area mode

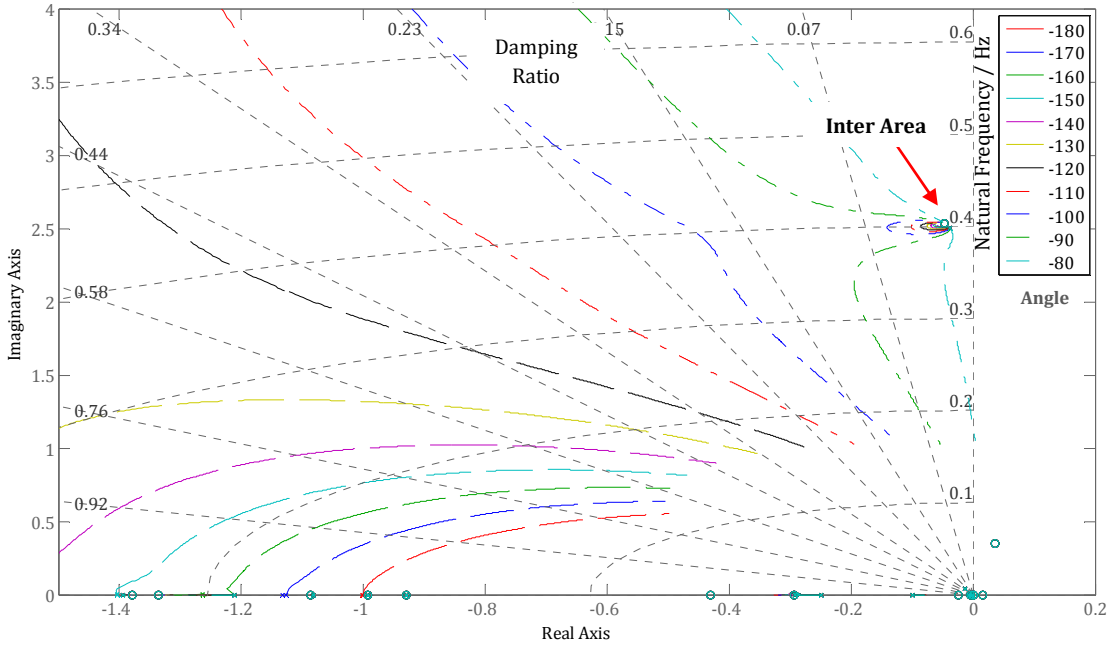

Figure 78: Root locus for the inter area mode, PSS-E for various angles of departures and controller gain K_{PSS-E} varied from 0-20, local signal P_d as input signal

Comparing the root traces of the inter area mode in Figure 77 and Figure 78 it can be concluded, that the PSS-G is more sensitive and thus more effective to damp the inter area mode than the PSS-E. In both figures the controller modes in the lower left corner remain sufficiently damped.

Input Signal	K_{PSS-G}	Angle of Departure	T_s	T_w	T_{lead}	T_{lag}	m	Maximum Damping
	p.u.	°	s	s	s	s		%
d_w	20	-140	0.01	10	0.4488	0.3554	2	4.1
P_d	13.4	-130	0.01	10	0.2141	0.745	2	15.7
P_{line}	0.75	-100	0.01	10	0.2672	0.5969	2	5.5
$d_{theta\ line}$	0.06	-150	0.01	10	0.1788	0.8919		19.1
Input Signal	K_{PSS-E}	Angle of Departure	T_s	T_w	T_{lead}	T_{lag}	M	Maximum Damping
	p.u.		s	s	s	s		
d_w	6.16	-100	0.01	10	0.8162	0.1954	2	2.0
P_d	3.96	-100	0.01	10	0.3507	0.4548	2	4.9
P_{line}	6.69	-120	0.01	10	0.2732	0.5837	2	7.7
$d_{theta\ line}$	0.158	-160	0.01	10	0.2054	0.7766	2	13.7

Table 14: Parameters of the PSS-G and PSS-E and expected damping for inter area mode, K_{PSS-X} controller cain, T_s transducer time constant, T_w wash-out time constant, T_{lead} lead time constant, T_{lag} lag time constant, m number of lead/lag compensators

Table 14 summarizes the expected damping of the inter area mode and the calculated parameters for the PSS-G and PSS-E based on varying transfer functions, respectively input signals.

It can be concluded that for the criterions (no influence on mode frequency and no other eigenvalue with damping ratio below 10 %) and for the target mode at 0.4 Hz, the PSS-G using the input signal $d_{theta\ line}$ is the best solution. This configuration is also the basis for the considerations in 6.4.3.
Regarding the expected mode damping, derived in the root locus plots for both devices, the best local signal is the accelerating power P_d as well as the best WAMS signal is $d_{theta\ line}$. Furthermore, the maximum damping is calculated for WAMS signals which is congruent with the expectation that the best handling of the inter area mode can be achieved using a WAMS signal.

Robustness against Variation of Grid and Operational Parameters

Varying grid conditions have a real background and are inherent to system operation. Changes in grid impedance or in grid inertia are from manifold root causes, described in more detail in chapter 2.1. The current grid inertia in the RG CE system is correlated to the infeed situation of renewable energy sources, such as wind or PV generating units. Furthermore, the active power output of the generator is varying according to the operational situation.
To determine the robustness of the damping devices the grid conditions are changed around the operating point of the base case and hence, the shift of the corresponding eigenvalue is visualized in root locus plots. Based thereon, trends of the damping of the inter area mode for varying grid conditions can be derived. As derived in chapter 6.4.2, generator 2 is equipped with a PSS-G or with a PSS-E.
In the following figures the system is exposed to changes in the operating point of generator 2 (variation of P_m) and the change in oscillation frequency (variation of grid inertia).
The arrows in the following figures indicate the direction of the variation and thus of the resulting eigenvalue shift of the inter area mode. Other modes correspond to controller modes and are of secondary interest for these observations.

Variation of Generator Active Power

The variation of the generator output power is provided for the range from P_{gen} = 0.6 p.u. up to P_{gen} = 1 p.u. The respective eigenvalue shifts are visualizes in pole zero maps for the PSS-G application in Figure 79 and for the PSS-E in Figure 80.
Analyzing Figure 79 one can see that the most promising input signals for the PSS-G (accelerating power P_d and tie line angle difference $d_{theta\ line}$) provide the expected high damping but with a comparable high sensitivity to generator output power variation. Also the tendency is towards decreasing mode damping for increasing operating points of the generator. In contrast the remote signals speed deviation and tie line active power

propose an increasing tendency in mode damping, whereas their contribution to damping is less.

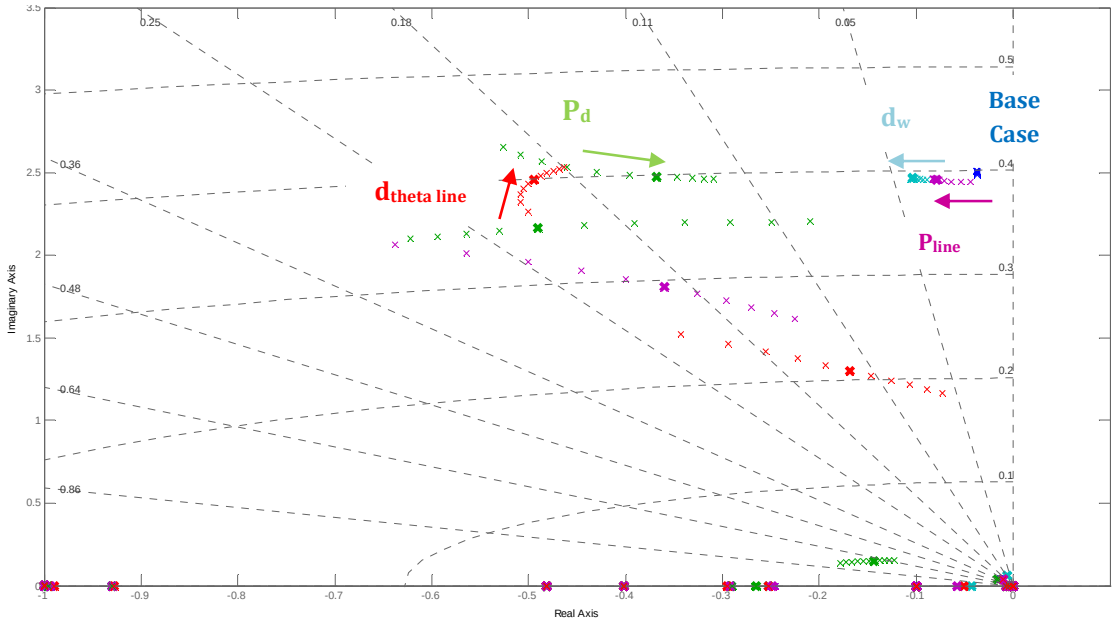

Figure 79: Scatterplot of the system eigenvalues with PSS-G applied, variation of active power of generator 2 of the base case (markers in bold), input signals d_w ,accelerating power P_d, tie line power P_{line} and voltage angle difference $d_{theta\ line}$ $d_{P\ line}$

The PSS-E parameterizations show an increasing mode damping throughout the variations of the operating point. At the same time the resulting oscillation frequency is almost unaffected by the variation of generator output power.

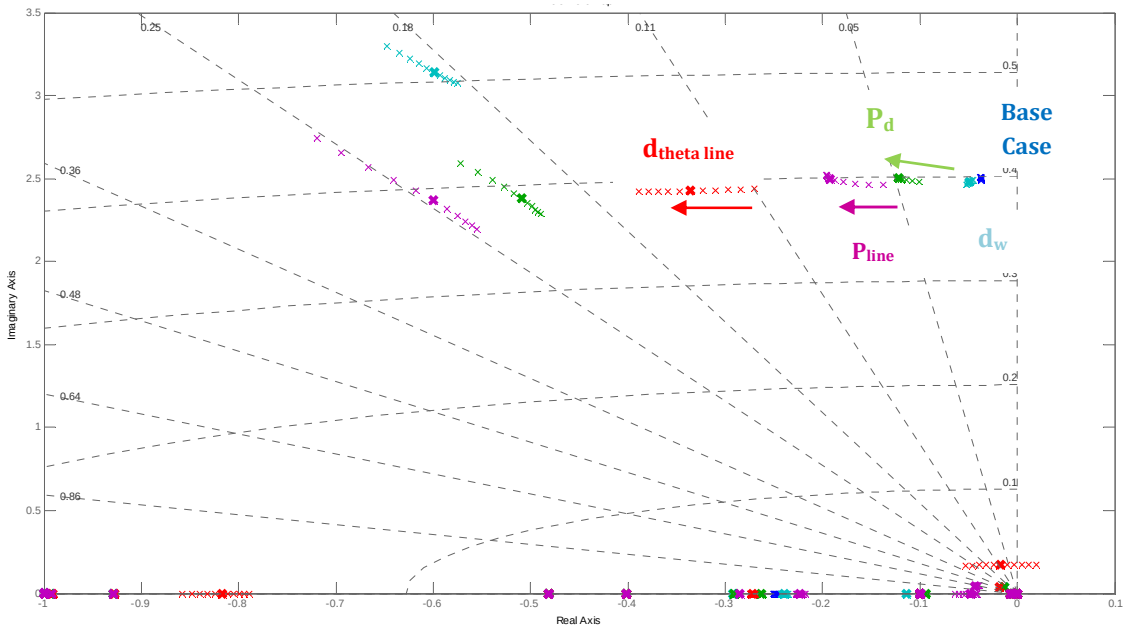

Figure 80: Scatterplot of the system eigenvalues with PSS-E applied, variation of active power of generator 2 of the base case (markers in bold), input signals d_w ,accelerating power P_d, tie line power P_{line} and voltage angle difference $d_{theta\ line}$ $d_{P\ line}$

Summarizing Figure 79 and Figure 80 a more robust behavior of the PSS-E parameterizations can be established. Although the highest damping is provided by the PSS-G, the PSS-E shows a comparably low sensitivity with a tendency towards stronger damping throughout the variation range.

Variation of Grid Inertia

For the investigation of the root shift of the eigenvalue, representing the inter area oscillation in case of variations of grid inertia, the root locus Figure 81 is analyzed. The grid inertia is varied from 0.8 p.u. to 1.2 p.u., resulting in a shift of the mechanical oscillation frequency around the value for the base case, given with 0.39 Hz. The arrows denote the decrease in oscillation frequency, respectively the increase of system inertia.

The root locus in Figure 81 shows the conditions with activated PSS-G for varying input signals. In the base case the damping of the inter area oscillation is slightly decreasing for lower oscillation frequencies. Similar characteristics can be observed for the local signal speed deviation d_w, as well as for the tie line active power P_{line}. For the input signals of accelerating power P_d, as well as for the angular difference $d_{theta\ line}$ the mode damping is increasing for lower frequencies.

Concluding Figure 81 with active PSS-G one can observe that input signals with a high impact on the damping of the inter area mode, like P_d and $d_{theta\ line}$, also show a quite high sensitivity to changes in the mode oscillation frequency. The trend of changes in damping shows a tendency towards increased damping for lower frequencies of the inter area mode. Nevertheless the introduced damping is much higher than the contributions using tie line active power and speed deviation whereas the sensitivity to varying oscillation frequencies is less.

In contrast, the root loci with the PSS-E, applied at generator 2, shows a trend in direction of a decreasing damping of the inter area mode for lower oscillation frequencies. This observation can be made for all applied input signals. The appropriate eigenvalue drifts are shown in Figure 82.

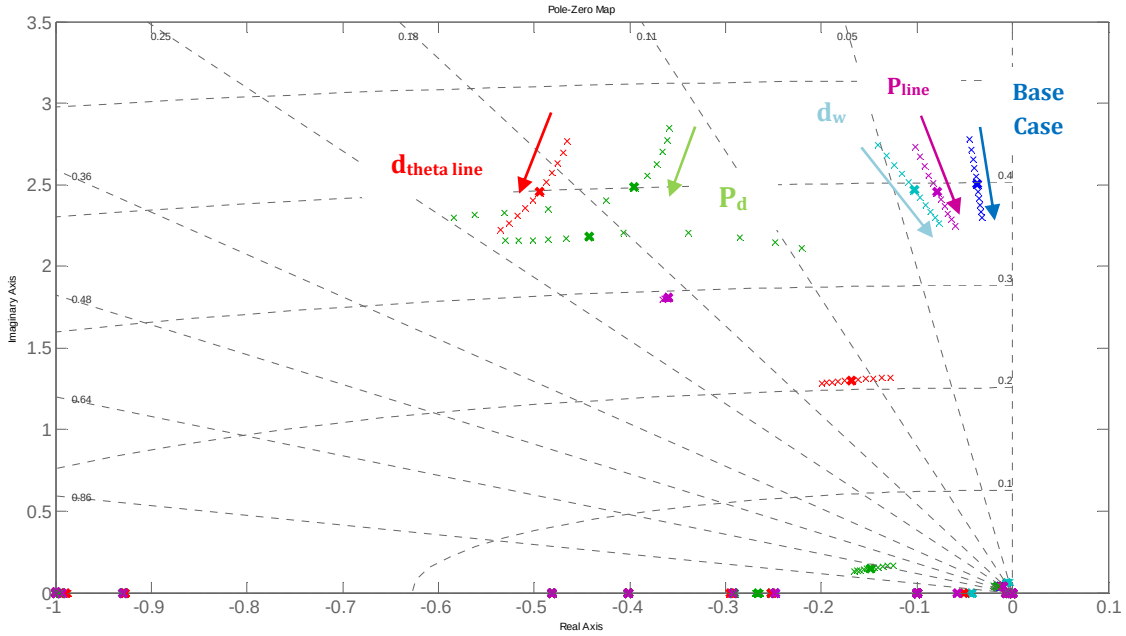

Figure 81: Scatterplots of the system eigenvalues with PSS-G applied, variation of oscillation frequency around the base case (markers in bold), speed deviation d_w, accelerating power P_d, tie line power P_{line} and voltage angle difference $d_{theta\ line}$ $d_{P\ line}$

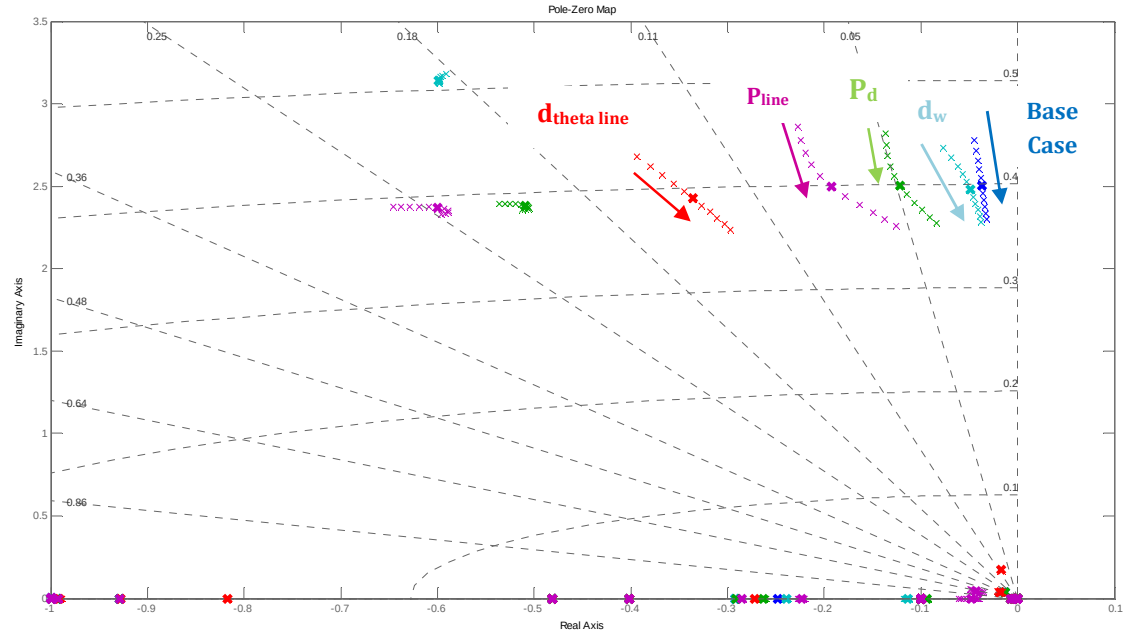

Figure 82: Scatterplots of the system eigenvalues with PSS-E applied, variation of oscillation frequency around the base case (markers in bold), input signals speed deviation d_w, accelerating power P_d, tie line power P_{line} and voltage angle difference $d_{theta\ line}$ $d_{P\ line}$

Figure 82 shows a decreasing tendency of mode damping for lower oscillation frequencies when the PSS-E is utilized with various input signals.

Comparison of PSS-E and PSS-G in Time Domain (Position optimal)

In the time domain simulation the parameterizations for the local signal P_d is investigated more closely. All other variants provide similar results in principle and are therefore not quoted in more detail at this point.

The excitation of the generator oscillations results from a three phase short circuit near the middle of the inter connection line. The fault lasts for 150 ms and is not causing and change in connection impedance of the generators, meaning a fault location outside the concerned two area system.

The time courses in Figure 83 and Figure 84 are obtained from the system with PSS-G active at generator 2 and using the local accelerating power P_d as an input signal. Each of them is divided in two diagrams. The left half plain contains generator 1, the right half plain generator 2 with the PSS-G activated. During the development of the inter area mode after t = 10 s, the magnitude of the mechanical power P_m of generator 2 provides nearly opposite phase to the speed deviation and high sensitivity resulting in a high magnitude compared to generator 1.

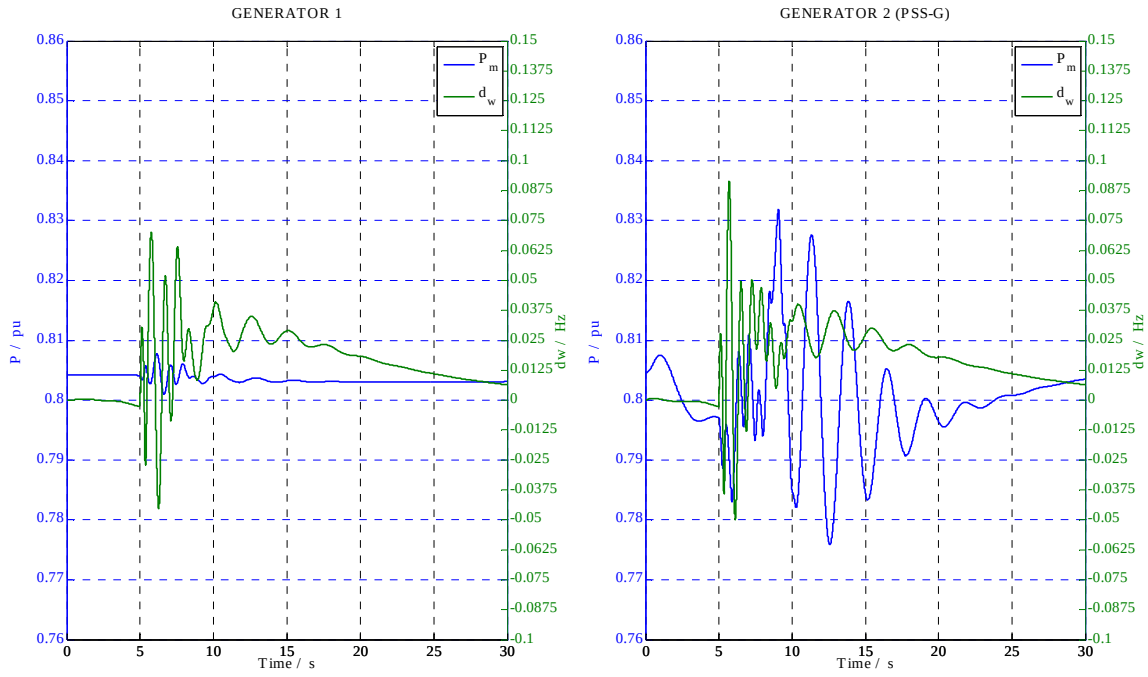

Figure 83: Mechanical power and speed deviation of Generator 1 and Generator 2 (with PSS-G)

Looking at Figure 84, one can see, that the magnitude of the mechanical power deviation is in the range of the electrical power deviation for generator 2 (right). Furthermore, the phase of the electrical and mechanical power shows quite good accordance. The reaction of the governor of generator 1 is thereby comparably small.

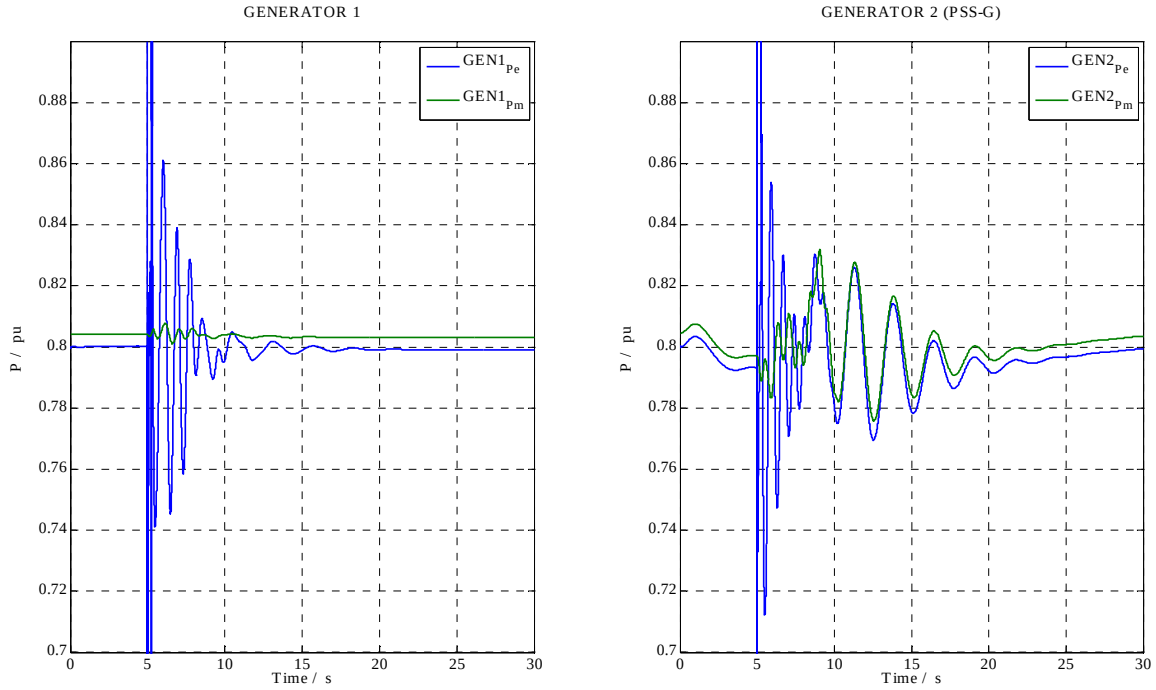

Figure 84: Active power and mechanical power of generator 1 and generator 2 (PSS-G)

The speed deviations in Figure 85 are results from the input signal of P_d for the PSS-G in the upper figure and for the PSS-E in the lower diagram. With the active PSS-G, after 5 seconds all modes with higher frequencies and a significant higher damping are decayed. The inter area oscillation, respectively the target mode is decayed after 20 s.
In the lower time course of Figure 85 the PSS-E is applied, also using the input signal P_d. Additionally to the lower damping resulting from the linear investigations, the PSS-E output is cut by the limiter. The result is a quite poor damping behavior.

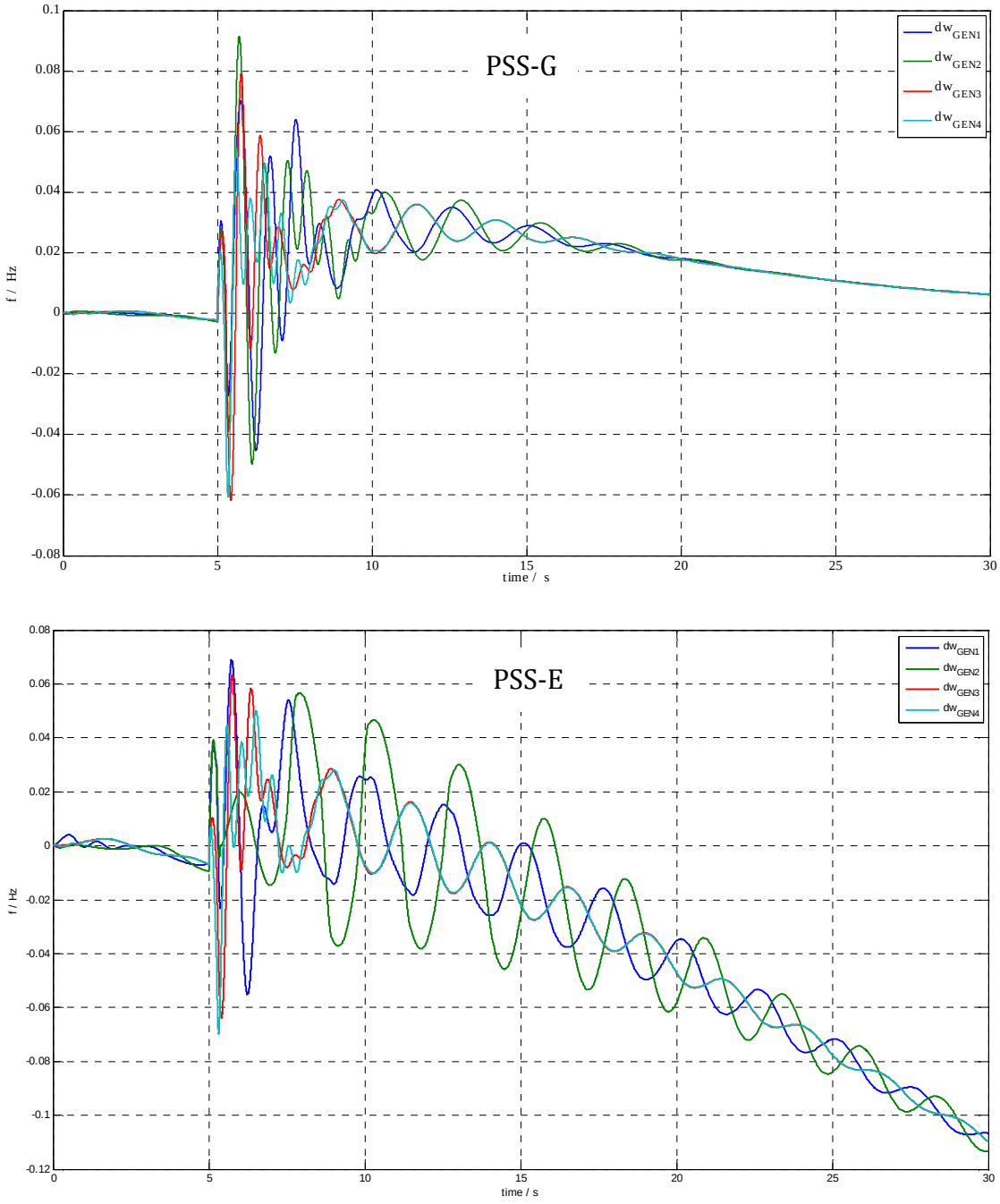

Figure 85: Speed deviations of the generators, input signal: accelerating power P_d applied for the PSS-G(above), for the PSS-E (below)

Both devices, the PSS-G as well as the PSS-G, act on their limits, as shown in Figure 86. For the PSS-G the output signals are limited between 8 s and 12 s, resulting in a triangular signal shape. For the PSS-E it is obvious that the output limit is reached at about 7 s.
This example shows the crossover of the linear and nonlinear characteristics of the model components and confirms the usage of a nonlinear time domain simulation.

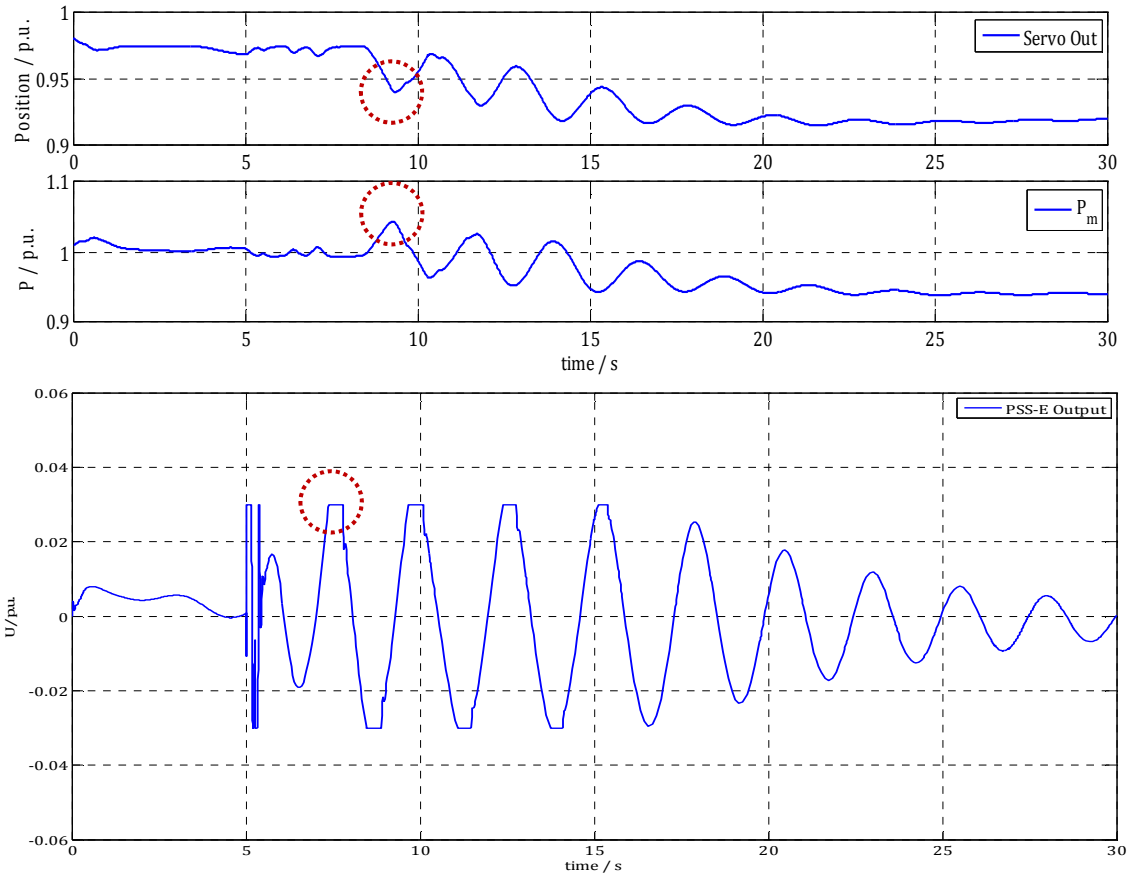

Figure 86: Limitations of governor output with PSS-G activated (upper figure) and PSS-E output (lower figure); inter area mode

6.4.3. **Detailed Description of Target Mode with optimal PSS**

Based on above derived parameter sets, the modal analysis in the following concentrates on the development of the inter area mode damping for the most effective local signal P_d and the most effective WAMS Signal $d_{\text{theta line}}$ for the application of a PSS-G.

Table 15 lists the relevant eigenvalues, obtained by the system without PSS-G and with PSS-G active for the input signals speed deviation and angular difference of the interconnection tie line.

Number of Eigenvalue λ	Base Case	P_d	$d_{theta\ line}$
	Eigenvalue	Eigenvalue	Eigenvalue
	1/s ± 1/s	1/s ± 1/s	1/s ± 1/s
1	-0.9495 ± 12.3576i	-7.2101 ± 14.1098i	-0.9495 ± 12.3577i
2	-1.2561 ± 9.5429i	-0.9495 ± 12.3577i	-1.2553 ± 9.5436i
3	-0.9385 ± 7.7824i	-1.2566 ± 9.5434i	-0.9338 ± 7.7920i
4	-0.6524 ± 6.7020i	-0.9712 ± 7.0829i	-0.6858 ± 6.7287i
5	-0.0371 ± 2.5041i	-0.3952 ± 2.4857i	-0.6227 ± 2.3824i
6	-0.0134 ± 0.0408i	-0.4429 ± 2.1821i	-0.1508 ± 1.4514i
7	-0.0105 ± 0.0402i	-0.0164 ± 0.0383i	-0.0105 ± 0.0403i

Table 15: Relevant system eigenvalues for the base case and with PSS-G active for two input signals, target mode: mode 5

The mode spectrum in Figure 87 provides the damping and mode frequency for the modes of interest.

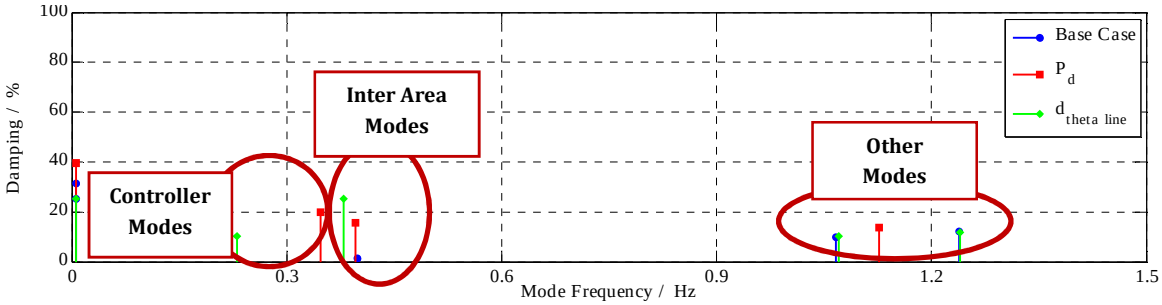

Figure 87: Mode spectrum base case compared to PSS-G; best local signal P_d and best Wide Area Signal $d_{theta\ line}$

The damping of the inter are mode, obtained by the input signal $d_{theta\ line}$, is increased as expected in Table 14, although the oscillation frequency is shifted slightly to a lower oscillation frequency. Global mode 3 and the local mode in area 2 remain unchanged for all parameterizations, whereas the local mode for area 1 is also stronger damped and shifted in oscillation frequency.

The two control modes, occurring due to the activation of the PSS are below the inter area oscillation frequency. The damping is 20 % for the input signal P_d compared to 10 % for the input signal $d_{theta\ line}$.

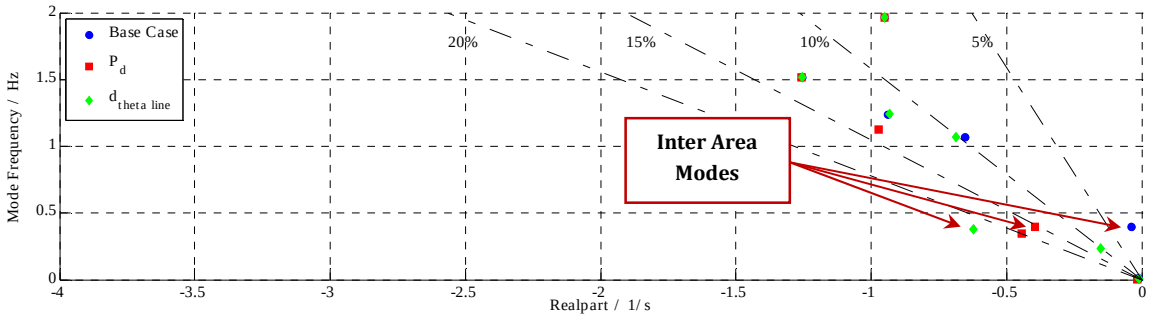

Figure 88: Scatter plot of the poles for the base case and the three

The root shift, drawn in Figure 88, confirms the results from above and illustrate the vertical shift of the root, corresponding to the inter area mode.
From the participation factors, plotted in Figure 89 and Figure 91, one can observe that the speed deviations of generator 2, of the substitute grid 1 and grid 2 and the states describing the PSS-G, respectively the governor, dominate the inter area mode and the controller mode.

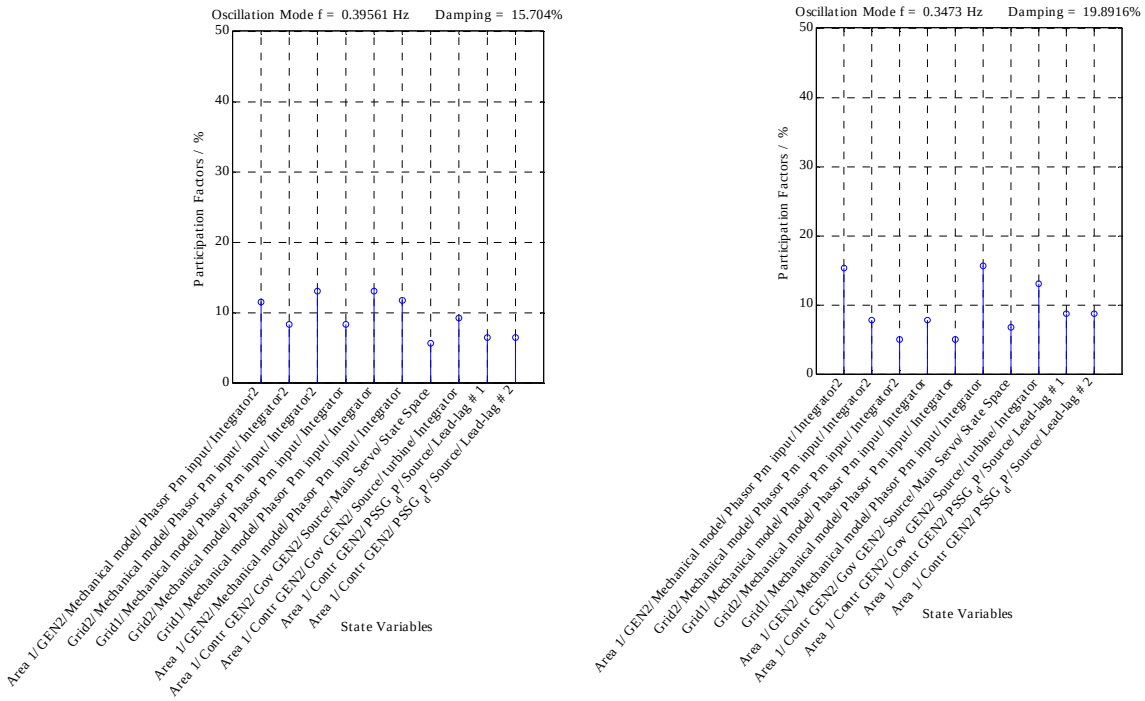

Figure 89: Participation factors of the dominant states for the inter area mode (left) and the control mode (right), PSS-G active using P_d as input signal

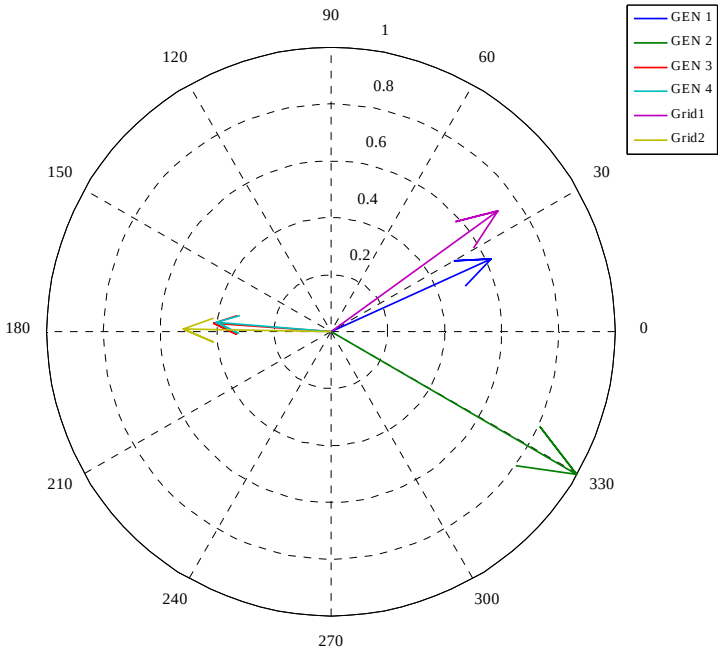

Figure 90: Mode shape of the inter area mode, PSS-G active using P_d as input signal

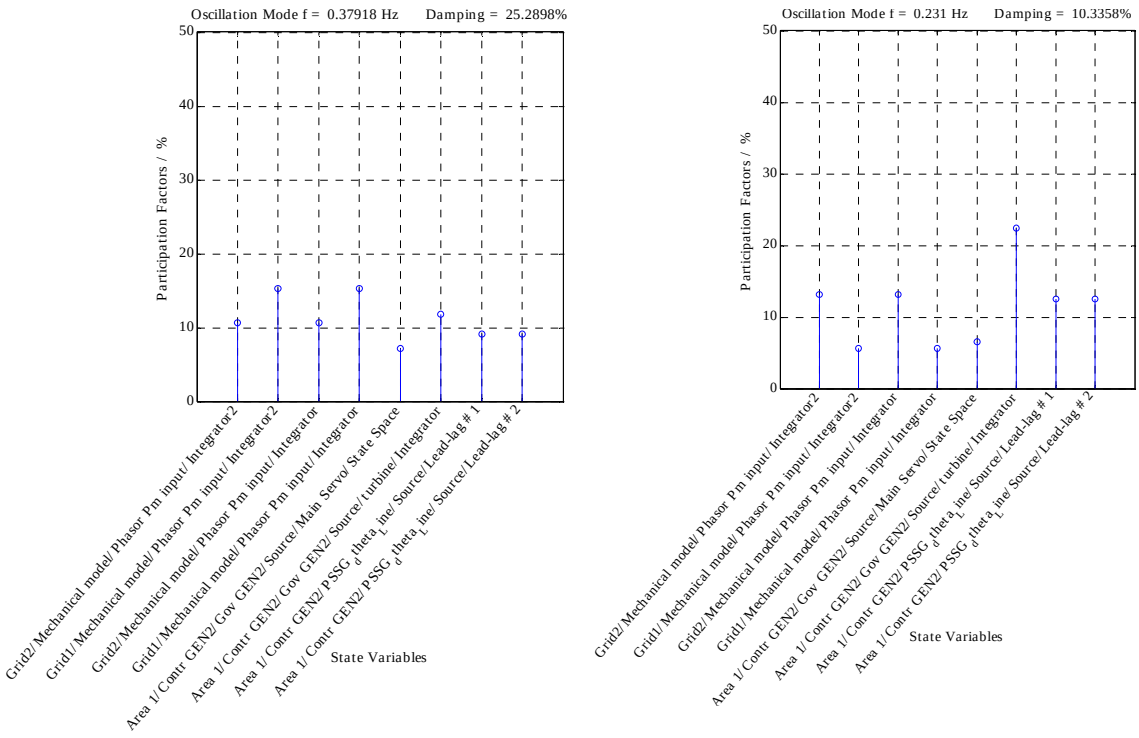

Figure 91: Participation factors of the dominant stated for the inter area mode (left) and the control mode (right), PSS-G active using $d_{theta\ line}$ as input signal

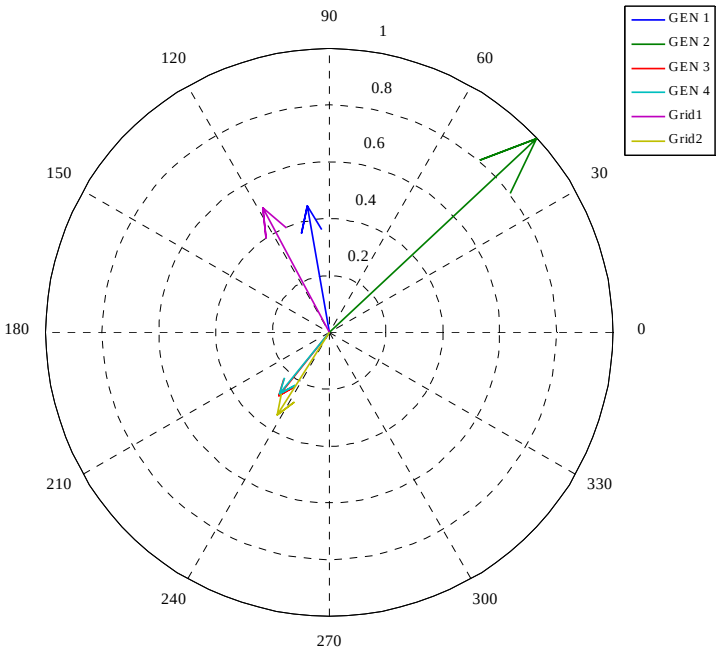

Figure 92: Mode shape of the inter area mode, PSS-G active using $d_{theta\ line}$ as input signal

Mode shapes plotted in Figure 90 Figure 92, point out the dominating speed deviation of generator 2 in area 1. The phase of oscillation has therefore spread in area 1 and is still in phase in area 2.

6.4.4. **Summary of Results**

The multi machine model forms the second step of investigation and focuses on the impact of the PSS-G on a poor damped inter area mode. In the multi machine system, the most suitable generator candidate for the application of a PSS is chosen by the analysis of participation factors and residues of proper transfer functions. Furthermore, the PSS-G and PSS-E parameter sets are derived for local signals and synthesized WAMS signals. In general the grid condition simulates a weak grid condition, including a bad voltage situation as well as high power transfers from area 1 to area 2.
The investigations are based on a detailed linear analysis with the aim to determine the potential of the governor control path, including the action of a PSS-G to improve the system damping. An additional nonlinear time domain simulation exposes the PSS-G and PSS-E to time domain limitations, such as actuator speed limit and voltage control output limit.

Similar to the results from the single machine infinite bus model the base case characteristics show a negative damping contribution of the governor control path of generator 2. The calculated value is in the same range as the positive damping torque, provided by the voltage control path. This result confirms the conclusion made in chapter 6.3.7 that the negative contribution, provided by the governor, should not be automatically

be neglected in small signal analysis. Especially for poor grid conditions, the governor characteristics should be taken into account.

To determine the robustness of the PSS-G, as well as of the PSS-E, the base case scenario is exposed to changes of active power output of generator 2 as well as to changes in grid inertia, resulting in a variation of the inter area oscillation frequency.
For the active PSS-G, the scatterplots of the eigenvalue shifts for varying output power show a comparable high sensitivity, especially the input signals which provide a high damping. In contrast the PSS-E parameterizations provide less sensitivity with a tendency towards increasing mode damping throughout the value range. Although the highest mode damping is dedicated to the use of the PSS-G, this leads to the conclusion that the PSS-E is more robust against changes of the generator output power for the investigated scenarios.
Regarding the variation of grid inertia and the accompanying variation in inter area oscillation frequency, the PSS-G shows advantageous behavior, especially towards lower oscillation frequencies. The PSS-E in contrast provides decreasing damping tendency for lower inter area frequencies. Similar to the observations for various operating points, the sensitivity is higher for input signals, providing higher mode damping.

In the time domain simulations the potential impact, determined from the linear analysis, is tested under the restrictions of the actuator speed limits.
The limiting factor for the impact of the PSS-G is the actuator speed limit, whereas for the PSS-E this is the output limit, according to the tolerable influence on the terminal voltage.

7. Conclusion

7.1. General Conclusions

This thesis presents a novel approach in damping inter area oscillations during poor grid conditions and very low frequency ranges at the generator side. The method is based on the application of single input PSS to the actuators of hydro governor systems without interfering with the standard operational utilizations, such as primary frequency control. Local signals, like speed deviation or accelerating power as well as signals provided by WAMS have been used as input signals.

As a major result the capability of hydro governor systems to act as a damping device was derived and demonstrated for an inter area oscillation at 0.4 Hz.
In general the hydro governor control path provides a favorable behavior for oscillation frequencies below 1 Hz down to very low oscillation frequencies from the linear point of view. In this range the governor control path shows favorable behavior compared to the excitation control path. The factual efficiency is determined also by the respective speed limits of the actuators of the hydro governor. Depending on the applied turbine type model these limitations can vary strongly, whether the limiting element is the vane system of a Francis type or the deflector system of an impulse turbine.
The application of the PSS-G to utilize the governor control path for damping has proven to extend the operational range of generator side damping towards low frequencies.

The studies are based on the method of model linearization and modal analysis, complemented by the application of the damping torque approach, using the extended Heffron-Phillips model. In time domain the nonlinear simulation model is used as the fundament of the investigations.

The results illustrate in general a weak coupling between the excitation and governor control path. The bode characteristic of the mechanical control loop shows a low pass behavior whereas the electrical control loop provides a high pass characteristic.

Furthermore the excitation control path in the linear domain provides the dominating contribution to the damping torque component at oscillations frequencies higher than 0.6 Hz. For variation in grid impedance the voltage control path shows comparatively high sensitivity, which impedes the calculation of optimal parameters for a certain mode of interest. The damping torque component, as well as the synchronizing torque component, provided by the voltage control path, decrease with increasing connection impedances of the generator. Furthermore a reduction of the damping torque in case of decreasing grid voltage has been observed.
In time domain the capability of the PSS-E is limited due to the opposite interaction with the control scheme of the voltage regulator. The influence is getting more dominant as the grid impedance, respectively the connection impedance of the generator, increases.

The governor path has shown negative damping contributions over a wide range of oscillation frequencies. In most stability studies assuming good grid conditions, this amount is justifiably neglected. However, for very poor damped low frequency modes the amount of positive damping, provided by the excitation path, has been shown to be in the range of the negative contribution provided by the governor. In such cases the inclusion of the governor system is recommended.
Furthermore root loci of the inter area modes and the control modes proof that the governor control path, including PSS-G, is comparably robust against changes in grid impedance. Especially for high grid impedances the contribution of damping torque has shown to be constant or even slightly increasing.
The robustness, concerning changes in grid inertia and therefore slight changes in the occurring target frequency, has shown to be sensitive to the choice of the remote signal. The most promising signal in this regard has been the generating accelerating power.

In the time domain, depending on actuator speed of the governor, the lower the oscillation frequency is, the higher is the potential impact of the PSS-G on the damping of the respective mode.

This leads to the final conclusion that PSS-E and PSS-G complement each other to extend the all over oscillation frequency spectrum towards lower frequencies and high connection impedances of the generator. Oscillations with frequencies below 1 Hz can be better handled with the PSS-G, depending on the respective actuator speed limits of the governor system and the prevailing operational conditions. As the ability of the governor system for damping concerns decreases at higher oscillation frequencies, the traditional PSS-E can be applied in the optimal operating range.

7.2. Future Work

7.2.1. Impact on Hydraulic Path and Governor Mechanics

Governor actions in general lead to changes of movement of the water volume. This coupling is inherent to the operation of hydro power plants and is, especially for transient movements with large actuator excursions, of great interest. The reason is the occurrence of hydraulic shock waves which can lead to destructive impact on the hydraulic system in case that the parameters of the respective governors do not prevent the actuators from excessive movements. As an example for the prevention, the transient governor droop is mentioned in this context.
As seen from the simulations in time domain, the governor system equipped with a PSS-G shows higher amplitudes of actuator excursions during the occurrence of inter area oscillations compared to systems without PSS-G.
Nevertheless, the detailed investigation of the impact of the increased actuator movements caused by the PSS-G is deemed necessary. The basement for this investigation was given in this work by introducing the various turbine and hydraulic systems models in chapter 4.3.4.

7.2.2. Interaction between Controllers

In [4] and [31] interactions between the governor control path and the excitation control path, respectively the excitation control path and the connected grid under prevailing grid conditions is discussed.
For generator side damping in general the interaction of these controllers requests future research. Furthermore the possible enhancement of the generator side damping behavior due to functional coordination of PSS-G and PSS-E, exemplary due to signal interchange among both devices, is seen to have potential.

7.2.3. Application of Hydro Governor as WAMPAC

This thesis focuses on the principal possibility, basic characteristics and the impact of the hydro governor utilized as a damping device. The input signals used in the simulations are predominant local signals. Experiences with WAMS in terms of visualization in Norway are described in [47]. The development of WAMS, which was set up in many power systems all over the world and also in RG CE in the last decade, offers the possibility to combine areas with high observability and damping devices (sites) with high controllability to an improved damping device. Especially for oscillation phenomena across long distances this topic has gained increased interest in the recent past. Monitoring of wide area measurement data has been also a topic in industry and academia whereas the challenge of visualization of relevant information for the system operator remains for the time being.
The extension of WAMS to an independent and automatically acting control system is found in literature as Wide Area Monitoring, Protection and Control - WAMPAC. For various actors like PSS-E or FACTS devices control algorithms have been developed and

tested up to the time being. An example is given in [48], where the authors describe the expected benefits from WAMPAC in the Nordic Power System along with controller design methods for PSS-E based on remote WAMS signals.
An enhancement of work, done in this thesis, would be the utilization of WAMS signals and the integration of PSS-G into an automatic control scheme as a fragment in a superior WAMPAC system.

8. References

[1] E.-E. Eurelectric, "Report on "Deterministic Frequency Deviations – Root Causes and Proposals for Potential Solutions"," November 2011. [Online]. Available: https://www.entsoe.eu/about-entso-e/working-committees/system-operations/ad-hoc-teams/aht-frequency-investigation/.

[2] P. Kundur, J. Paserba, V. Ajjarapu, G. Andersson, A. Bose, C. Canizares, N. Hatziargyriou, D. Hill, A. Stankovic, C. Taylor, T. Van Cutsem and V. Vittal, "Definition and Classification of Power System Stability," *IEEE Transactions on Power Systems*, 2004.

[3] J. Paserba, "Analysis and control of power system oscillations," in *CIGRE Special Publication, Technical Brochure 111*, 1996.

[4] J. V. Milanovic, *Damping of the low-frequency oscillations of the generator: dynamic interactions and the effectiveness of the controllers*, 2002.

[5] P. Kundur, Power sytsem Stability and Control, McGraw-Hill, Inc., 1994.

[6] S. Yee, J. Milanovi´c and F. Hughes, "Damping of system oscillatory modes by a phase compensated gas turbine governor," *Electric Power Systems Research 80*, pp. 667-674, 2010.

[7] I. P. Engineering, *IEEE Recommended Practice for Excitation System Models for Power System Stability Studies, IEEE Std 421.5™-2005*, New York, NY 10016-5997, USA, 2006.

[8] W. G. Heffron and R. A. Phillips, *Effect of a Modern Amplidyne Voltage Regulator on Underexcited Operation 0o Large Turbine Generators*, Vols. 71:692-697, 1952.

[9] B. Pal and B. Chaudhuri, Robust Control in Power Systems, Springer Science+Business Media Inc., 2005.

[10] P. H. Krishna, S. P. Venkatesh, E. Ramesh and S. G. Sudheer, "Design Of Power System Stabilizer To Improve Small Signal Stability By Using Modified Heffron-Phillip's Model," in *International Journal of Engineering Science and Technology*, 2011.

[11] H. B. Gooi, E. F. Hill, M. A. Mobarak, D. H. Thorne and T. H. Lee, "Coordinated Multi-Machine Stabilizer Settings without Eigenvalue Drift," in *IEEE Transactions on Power Apparatus and Systems*, 1981.

[12] M. Soliman, D. Westwick and O. P. Malik, "Identification of Heffron–Phillips

model parameters for synchronous generators operating in closed loop," in *IET Generation, Transmission & Distribution*, 2008.

[13] F. R. Schleif, G. E. Martin and R. R. Angell, "Damping of System Oscillations with a Hydrogenerating Unit," in *IEEE TRANSACTIONS ON POWER APPARATUS AND SYSTEMS*, 1967.

[14] F. P. De Mello, R. J. Koessler, J. Agee, P. M. Anderson, J. H. Doudna, J. H. Fish, P. A. Hamm, P. Kundur, D. C. Lee, G. J. Rogers and C. Taylor, *Hydraulic Turbine and Turbine Control Models for Ssystem Dynamic Studies*, 1992.

[15] IEEE Std 1207, *IEEE Guide for the Application of Turbine Governing Systems for Hydroelectric Generating Units*, 2004.

[16] W. Li, L. Vanfretti and Y. Chompoobutrgool, "Development and implementation of hydro turbine and governor models in a free and open source software package," in *Simulation Modelling Practice and Theory*, 2012.

[17] I. Kamwa, D. Lefebvre and L. Loud, "Small Signal Analysis of Hydro-Turbine Governors in Large Interconnected Power Plants," in *Power Engineering Society Winter Meeting*, 2002.

[18] I. Kamwa and L. Gkrin-Lajoie, "State-Space System Identification-Toward MIMO Models for Modal Analysis and Optimization of Bulk Power Systems," in *IEEE TRANSACTIONS ON POWER SYSTEMS*, 2000.

[19] S. Yee, J. Milanovi´c and F. Hughes, "Phase compensated gas turbine governor for damping oscillatory modes," *Electric Power Systems Research 79*, p. 1192–1199, 2009.

[20] M. Jin, W. Hu, F. Liu, S. Mei and Q. Lu, "Nonlinear co-ordinated control of excitation and governor for hydraulic power plants," 2005. [Online].

[21] T. Xiangyu, W. Guanhong, L. Wenfeng, L. Zenghuang, Z. Hongguang and C. Liu, *Mechanism of Impact of Governor Control on Power System Dynamics and Introduction of Boundary Frequency*, 2011.

[22] J. C. Mantzaris, A. Metsiou and C. D. Vournas, *Analysis of Interarea Oscillations Including Governor Effects and Stabilizer Design in South-Eastern Europe*, 2013.

[23] H. F. Wang, Y. S. Hao, B. W. Hogg and Y. H. Yang, "Stabilization of power systems by governor-turbine control," *Electrical Power & Energy Systems*, 1993.

[24] D. M. Dobrijevic and M. V. Jankovic, "An Approach to the Damping of Local Modes of Oscillations Resulting from Large Hydraulic Transients," *IEEE Transactions on Energy Conversion*, pp. 754-758, September 1999.

[25] L. A. Lucero Tenorio, *Hydro Turbine and Governor Modelling*, 2010.

[26] J. Turunen, A Wavelet-based Method for Estimating Damping in Power Systems, 2011.

[27] T. Bödefeld and H. Sequenz, Elektrische Maschinen, Wien: Springer-Verlag, 1962, pp. 331-332.

[28] "Analysis of CE Inter-Ares Oscillations of 19 and 24 February 2011," *ENTSO-E SG SPD REPORT*, 2011.

[29] A. Dysko, W. E. Leithead and J. O'Reilly, *Enhanced Power System Stability by Coordinated PSS Design*, 2010.

[30] M. J. Gibbard, *Co-ordinated design of multimachine power system stabilisers based on damping torque concepts*, 1988.

[31] J. Hell, A. Glaninger-Katschnig, R. Schürhuber and M. Egretzberger, *Interference of parallel operating hydro generating units connected to a weak grid*, 2010.

[32] H. Ni, G. T. Heydt and L. Mili, *Power System Stability Agents Using Robust Wide Area Control*, 2002.

[33] A. Mendonca and J. A. Pecas Lopes, *Robust Tuning of PSS in Power Systems with Different Operating Conditions*, Bologna, 2003.

[34] M. E. Aboul-Ela, A. A. Sallam, J. D. McCalley and A. A. Fouad, "Damping Controller Design for Power System OScillations using Global Signals," *IEEE Transactions on Power Systems, Vol. 11*, pp. 767-773, Mai 1996.

[35] Y. Chompoobutrgool, L. Vanfretti and M. Ghandhari, *Survey on power system stabilizers control and their prospective applications for power system damping using Synchrophasor-based wide-area systems*, 2011.

[36] S. Brandl, *Dynamic modelling of a grid in islanded operation and evaluation of islanded grid operation tests*, Graz: University of Technology Graz, 2010.

[37] J. M. Undrill and J. L. Woodward, *Nonlinear Hydro Governing Model and Improved Calculation for Determining Temporary Droop*, 1967.

[38] J. Machowski, J. W. Bialek and J. R. Bumby, in *POWER SYSTEM DYNAMICS*, 2008, pp. 172-175.

[39] M. Weixelbraun and H. Renner, *Damping of Low Frequency Oscillations in Power Systems*, Budapest, 2009.

[40] D. Schafer and J. J. Simond, "Adjustable speed Asynchronous Machine in Hydro

Power Plants and its Advantages for the Electric Grid Stability," in *Cigré Session*, Paris, 1998.

[41] J. J. Simond, A. Sapin and D. Schafer, "Expected benefits of adjustable speed pumped storage in the European network," 1999. [Online].

[42] D. Schafer and J. J. Simond, "Adjustable speed Asynchronous Machine in Hydro Power Plants and its Advantages for the Electric Grid Stability," 1998. [Online].

[43] G. Tsourakis, B. M. Nomikos and C. D. Vournas, *Contribution of Doubly Fed Wind Generators to Oscillation Damping*, vol. 24, 2009.

[44] F. Mei and B. C. Pal, *Modelling and Small-Signal Analysis of a Grid Connected Doubly-Fed Induction Generator*, 2005.

[45] IEEE Std 1110, *IEEE Guide for Synchronous Generator Modeling Practices in Stability Analyses*, 1991.

[46] MATLAB, "Simulink Library Browser".

[47] A. B. Leirbukt, J. O. Gjerde, P. Korba, K. Uhlen, L. K. Vormedal and L. Warland, "Wide Area Monitoring Experiences in Norway," 2006. [Online].

[48] E. Johansson, K. Uhlen, A. B. Leirbukt, P. Korba, J. O. Gjerde and L. K. Vormedal, *Coordinating Power Oscillation Damping Control using Wide Area Measurements*, Trondheim, 2009.

[49] D. H. Wilson, "Wide-Area Measurement and Control for Dynamic Stability," 2007. [Online].

9. Appendix

Single Machine Infinite Bus Model, Participation Factors of PSS-G Parameter Sets

In Figure 93, Figure 94 and Figure 95 selected participation factors with a contribution greater than 5 % to the mechanical mode as well as the occurring controller mode are shown for the three PSS-G parameterizations.
In Figure 95 one can see that the contribution of the high- and intermediate band of the multiband device is dominant in the mechanical mode and in the controller mode.

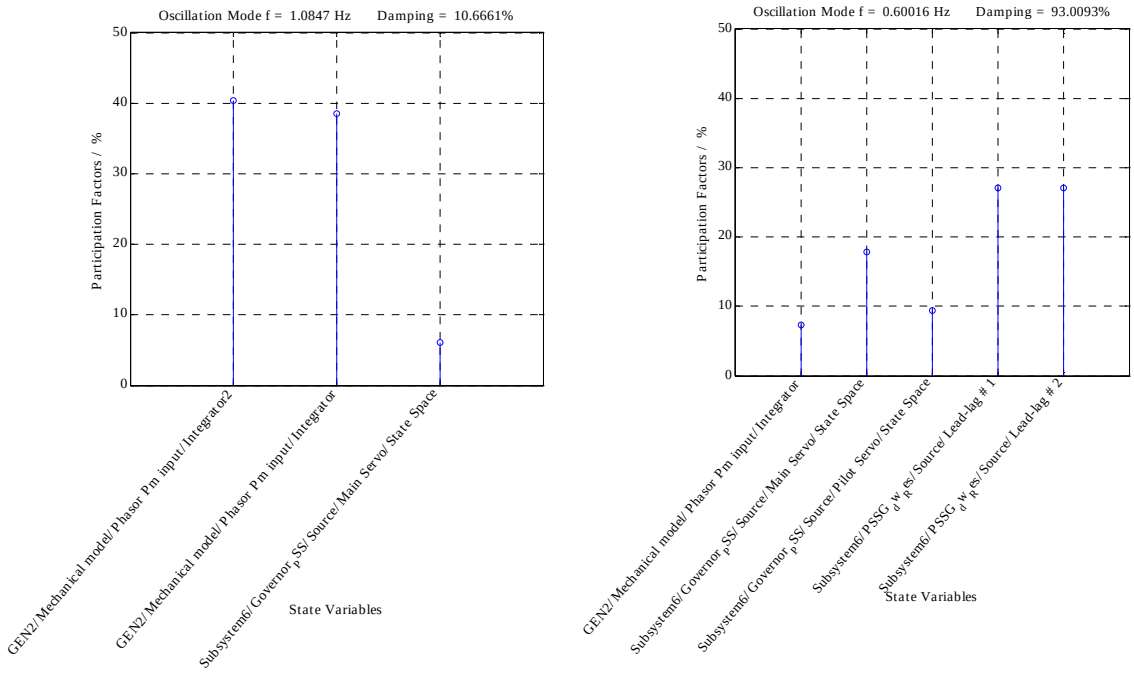

Figure 93: Residue method, dominant participation factors of the mechanical mode (left) and the controller mode (right)

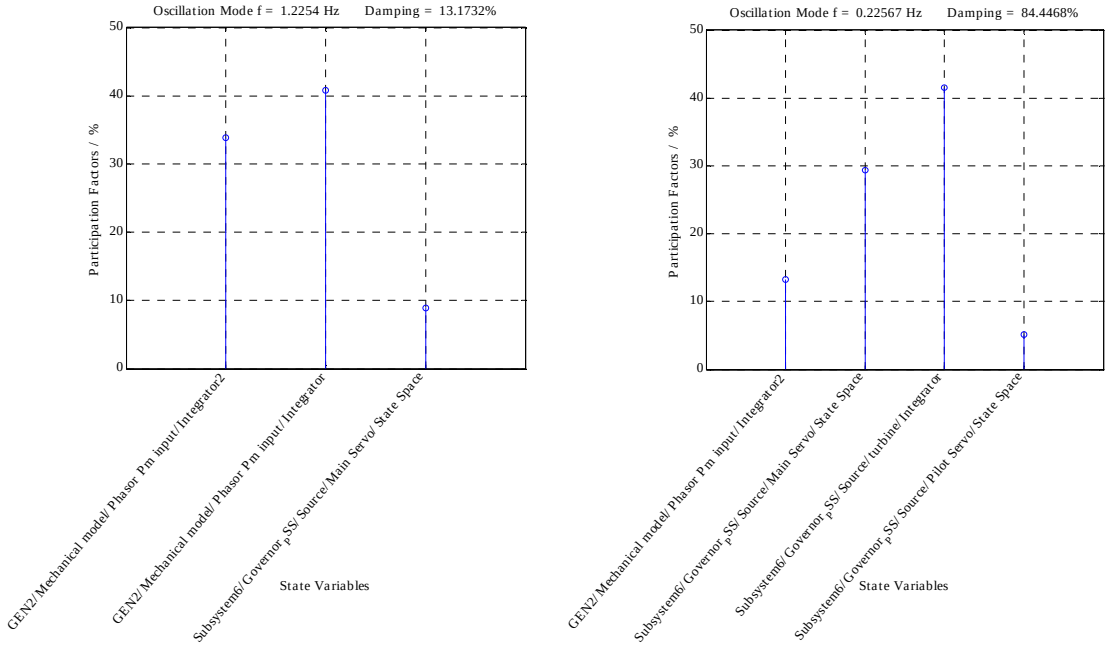

Figure 94: Kundur parameterization, dominant participation factors of the mechanical mode (left) and the controller mode (right)

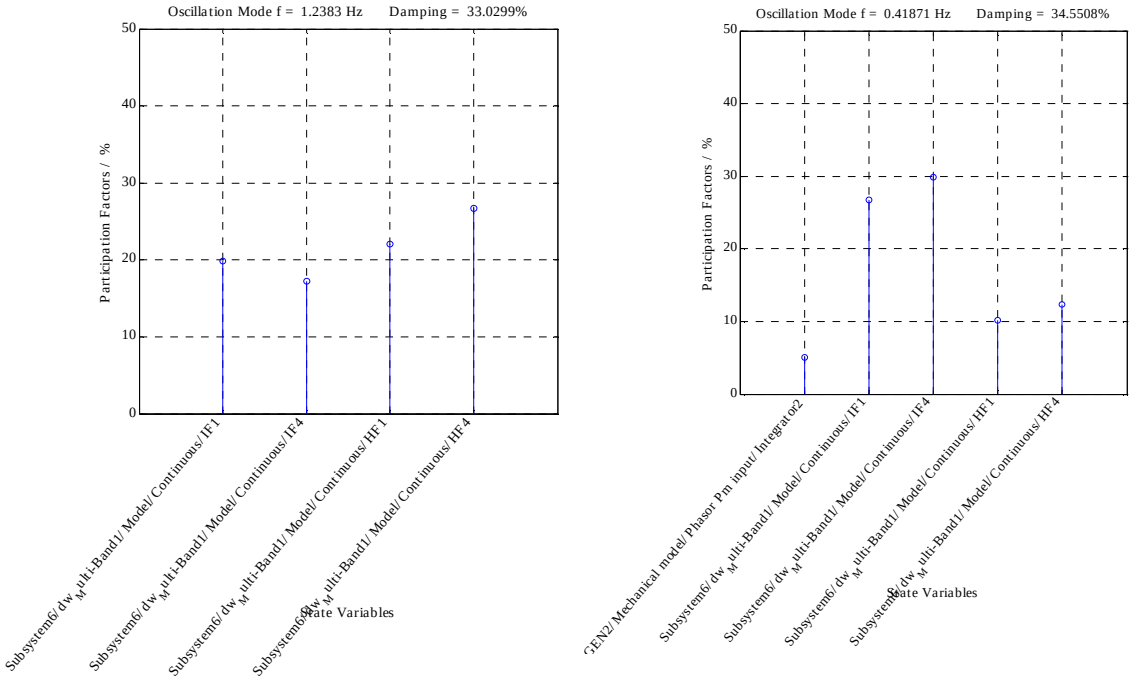

Figure 95: Multiband parameterization, dominant participation factors of the mechanical mode (left) and the controller mode (right)